Abnormal brain development in mice with region- and cell-type-specific inactivation of ST8SIA2

Von der Naturwissenschaftlichen Fakultät der
Gottfried Wilhelm Leibniz Universität Hannover

zur Erlangung des Grades
Doktorin der Naturwissenschaften (Dr. rer. nat.)

genehmigte Dissertation
von

Ute Elisabeth Schuster, M. Sc.
geb. Diederichs

2017

Abstract

Polysialylation of the neural cell adhesion molecule NCAM by the two polysialyltransferases ST8SIA2 and ST8SIA4 plays an essential role during brain development. Ablation of polysialic acid (polySia) causes neuroanatomical defects associated with psychiatric disorders. This thesis addresses (i) the role of polySia, ST8SIA2 and ST8SIA4 during migration of interneurons derived from the medial ganglionic eminence (MGE) into the neocortex, (ii) the differential impact of ST8SIA2 expressed in MGE-derived interneurons compared to their cortical environment and (iii) the consequences of *St8sia2*-deficiency for the long-range connectivity of the thalamus and the mammillary body. Based on the generation and phenotypical evaluation of conditional knockout models, the presented results dissect the differential impact of ST8SIA2 in different brain regions and cell types.

The first part of this thesis assesses different interneuron populations in the medial prefrontal cortex of polySia-deficient mice and demonstrates a loss of parvalbumin- and somatostatin-positive interneurons in adult as well as reduced GABAergic cells in neonatal mice. Analysis of embryonic polySia-deficient mice revealed an accumulation of precursor cells accompanied by increased apoptosis in the MGE. Removal of polySia by endosialidase caused impaired entry of migrating interneurons into the neocortex and reduced migration velocities. Furthermore, endosialidase-treatment resulted in shorter leading processes of interneurons in slice and primary cultures. Hence, disturbed polysialylation impacts interneuron migration from the MGE towards the neocortex, resulting in altered interneuron populations.

The second part aims at analyzing, whether ST8SIA2 impacts the development of MGE-derived interneurons cell-autonomously or non-cell-autonomously. Conditional knockout of *St8sia2* in MGE-derived interneurons and their cortical environment resulted in alterations of interneuron distributions in selected regions of the anterior cortex. Together with analysis of interneuron migration *in situ*, the data argue for a cell-autonomous role of ST8SIA2. Both approaches also indicated a polySia-dependent interaction between interneurons and their cortical environment. Live imaging experiments revealed polySia-dependent sensing of the brain-derived neurotrophic factor BDNF. Together, these results demonstrate a major cell-autonomous impact of ST8SIA2 on interneuron development, which may be connected to polySia-dependent BDNF-perception.

In the third part, the role of ST8SIA2 in establishing the long-range connectivity of the thalamus and the mammillary body was analyzed. Evaluation of mice with a loss of *St8sia2* in the diencephalon (*Foxb1-Cre;St8sia2$^{f/f}$*) revealed severe hypoplasia of the mammillary body and the mammillothalamic tract as well as minor reductions of the fornix. In contrast, mice with a cortex-specific inactivation of ST8SIA2 (*Emx1-Cre;St8sia2$^{f/f}$*) displayed minor reductions of the mammillothalamic tract and major hypoplasia of the fornix. Further analyses of these mice demonstrated that ST8SIA2-depletion in thalamocortical and corticofugal fibers is not sufficient to mimic the aberrant pathfinding observed in mice with constitutive ablation of *St8sia2*.

Taken together, this thesis reveals novel neuropathological changes caused by loss of ST8SIA2 and discloses some of the underlying developmental mechanisms. Based on the distinct phenotypical features in mice with conditional knockout of *St8sia2* in MGE-derived interneurons, cortex and diencephalon, future studies will be able to analyze, whether behavioral changes observed in *St8sia2*-negative mice can be attributed to specific defects of brain morphology.

Zusammenfassung

Polysialylierung des neuralen Zelladhäsionsmoleküls NCAM durch die zwei Polysialyltransferasen ST8SIA2 und ST8SIA4 ist essentiell für die Gehirnentwicklung. Verlust von Polysialinsäure (PolySia) verursacht neuroanatomische Defekte, die mit psychiatrischen Erkrankungen in Verbindung gebracht werden. Diese Arbeit thematisiert (i) die Rollen von PolySia, ST8SIA2 und ST8SIA4 während der Migration von Interneuronen, die aus dem medialen Ganglionhügel (MGE) stammen und in den Cortex einwandern, (ii) unterschiedliche Einflüsse von ST8SIA2 in MGE-abstammenden Interneuronen im Vergleich zu deren kortikalen Umgebung und (iii) die Folgen von ST8SIA2-Defizienzen auf lange Axon-Verbindungen des Thalamus und des Mammillarkörpers. Durch Generierung und Phänotyp-Analysen von konditionalen Knockout-Modellen, werden hier unterschiedliche Einflüsse von ST8SIA2 in verschiedenen Gehirnregionen und Zelltypen analysiert.

Der erste Abschnitt dieser Arbeit behandelt verschiedene Interneuronen-Populationen im medialen präfrontalen Kortex von PolySia-defizienten Tieren und weist einen Verlust von Parvalbumin- und Somatostatin-positiven Interneuronen in adulten Tieren, sowie eine Reduktion von GABAergen Zellen in neonatalen Mäusen nach. Untersuchungen von embryonalen PolySia-defizienten Tieren offenbarte eine Akkumulation von Vorläuferzellen sowie erhöhtes Zellsterben in der MGE. Enzymatischer Verdau von PolySia durch Endosialidase führte zu beeinträchtigter Einwanderung von migrierenden Interneuronen in den Kortex und zu einer verminderten Migrationsgeschwindigkeit. Außerdem verursachte Endosialidase-Behandlung kürzere Leitfortsätze von Interneuronen in Gewebe- und Primärkulturen. Folglich beeinträchtigt fehlerhafte Polysialylierung die Migration von Interneuronen aus der MGE in den Kortex und verursacht Veränderungen in Interneuronen-Populationen.

Der zweite Abschnitt befasst sich mit der Frage, ob ST8SIA2 die Entwicklung von MGE-abstammenden Interneuronen zellautonom oder nicht-zellautonom beeinflusst. Konditionaler Knockout von *St8sia2* spezifisch in MGE-abstammenden Interneuronen und deren kortikaler Umgebung führte zu Veränderungen in der Interneuron-Verteilung in bestimmten Regionen des vorderen Kortex. Zusammen mit Migrationsanalysen *in situ*, sprechen diese Daten für einen zellautonomen Einfluss von ST8SIA2. Beide Ansätze deuteten außerdem eine PolySia-abhängige Interaktion zwischen Interneuronen und ihrer kortikalen Umgebung an. *Live cell imaging* Analysen offenbarten eine PolySia-abhängige Wahrnehmung des *brain-*

derived neurotrophic factors BDNF. Zusammengenommen sprechen diese Daten für einen starken, zellautonomen Einfluss von ST8SIA2 auf die Interneuronen-Migration, die im Zusammenhang mit PolySia-abhängiger BDNF-Wahrnehmung stehen könnte.

Im dritten Abschnitt wird der Einfluss von ST8SIA2 auf die Etablierung von langen Faserverbindungen des Thalamus und des Mammillarkörpers analysiert. Untersuchungen von Mäusen mit spezifischer Inaktivierung von ST8SIA2 im Diencephalon (*Foxb1-Cre;St8sia2$^{f/f}$*) offenbarten eine stark ausgeprägte Hypoplasie des Mammillarkörpers und des mammillothalamischen Traktes, sowie eine geringer ausgeprägte Atrophie der Fornix. Im Gegensatz dazu zeigten Tiere mit spezifischer Inaktivierung der ST8SIA2 im Kortex (*Emx1-Cre;St8sia2$^{f/f}$*) nur eine geringe Hypoplasie des mammillothalamischen Traktes, jedoch eine stark ausgeprägte Atrophie der Fornix. Weitere Analysen zeigten, dass ST8SIA2-Verlust in thalamokortikalen sowie in kortikofugalen Fasern nicht ausreicht, um fehlerhafte Wegfindung von Fasern zu rekapitulieren, die bei vollständiger Deletion von *St8sia2* auftritt.

Diese Arbeit offenbart neue neuropathologische Veränderungen durch Verlust von ST8SIA2 und enthüllt manche der zugrundliegenden Mechanismen. Auf Grundlage von verschiedenen neuropathologischen Phänotypen in Mäusen mit konditionalem Verlust von ST8SIA2 in MGE-abstammenden Interneuronen, deren kortikaler Umgebung sowie im Diencephalon, können künftige Studien Zusammenhänge zwischen Verhaltensauffälligkeiten in Mäusen mit vollständigem ST8SIA2-Verlust und dem Fehlen von ST8SIA2 in spezifischen Hirnregionen herausfinden.

Schlüsselwörter: Polysialyltransferase, konditionaler Knockout, Interneurone

Contents

Contents

List of Figures

List of Abbreviations

5HT3aR	ionotropic serotonin receptor 5HT3a
AMPA	2-amino-3-(3-hydroxy-5-methyl-isoxazol-4-yl)propanoic acid
ANOVA	analysis of variance
BDNF	brain-derived neurotrophic factor
CB	calbindin
cc	corpus callosum
cDNA	complementary DNA
Cg1	cingulate cortex area 1
CGE	caudal ganglionic eminence
CR	calretinin
CXCL12	C-X-C motif chemokine 12
DAPI	4',6-diamidino-2-phenylindole
DIV	days in vitro
DNA	deoxyribonucleic acid
DNase	deoxyribonuclease
DT	dorsal thalamus
E	embryonic day
Endo	endosialidase
FGF	fibroblast growth factor
FnIII	fibronectin-type III
GABA	γ-aminobutyric acid
GAD	glutamate decarboxylase
GAPDH	glyceraldehyde-3-phosphate dehydrogenase
GFP	green fluorescent protein
HGF	hepatocyte growth factor
ic	internal capsule
Ig	immunoglobulin
LGE	lateral ganglionic eminence
M1	motorcortex 1
M2	motorcortex 2
mAb	monoclonal antibody
mb	mammillary body
MGE	medial ganglionic eminence
mPFC	medial prefrontal cortex
mRNA	messenger ribonucleic acid
mtg	mammillotegmental tract
mth	mammillothalamic tract
NCAM	neural cell adhesion molecule
NF	neurofilament
NMDA	N-methyl-D-aspartate

List of Abbreviations

NPY	neuropeptide Y
Nrg1	neuregulin 1
Nrg1-CRD	cysteine-rich domain-containing neuregulin 1
Nrp2	neuropilin 2
OB	olfactory bulb
P	postnatal day
pAb	polyclonal antibody
PAGE	polyacrylamide gel electrophoresis
PBS	phosphate buffered saline
PCR	polymerase chain reaction
PDGF	platelet-derived growth factor
PFC	prefrontal cortex
pm	principal mammillary tract
PNN	perineuronal net
POA	preoptic area
polySia	polysialic acid
PV	parvalbumin
qPCR	real-time quantitative polymerase chain reaction
RMS	rostral migratory stream
RNA	ribonucleic acid
RNase	ribonuclease
Rt	reticular thalamic nucleuss
S1	somatosensory cortex 1
SDS	sodium dodecyl sulfate
SEM	standard error of the mean
SEMA	semaphorin
Sst	somatostatin
SVZ	subventricular zone
SZ	schizophrenia
TrkB	tyrosine-related kinase B
TUNEL	terminal deoxynucleotidyl transferase-mediated digoxigenin-dUTP nick end labeling
VGLUT	vesicular glutamate transporter
VIP	vasointestinal peptide
VZ	ventricular zone
WFA	Wisteria floribunda agglutinin
ErbB4	Erb-B2 receptor tyrosine kinase 4
Pax6	paired box protein 6
GE	ganglionic eminence
HEPES	2-[4-(2-hydroxyethyl)piperazin-1-yl]ethanesulfonic acid
IL	infralimbic cortex
IZ	intermediate zone
NT4	neurotrophin 4
PFA	paraformaldehyde
PrL	prelimbic cortex

1

General Introduction

Most eukaryotic, but also prokaryotic cells are encased in a glycoprotein coat, called the glycocalyx. As the outermost structure of a cell, the glycocalyx is essential for communication with the cell's surroundings. For instance, it is involved in adhesion and cell-cell as well as cell-matrix recognition including, e.g., discrimination between host cells and invading pathogens. Typically, the terminal sugars of a glycan structure are sialic acid residues, which therefore have been associated with the molecular interactions underlying the glycocalyx functions (Varki 2017). In the brain, a special form of sialylation occurs by polymerization of sialic acid residues. The resulting long homopolymer is called polysialic acid or short polySia (Schnaar et al. 2014). As explained in the following sections, the accumulation of negative charges in the carboxyl group of each residue results in a high hydration volume, which is the underlying cause of some, but not all polySia functions. Astonishingly, the vast majority of polySia in the developing and adult nervous system is found on the neural cell adhesion molecule NCAM, but it also has been found on several other carrier proteins (Curreli et al. 2007; Galuska et al. 2010; Mühlenhoff et al. 2013; Kiermaier et al. 2016; Werneburg et al. 2016).

Deficits in polysialylation result in phenotypes reminiscent to those observed in patients with neurodevelopmental psychiatric disorders. Several studies therefore analyzed structural and behavioral phenotypes of mice with perturbed balance between polySia and NCAM-expression in respect to these abnormalities. However, there is still little knowledge as to where and when during development, polySia may contribute to the etiology of these disorders. Identifying the brain regions or cell types, in which polySia-deficiency causes neuropathological changes will be essential to understand how aberrant polySia synthesis translates into neurodevelopmental mechanisms and ultimately may cause a predisposition for psychiatric diseases.

1.1 Structure of NCAM and polysialic acid

Adhesion and communication between cells and their surrounding is indispensable in order to establish proper tissue architecture and to ultimately form a functional organism. Both functions involve a variety of cell-surface proteins called cellular adhesion molecules, or short CAMs. These proteins can be categorized by their dependence on calcium. Cellular interactions mediated by cadherins or by mucin-like CAMs with selectins as well as cell-matrix interactions mediated by integrins are calcium-dependent. Interactions by CAMs of the immunglobulin (Ig) superfamily on the other hand are calcium-independent. The most prominent member of the Ig-superfamily is the neural cell adhesion molecule NCAM (Edelman 1987; Rutishauser *et al.* 1988). This name suggests expression confined to the nervous system and, indeed, NCAM is ubiquitously expressed throughout the entire brain. However, NCAM is also expressed in other organs, as for example the heart, the digestive and the reproductive systems (Uhlén *et al.* 2015; *Human Protein Atlas* 2017). The *Ncam1* gene comprises 19 exons (Fig 1.1a) enabling the production of numerous isoforms by alternative splicing, with 27 different isoforms experimentally verified (Murray *et al.* 1986; Cunningham *et al.* 1987; Reyes *et al.* 1991). The most common isoforms are named NCAM-120, -140 and -180, based on their apparent molecular weight in denaturing gel electrophoresis (Hirn *et al.* 1983). While all three isoforms share a common extracellular structure consisting of five Ig-like domains and two fibronectin type III repeats (Fig 1.1b), they differ in their cytoplasmic region. NCAM-140 and -180 are transmembrane proteins and differ solely in the usage of exon 18 leading to the longer cytoplasmic tail of NCAM-180 (Gennarini *et al.* 1984; Rougon and Marshak 1986; Cunningham *et al.* 1987). NCAM-120 arises from transcription of exon 15, which codes for a glycophosphatidylinositol anchor and carries a stop codon, resulting in the loss of the intracellular domain (He *et al.* 1986, 1987). Other isoforms arise from variable exon usage, like the variable alternative spliced exon VASE (π exon in mice) that can be inserted between exon 7 and 8 (Santoni *et al.* 1989; Small and Akeson 1990), the AAG-trinucleotide or the α-exons that can be inserted between exon 12 and 13 (Santoni *et al.* 1989) forming the NCAM muscle-specific domain 1 (MSD1) expressed in differentiated myotube cells (Thompson *et al.* 1989). A secreted isoform of NCAM, which lacks the hydrophobic domain required for plasma membrane insertion, arises from incorporation of the SEC-exon (Gower *et al.* 1988). Furthermore, NCAM molecules are subject to ectodomain shedding implicated in the regulation of neurite outgrowth by members of a disintegrin and metalloproteinase (ADAM) protein family (Diestel *et al.* 2005; Hübschmann *et al.* 2005; Hinkle *et al.* 2006; Kalus *et al.* 2006).

All NCAM isoforms can be posttranslationally modified, which further amplifies the diversity of NCAM. Sulfation, phosphorylation and palmitoylation of the cytoplasmic domain (Sorkin *et al.* 1984; Little *et al.* 1998) have been reported as well as glycosylation of the extracellular domains (Finne *et al.* 1983; Geyer *et al.* 2001; Liedtke *et al.* 2001; von der Ohe *et al.* 2002). The Ig domains contain six N-glycosylation sites (Albach *et al.* 2004), of which the 5th and the 6th are polysialylated (Fig 1.1b) (Nelson *et al.* 1995; Liedtke *et al.* 2001; von der Ohe *et al.* 2002). On NCAM, polySia consists of up to 90 and more 5-acetylneuraminic acid (Neu5Ac) monomers in α-2,8-linkage (Fig 1.1c) (Inoue *et al.* 2000; Galuska *et al.* 2006, 2008) attached to a highly variable di-/tri- or tetraantennary core glycan (Nelson *et al.* 1995; Liedtke *et al.* 2001; von der Ohe *et al.* 2002). Polysialylation is implemented by the two Golgi-resident polysialyltransferases ST8SIA2 and ST8SIA4 (Eckhardt *et al.* 1995; Kojima *et al.* 1995; Scheidegger *et al.* 1995). As members of the mammalian sialyltransferase family, both enzymes are type II transmembrane proteins with high structural homology. They consist of a short N-terminal cytoplasmic tail, a stem region and a catalytic domain, which contains the conserved sialyl motifs L, S and VS that are involved in substrate binding (see Schnaar *et al.* 2014). The catalytic domain is situated in the Golgi lumen (Datta and Paulson 1995; Datta *et al.* 1998; Harduin-Lepers *et al.* 2001, 2005). Compared to other members of the sialyltransferase family, polysialyltransferases contain two additional unique polybasic motifs, one in the polysialyltransferase domain as part of the catalytic domain (Nakata *et al.* 2006) and one in the stem region (Foley *et al.* 2009; Zapater and Colley 2012).

1.2 Functions of polySia and NCAM

Based on *in vitro* findings that polysialylation decreases NCAM binding (Hoffman and Edelman 1983; Sadoul *et al.* 1983), polySia emerged as a modulator of cellular interactions. The different functions of polySia can be categorized as indirect and direct (as reviewed in Schnaar *et al.* 2014). Due to the increase of NCAM's hydrodynamic radius (Rougon 1993; Yang *et al.* 1994), polySia prevents cellular interactions as a consequence of sterical hindrance (Rutishauser and Landmesser 1996). Apart from the unspecific enlargement of the intercellular space, polySia also shields the underlying carrier protein from interactions (Johnson *et al.* 2005b,a). Regulation of polysialylation is therefore indispensable to control NCAM functions. These interactions can be homophilic, i.e. NCAM-NCAM interactions or heterophilic interactions of NCAM with other cell surface proteins. For instance, interactions with the fibroblast growth factor (FGF) receptor result in ERK1/2 activation promoting survival, neuronal differentiation and migration (Fig 1.1d, Kolkova *et al.* 2000; Niethammer *et al.* 2002; Francavilla *et al.* 2009). In the absence of polySia,

NCAM interactions with a so far unknown cellular receptor leads to the activation of the focal adhesion kinase FAK resulting in enhanced cell-matrix interactions (Eggers *et al.* 2011). Moreover, NCAM interacts with the chondroitin sulfate proteoglycans neurocan and phosphacan, essential members of the brain extracellular matrix. It can be assumed that this interaction can be blocked by polysialylation (Fig 1.1e, Grumet *et al.* 1993; Friedlander *et al.* 1994; Milev *et al.* 1994). On the other hand, polySia has been shown to facilitate NCAM binding to heparan sulfate proteoglycans (Storms and Rutishauser 1998).

Apart from implications in inhibiting interactions of the underlying carrier protein, several studies have shown that polySia itself has the potential to interact with soluble factors or cell surface proteins. For instance, polySia was shown to enhance local concentrations of the brain-derived neurotrophic factor BDNF (Fig 1.1g, Muller *et al.* 2000; Vutskits *et al.* 2001). Other observations, however, argue for a role in limiting the binding of BDNF to its receptor (Burgess and Aubert 2006). Only later, evidence emerged that polySia indeed binds BDNF and that this binding is dependent on the chain length. The same holds true for the neurotrophins NT3 and NT4 (Kanato *et al.* 2008). Moreover, trimming of polySia by secreted Neuraminidase-1 coincides with release of BDNF (Sumida *et al.* 2015). Apart from interactions with BDNF, polySia has been shown to interact with several other factors. For one, polySia increases the sensitivity of hypothalamic neurons towards the ciliary neurotrophic factor (Vutskits *et al.* 2003). Oligodendrocyte precursor cells (OPCs) sense a gradient of platelet-derived growth factor utilizing polySia (Zhang *et al.* 2004) and polySia on the chemokine receptor CCR7 is essential for the recognition of the respective chemokine CCL21 (Kiermaier *et al.* 2016). Other studies demonstrated interactions of polySia with FGF2 (Ono *et al.* 2012) and the neurotransmitter dopamine (Isomura *et al.* 2011).

Moreover, polySia has been shown to interact with certain cell surface receptors. Both soluble polySia and soluble polySia-NCAM are able to specifically modify the activity of particular glutamate receptors. Treatment with soluble polySia potentiates AMPA (α-amino-3-hydroxy-5-methyl-4-isoxazolepropionic acid) -type glutamate receptor currents (Vaithianathan *et al.* 2004) and NR2B subunit containing NMDA (N-Methyl-D-aspartic acid)-receptors were inhibited (Hammond *et al.* 2006; Kochlamazashvili *et al.* 2010). PolySia has also been reported to bind to Siglec-11 in human macrophages and microglia resulting in a reduction of inflammatory and neurotoxic responses (Wang and Neumann 2010; Shahraz *et al.* 2015; Karlstetter *et al.* 2017).
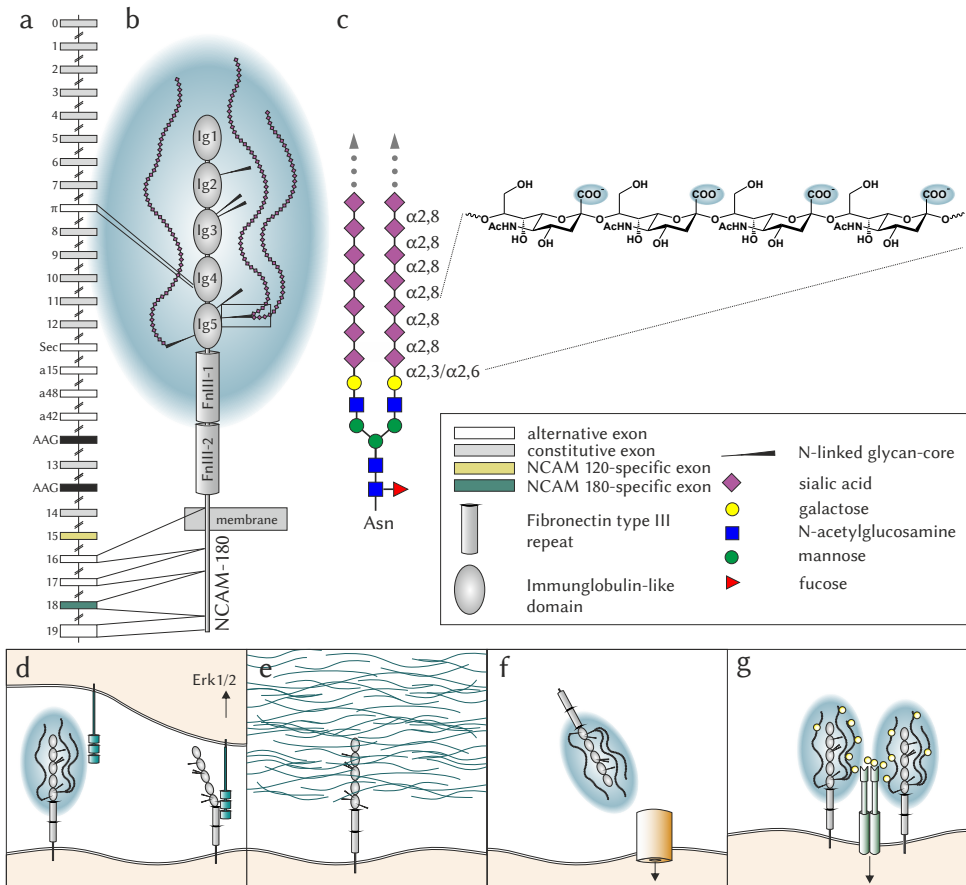
Figure 1.1: Structure and proposed function of NCAM and polySia. (a) Exon struc-
ture of the *Ncam* genetic locus, with constitutive exons depicted in gray. Variable usage of
the π-, the Sec- and α-exons (white), the AAG triplet (black), exon 15 and 18 leads to a variety
of NCAM isoforms. (b) Translation of exon 18 results in NCAM-180, which consists of a
long cytoplasmic tail, two fibronectin type III repeats (FnIII) and five immunoglobulin-like
domains (Ig). Polysialylation occurs in Ig5 on two N-glycosylation sites. (c) The core glycan
with attached polysialic acid chains and its chemical structure. (d) Due to the polyanionic
nature of polySia, it increases the intracellular space and prevents signaling of the under-
lying carrier protein, e.g. the interaction of NCAM with the FGF-receptor, resulting in
Erk1/2 signaling. (e) NCAM devoid of polySia can interact with the extracellular matrix. (f)
Soluble polySia-NCAM can directly interact with certain surface receptors (g) and polySia
has been proposed to sequester soluble molecules to facilitate binding to the respective
receptor. Figure was created based on information as reviewed in Schnaar *et al.* 2014.

1.3 Developmental regulation of polysialylation

As outlined below, comparison between enzyme-levels and substrate-amounts suggests that lower levels of polysialyltransferases would suffice for polysialylation of the entire substrate-pool. From an evolutionary perspective, the emergence of two enzymes involved in polysialylation of NCAM, that do not operate at their full capacity and are able to compensate for the loss of the other argues for a tightly regulated system demonstrating the importance of polySia in the developing brain. Thus, the correct formation of polySia on NCAM and by association, the temporally appropriate shielding of NCAM to prevent interactions, seems to be of major importance for proper brain development (Weinhold *et al.* 2005; Hildebrandt *et al.* 2009).

   In mice, expression of both polysialyltransferases starts around the time of neural tube closure and first transcripts can be detected at embryonic day (E) 8 (Ong *et al.* 1998), resulting in the first appearance of polySia around E9 (Probstmeier *et al.* 1994). Peaking around E14.5, expression levels of both transferases are upregulated, then stay fairly constant with only a slight reduction towards postnatal day (P) 1 (Schiff *et al.* 2009). While the expression of *St8sia4* declines only mildly and persists throughout adulthood (Kurosawa *et al.* 1997; Hildebrandt *et al.* 1998; Ong *et al.* 1998; Angata *et al.* 2007), *St8sia2* expression drops sharply between P5 and P11 (Oltmann-Norden *et al.* 2008). Perinatally, the entire NCAM pool is polysialylated. Subsequent to the downregulation of *St8sia2*, the percentage of polysialylated NCAM drops by 70% between P9 and P17 and further declines, coinciding with first polySia-free NCAM 140/180 (Finne *et al.* 1983; Galuska *et al.* 2006; Oltmann-Norden *et al.* 2008). In brains of 6 months old mice, only 10% of the perinatal polySia-levels can be detected (Oltmann-Norden *et al.* 2008). Of note, expression of NCAM 120, which is characteristic for mature oligodendrocytes and the myelin sheath, is strongly upregulated around P5, yet never polysialylated (Oltmann-Norden *et al.* 2008).

   PolySia is prevalent in the embryonic mouse brain. Basically all neurons are polySia-positive at some point during their development (Bonfanti 2006), but polySia can be found on other cell types as well. For instance, polySia is found on oligodendrocytes precursor cells (OPCs) (Ben-Hur *et al.* 1998; Vitry *et al.* 1999; Werneburg *et al.* 2015), on specific astrocyte populations in the hypothalamus (Theodosis *et al.* 1991; Theodosis *et al.* 1999) and on radial glia in the cortex, the mesencephalon, the cerebellum and the retina (Bartsch *et al.* 1990; Hekmat *et al.* 1990; Li *et al.* 2004; Schiff *et al.* 2009; Kustermann *et al.* 2010). *In vivo* findings of aberrantly localized pyramidal cells in the neocortex after loss of polySia led to the proposal that polySia might be involved in radial migration (Angata *et al.* 2007). In the visual cortex, loss of polySia shortly after eye opening at P14 causes maturation of inhibitory synapses, a process involved in the regulation of the critical period necessary for cortical plasticity (Di Cristo 2007). In the adult mouse

brain, polySia-expression is confined to regions of adult neurogenesis. One of these neurogenic niches is the anterior subventricular zone (SVZ), from where polySia-positive neuroblasts migrate towards the olfactory bulb (Bonfanti and Theodosis 1994; Rousselot and Nottebohm 1995; Kornack and Rakic 2001; Ponti *et al.* 2006). Another neurogenic niche is the dentate gyrus of the hippocampus with its polySia-positive postmitotic precursors of granule cells (Seki and Arai 1991, 1993; Doetsch 2003). Furthermore, polySia can be found on some mature interneurons in the neocortex, the hippocampus, the amygdala and on immature neurons in layer 2 of the paleocortex (Nacher *et al.* 2002a,b; Varea *et al.* 2005; Varea *et al.* 2007; Gilabert-Juan *et al.* 2011; for overview see Nacher *et al.* 2013). Of note, polySia on mature interneurons of the adult cortex is solely implemented by ST8SIA4 (Nacher *et al.* 2010).

1.4 PolySia-deficient mouse models

In order to analyze the role of polysialic acid in the brain, several mouse knockout lines have been generated. Despite the high developmental impact of polySia-NCAM, NCAM knockout animals ($Ncam^{-/-}$) that are almost completely devoid of polySia show relatively mild defects (Cremer *et al.* 1994). They are viable and fertile, but display defective lamination of mossy fibers and a pronounced size reduction of the olfactory bulb (Cremer *et al.* 1994; Ono *et al.* 1994; Seki and Rutishauser 1998). Further experiments in these animals revealed that loss of polySia leads to disruption of the migratory chains characteristic for olfactory bulb interneuron migration due to reduced compaction and disintegration of glial tubes that form a scaffold for migratory neuroblasts (Chazal *et al.* 2000).

A different approach to obtain polySia-negative mice was the generation of a double knockout of the two polysialyltransferases ($St8sia2^{-/-} St8sia4^{-/-}$, Weinhold *et al.* 2005). These animals show phenotypes that can be categorized into two groups. Defects that appear in both the double knockout and the NCAM knockout depend on polySia and comprise a smaller olfactory bulb and delamination of mossy fibers. Deficits on the other hand, that do not occur in $Ncam^{-/-}$ but only in polysialyltransferase-negative animals result from the untimely appearance of unpolysialylated NCAM. These phenotypes comprise precocious death, postnatal retardation, increased incidence of hydrocephalus as well as defects of major brain axon tracts, such as the anterior commissure, the corpus callosum, the internal capsule and the mammillothalamic tract (Weinhold *et al.* 2005; Hildebrandt *et al.* 2009; Schiff *et al.* 2011). Since these defects arise from a gain of NCAM-function, they are rescued by an additional knockout of NCAM ($St8sia2^{-/-} St8sia4^{-/-} Ncam^{-/-}$,

Weinhold *et al.* 2005). This is strongly supported by the observation that the severity of these phenotypes correlates not with the reduction of polySia, but directly with the amount of NCAM erroneously devoid of polySia (Hildebrandt *et al.* 2009).

To address possible differences between the two polysialyltransferases, both enzymes were knocked out individually. Analysis of *St8sia4* mRNA levels indicates that ST8SIA4 is the major polysialyltransferase in adult mice (Angata *et al.* 1997; Hildebrandt *et al.* 1998). In a first study of *St8sia4*$^{-/-}$ animals, no developmental defects were found. However, postnatal *St8sia4*$^{-/-}$ mice display a strong reduction of polySia levels in most parts of the brain and adult knockout brains were almost completely devoid of polySia (Eckhardt *et al.* 2000; Nacher *et al.* 2010). Knockout of *St8sia2* on the other hand causes developmental deficits such as mossy fiber defects (Angata *et al.* 2004). Although moderate if compared to the *St8sia2*$^{-/-}$ *St8sia4*$^{-/-}$ double knockout mice, *St8sia2*$^{-/-}$ animals display hypoplasia of the internal capsule (Hildebrandt *et al.* 2009), disorganized thalamocortical and corticofugal fibers, which are major constituents of the internal capsule, as well as a smaller thalamus (Kröcher *et al.* 2015). However, it is completely unclear, which fibers or cell types of the thalamic system need ST8SIA2 for normal development and which cellular mechanisms depend on the presence of ST8SIA2.

Apart from its implication in thalamus-cortex connectivity, polySia has been associated with the migration of olfactory interneurons in the rostral migratory stream (RMS, Röckle *et al.* 2008; Röckle and Hildebrandt 2016). As one of the neurogenic niches, the anterior SVZ of the lateral ventricle gives rise to neuroblasts that migrate tangentially along the RMS into the olfactory bulb. There, they differentiate into granule cells and periglomerular cells (Lois *et al.* 1996). Depletion of polySia on these cells results in loss of interneurons likely caused by impaired migration (Röckle and Hildebrandt 2016). Although different in detail, another prominent example of tangential migration is the migration of cortical interneurons from the subpallium into the neocortex (Marín and Rubenstein 2001).

1.5 Cortical interneurons in the developing brain

Neurons categorize into two principal groups – pyramidal neurons and interneurons. Pyramidal neurons are excitatory neurons and comprise roughly 70-80% of all neurons. They are characterized by using glutamate as a neurotransmitter and by forming long axons that are able to span different brain regions to ensure communication between remote locations. Interneurons on the other hand constitute 20-30% of cortical neurons (Ren *et al.* 1992), utilize the neurotransmitter γ-aminobutyric acid (GABA) and form short extensions. Their role is not to establish communication between remote structures but to regulate the activity of pyramidal neurons.

Unlike pyramidal neurons, cortical interneurons do not arise from the ventricular zone of the cortex but from the subpallium, from where they migrate tangentially into the developing neocortex. The major contribution to cortical interneurons comes from the ganglionic eminences that are further divided, based on the spatial localization, into the medial, lateral and caudal ganglionic eminences (MGE, LGE and CGE respectively). While most LGE-derived interneurons migrate towards the olfactory bulb via the RMS, most, if not all, cortical interneurons arise from the MGE, the CGE and the preoptic area (POA). These three structures can not only be characterized by their localization but also by a region-specific expression of transcription factors. Fate-mapping analyses of respective populations revealed a correlation between the expression of transcription factors and the specification into subpopulations. These can be characterized by the expression of certain calcium-binding proteins like parvalbumin (PV), calbindin (CB) and calretinin (CR) or a number of other markers like somatostatin (Sst), neuropeptide Y (NPY), the vasointestinal peptide (VIP), the ionotropic serotonin receptor 5HT3a (5HT3aR) or Reelin (Gelman and Marín 2010; Rudy *et al.* 2011). The homeodomain-containing transcription factor NKX2.1 is expressed in the proliferative zone of the MGE and the POA. In *Nkx2.1* knockout animals, which die at birth, the formation of the MGE fails and the amount of GABAergic cells in the neocortex is reduced by 50%, highlighting the major contribution of the MGE to the cortical interneuron population (Sussel *et al.* 1999). In particular, cortical interneurons expressing Sst or NPY are completely absent from *Nkx2.1* knockout brains at E18.5 (Anderson *et al.* 2001) and upon cultivation of dissociated cortical tissue for two to four weeks, the typically present PV-positive interneurons are absent in knockout brains, as well (Xu *et al.* 2004). While *Nkx2.1* is downregulated in cortical interneurons prior to their entry into the neocortex, expression persists to juvenile ages in striatal interneurons (Marín *et al.* 2000). A downstream-target of *Nkx2.1* is the LIM homeodomain factor *Lhx6* (Du *et al.* 2008) that is expressed in the SVZ of the MGE and is used as a marker for MGE-derived interneurons (Grigoriou *et al.* 1998). Unlike *Nkx2.1*, *Lhx6*-expression persists even after invasion of the neocortex (Lavdas *et al.* 1999; Gong *et al.* 2003). As the CGE emerges caudally from the fusion of MGE and LGE, the borders between the three regions are not always clear. For instance, the ventral CGE displays *Nkx2.1* expression and the CGE-specific transcription factor COUP-TF2 (Kanatani *et al.* 2008), was later shown to be expressed in the MGE as well (Lodato *et al.* 2011). Moreover, some MGE-derived interneurons migrate caudally and pass the CGE on their way towards the cortex (Butt *et al.* 2005; Yozu *et al.* 2005). Although the expression of transcription factors in insufficient to dissect both regions, MGE- and CGE-derived interneurons can be distinguished by their specification. While MGE-derived interneurons specify towards PV and Sst, interneurons arising from the CGE can be characterized by CR, Reelin and VIP (Gelman and Marín 2010). Interneurons derived from MGE and CGE also differ in

their laminar localization in the mature cortex. MGE-derived interneurons start to migrate towards the cortex around E11.5 (Anderson *et al.* 2001) and populate the cortical layers in an inside-out pattern with a lateral to medial gradient. While early-born interneurons preferentially settle in deep layers of lateral regions, late-born interneurons populate the more superficial layers of medial regions (Ang *et al.* 2003). PV-interneurons can be subdivided based on their morphology into basket and chandelier cells (Gelman and Marín 2010). While both subtypes can be found in upper cortical layers, PV-positive cells of the basket-type preferentially colonize deep cortical layers (Brandão and Romcy-Pereira 2015; Miyamae *et al.* 2017). CGE-derived interneurons on the other hand arise later during developing (around E15.5) and preferably populate superficial layers in an outside-in pattern (Miyoshi *et al.* 2007; Rymar and Sadikot 2007).

Since the majority of cortical interneurons arise from the MGE, numerous studies analyzed the mechanisms by which these interneurons migrate towards the cortex. Driven by chemorepellents in the MGE itself, the POA and the striatum, MGE-derived interneurons migrate towards the cortex. In the subpallium, they are influenced by motogenic cues like the hepatocyte growth factor HGF (Powell *et al.* 2001). Unlike striatal interneurons, cortical interneurons express the receptors neuropillin (Nrp) 1 and 2, which enable them to react to the chemorepellents semaphorin 3A and 3F expressed in the striatal mantle zone in order to evade the striatum (Marín and Rubenstein 2001). By expression of ErbB4 (Li *et al.* 2012), interneurons sense the chemoattractive factor neuregulin-1 (Nrg1). In the subpallium it is presented in a membrane-bound form (Nrg1-CRD), whereas in the cortex, the soluble Nrg1-Ig is predominant and forms a gradient in the cortical proliferative zone (Flames *et al.* 2004). In the cortex, interneurons migrate via two distinct migratory streams. In mice, a first cohort of cells starts migrating towards the cortex around E11.5 and mainly invades the preplate. A second, more prominent cohort arises from the MGE from E13 to E15 and migrates mainly through the cortical intermediate zone (Anderson *et al.* 2001, see Fig 1.2). Once in the cortex, interneurons respond to soluble factors, such as NT4 and BDNF, which have been proposed as motogenic factors (Polleux *et al.* 2002). Another soluble factor, CXCL12, is expressed in the meninges and the SVZ of the cortex (Stumm *et al.* 2003; Tiveron *et al.* 2006). Studies revealed a motogenic impact of CXCL12 on migrating interneurons (López-Bendito *et al.* 2008). Additionally, by suppressing branch formation, it prevents interneurons from prematurely exiting the migratory stream. During maturation interneurons supposedly loose responsiveness to CXCL12 and upon that cue, switch from tangential to radial migration and leave the migratory stream to populate the cortical layers (López-Bendito *et al.* 2008; Lysko *et al.* 2011; Abe *et al.* 2014).
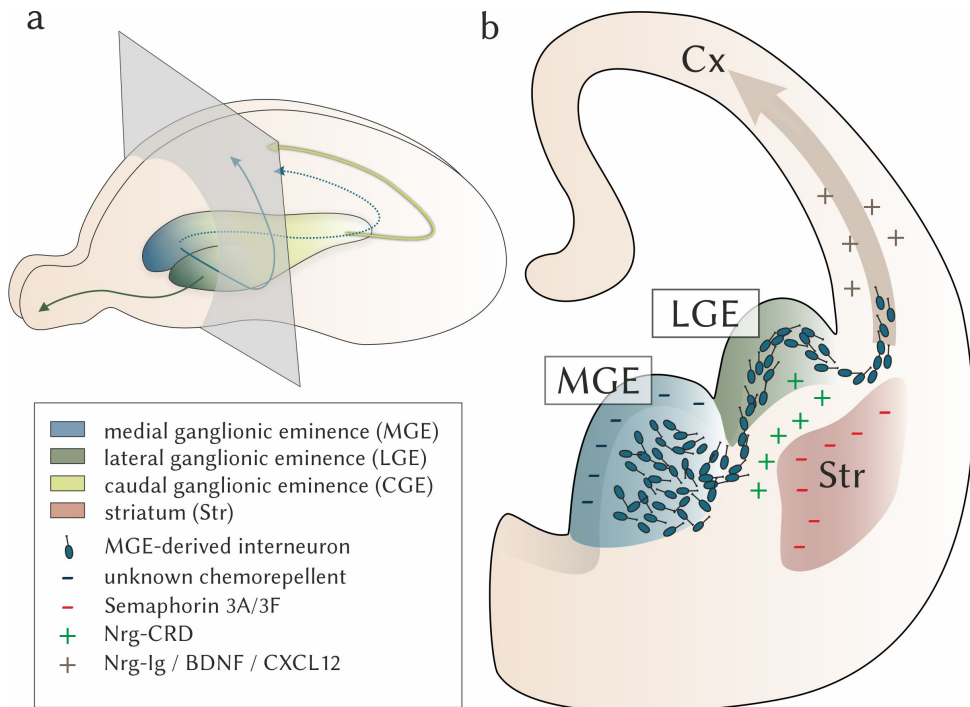
Figure 1.2: Interneuron migration from the ganglionic eminence to the cortex. (a) Schematic of an E14.5 mouse brain with the ganglionic eminences depicted in blue (MGE), green (LGE) and yellow (CGE) as well as the migratory paths of respective interneuron populations (colored arrows). (b) Schematic of a coronal section as indicated by gray box in a. The major migratory stream of MGE-derived interneurons is illustrated. Interneurons exit the MGE, pass the LGE and invade the cortex. This migration is influenced by different chemorepellents expressed in the VZ of the MGE and in the striatum as well as by chemoattractants and motogenic factors expressed in the LGE and the cortex. Figure was created based on information gathered from citations in the text.

1.6 Development of the cortex-thalamus connectivity

The thalamus, as part of the diencephalon, receives visual, auditory and somatosensoric input in specific thalamic nuclei and is responsible to relay these information to the cerebral cortex. The communication between both structures is enabled by mutual projections that are formed during development to ensure reciprocal input. In mice, first thalamocortical axons (TCAs) start to emerge from the thalamus around E13 (Molnár and Blakemore 1995). From there, they pass through the internal capsule and meet the reciprocal corticofugal fibers in the basal telencephalon around E14.5 in a process referred to as the "handshake" (Fig 1.3a, Blakemore and Molnar 1990). Several factors impact the pathfinding of corticofugal and thalamo-

cortical fibers. For instance, the chemorepulsive factors Slit1 and Slit 2, expressed in the hypothalamus, prevent Robo-positive thalamic axons from approaching the hypothalamus and instead cause them to turn sharply into the internal capsule (Braisted *et al.* 2009). After passing the internal capsule, repulsive activities in the globus pallidus as well as in the MGE prevent fibers to innervate these structures. Located in between both structures are *Islet1*-positive cells that express the chemoattractive Nrg1-CRD and form a permissive corridor. These cells originate in the LGE and migrate tangentially towards the MGE (Molnár and Blakemore 1995; López-Bendito *et al.* 2006).

In adult mice, thalamocortical and corticofugal fibers form a major part of the internal capsule. The reticular thalamic nucleus (Rt) forms a sheet of GABAergic neurons at the interface between internal capsule and thalamus (Guillery *et al.* 1998; Pinault 2004). Thus, virtually all thalamocortical and corticofugal fibers traverse the Rt (see Fig 1.3b) and provide major excitatory input via collaterals (Harris 1987). Unlike other thalamic nuclei, Rt neurons do not project to the cortex. Instead, its axons terminate locally and project to basically all thalamic nuclei (Pinault 2004). The Rt has been proposed to be involved in the control of internal attention and thalamocortical circuits (Crick 1984; Pinault 2004; Zikopoulos and Barbas 2012; Young and Wimmer 2017). Originating in the ventral thalamus (Angevine 1970), Rt precursor cells start to migrate dorsally around E10-11 to envelop the dorsal thalamus (Guillery *et al.* 1998; Pinault 2004). Early during development, they express *Islet1*, which can be utilized as a marker for the Rt. Starting around P10, all Rt-neurons begin to express PV (Schiff *et al.* 2011).

As described above, the loss of both polysialyltransferases and to a lesser extent the loss of ST8SIA2 led to a hypoplasia of the internal capsule (Hildebrandt *et al.* 2009). Therefore, it was hypothesized that this might be due to impaired pathfinding of thalamocortical and corticofugal axons. Indeed, during embryonic development, thalamocortical fibers in *St8sia2$^{-/-}$ St8sia4$^{-/-}$* mice fail to turn dorsally into the permissive corridor of *Islet1* cells and display a loss of corticofugal fibers (Schiff *et al.* 2011). Moreover, thalamocortical and corticofugal fibers traversing the Rt are highly disorganized, leading to a postnatal degeneration of the Rt (Schiff *et al.* 2011). *St8sia2*-knockout mice also show less organization of fibers traversing the Rt (Kröcher *et al.* 2015). Since ST8SIA2 seems necessary for proper development of the Rt and knockout mice display a phenotype reminiscent to schizophrenia (Kröcher *et al.* 2015), it would be interesting to understand which fibers or cells are dependent on ST8SIA2 for the development of functional thalamus-cortex connectivity.

Figure 1.3: Reciprocal input from thalamus and cortex. (a) Thalamocortical grow out of the dorsal thalamus (DT) and traverse the internal capsule (IC), guided by *Islet1* expressing guidepost cells dorsal to the globus pallidus (GP) and meet corticofugal axons leaving the cortex (Cx) dorsal to the striatum (Str) in a process called "handshake" at E14.5. (b) In adult mice, all thalamocortical and corticofugal projections pass the reticular thalamic nucleus (Rt) and give off collaterals. Rt neurons project to the Rt itself and to thalamic nuclei. Figure was created based on information gathered from publications cited in the text.

1.7 Implications of polySia in schizophrenia and other psychiatric disorders

Deficits in the thalamic system of *St8sia2*$^{-/-}$ animals have been linked to behavioral abnormalities, which are reminiscent to features of schizophrenia (Kröcher *et al.* 2015). Schizophrenia (SZ) is a mental disorder that affects roughly 1% of the population. Symptoms comprise positive symptoms, such as delusions and hallucinations, negative symptoms including social withdrawal and apathy as well as cognitive deficits like deficits in attention, executive functioning and working memory. Despite extensive research efforts, the causes of schizophrenia are still largely unknown. In addition to genetic factors (Ehrenreich and Nave 2014; for review, see Blokland *et al.* 2016), several lines of evidence point towards a strong neurodevelopmental component (Lewis and Levitt 2002; Rapoport *et al.* 2012) and both interact with environmental factors, acting as "second hits" to finally cause the outbreak of the disease in individuals with unfavorable predisposition (Brown 2011; Stepniak *et al.* 2014).

Post mortem studies of schizophrenic patients indicate alterations of NCAM or polySia. For instance, elevated levels of soluble NCAM were detected in the prefrontal cortex, the hippocampus and the cerebrospinal fluid (Poltorak *et al.* 1995; Kammen *et al.* 1998; Vawter *et al.* 2000, 2001). Moreover, in the hilus region of the hippocampus and in layers 4 and 5 of the dorsolateral prefrontal cortex, reduced polySia levels have been reported (Barbeau *et al.* 1995; Gilabert-Juan *et al.* 2012). A recent study reports elevated serum levels of polySia-NCAM in schizophrenia, which might reflect enhanced proteolytic cleavage or clearance of polySia-NCAM from the schizophrenic brain (Piras *et al.* 2015). Notably, the increased polySia-NCAM serum levels correlate with negative and cognitive symptoms, and with decreased volume of Brodmann area 46 in the left prefrontal cortex of schizophrenic patients, an area that plays an important role in working memory and whose early alteration is one of the most replicated findings in SZ (Piras *et al.* 2015). Furthermore, a number of genetic studies demonstrate associations of single nucleotide polymorphisms in the *NCAM1* and the *ST8SIA2* genetic locus with SZ and bipolar disorder (Arai *et al.* 2006; Sullivan *et al.* 2006; Atz *et al.* 2007; Tao *et al.* 2007; McAuley *et al.* 2012; Gilabert-Juan *et al.* 2013; Yang *et al.* 2015), and genome wide association studies (GWAS) revealed correlations between *ST8SIA2* variants and autism as well as bipolar disorder (Anney *et al.* 2010; McAuley *et al.* 2012). Altogether, the available data strongly point towards a role for *NCAM*, polySia and *ST8SIA2* in these psychiatric disorders.

Not only ST8SIA2 has been linked to psychiatric disorders but especially in schizophrenic patients, a variety of alterations were reported, that are also found in *St8sia2*-deficient mice. For instance, analysis of schizophrenic patients revealed alterations of major brain axon tracts, such as the corpus callosum and the internal capsule (Woodruff *et al.* 1995; Wobrock *et al.* 2008; Rosenberger *et al.* 2012; Ellison-Wright *et al.* 2014; Gu *et al.* 2016). Moreover, dysfunction of the Rt has been associated with hallucinations and schizophrenia (Sharp *et al.* 2001; Krause *et al.* 2003; Behrendt 2006; Zikopoulos and Barbas 2006). Analysis of the mammillary bodies of schizophrenic patients revealed a reduction of parvalbumin-positive neurons but no hypoplasia of the mammillary bodies (Bernstein *et al.* 2007). Given that polySia and particularly ST8SIA2 are essential for interneuron migration to the olfactory bulb (Chazal *et al.* 2000; Hu 2000; Röckle and Hildebrandt 2016) and hypoplasia of the olfactory bulb as well as olfactory deficits have been implicated in SZ (Turetsky *et al.* 2000, 2009; Moberg *et al.* 2013), polySia might also be involved in the establishment of the cortical interneuron system. Indeed, a frequent observation not only in schizophrenia, but also in autism and bipolar disorder is the reduction of interneuron populations in the prefrontal cortex (Benes and Berretta 2001; Todtenkopf *et al.* 2005; Sakai *et al.* 2008; Lewis *et al.* 2012; Hashemi *et al.* 2016).

1.8 Conditional approach and objectives

In order to further analyze the role of ST8SIA2 and its implications in schizophrenia, we seek to investigate in which brain region or cell types the expression of ST8SIA2 is necessary to prevent the observed phenotypes in the thalamic system. Moreover, since ST8SIA2 impacts interneuron migration from the LGE to the olfactory bulb and loss of cortical interneurons is a common phenotype in neurodevelopmental disorders, we aim to analyze the impact of polySia on cortical interneuron populations. To remove ST8SIA2 in specific brain regions and cell-types, a conditional *St8sia2* mouse line was generated. *Loxp*-sequences were inserted flanking exon 4, which is essential for sialyltransferase-activity (Datta and Paulson 1995). By cross-breeding with *Lhx6-Cre* mice (Fragkouli *et al.* 2009), *St8sia2* is specifically deleted in MGE-derived interneurons. Cross-breeding with *Foxb1-Cre* mice (Zhao *et al.* 2007) results in a diencephalon-wide depletion of ST8SIA2. To delete *St8sia2* in the cortical environment, mice were cross-bred with *Emx1-Cre* mice (Gorski *et al.* 2002) and crossbreeding with *Zp3-Cre* (Lewandoski *et al.* 1997), which is already activated in the oocyte, led to generation of ST8SIA2-negative mice.

The first part of this thesis addresses the impact of ST8SIA2 and ST8SIA4 on the establishment of cortical interneuron populations in adult mice. Based on observed alterations in interneuron densities, the developmental impact of polySia on cortical interneuron migration was analyzed.

As demonstrated in the first part of this thesis, ST8SIA2 strongly impacts the development of cortical interneurons. The second study therefore assesses whether ST8SIA2 has a cell-autonomous or non-cell-autonomous impact on interneuron development. Cell-autonomy was addressed by analysis of interneuron populations in mice with a deletion of *St8sia2* specifically in MGE-derived interneurons (*Lhx6-Cre;St8sia2$^{f/f}$*) or in the cortex (*Emx1-Cre;St8sia2$^{f/f}$*) and utilization of a co-culture assay. Live imaging experiments involving BDNF-treatment were used to evaluate the BDNF-response of *St8sia2*-deficient interneurons.

As previously presented, ST8SIA2 is implicated in long-range connectivity of the thalamus and the mammillary body. In the third manuscript, *Foxb1-Cre;St8sia2$^{f/f}$* and *Emx1-Cre;St8sia2$^{f/f}$* mice were used to assess whether ST8SIA2-produced polySia on thalamocortical or corticofugal fibers is essential for axonal pathfinding. By morphological analyses, the impact of ST8SIA2 on long-range connectivity of the mammillothalamic tract was assessed.

A crucial role for polysialic acid in developmental interneuron migration and the establishment of interneuron densities in the mouse prefrontal cortex

Tim Kröcher[1,2,*], Iris Röckle[1,*], Ute Diederichs[1], Birgit Weinhold[1], Hannelore Burkhardt[1], Yuchio Yanagawa[3], Rita Gerardy-Schahn[1,2], Herbert Hildebrandt[1,2,#]

[1] *Institute of Cellular Chemistry, Hannover Medical School, Carl-Neuberg-Str. 1, 30625 Hannover, Germany*
[2] *Center for Systems Neuroscience Hannover (ZSN), Hannover, Germany*
[3] *Department of Genetic and Behavioral Neuroscience, Gunma University Graduate School of Medicine and CREST, 3-39-22 Showamachi, Maebashi 371-8511, Japan*
[*] *These authors contributed equally to this work*
[#] *Corresponding author: Herbert Hildebrandt*

Institute of Cellular Chemistry (4330), Hannover Medical School,
Carl-Neuberg-Str. 1, 30625 Hannover, Germany
Phone: +49 511 532 9808, Fax: +49 511 532 8801
e-mail: hildebrandt.herbert@mh-hannover.de

This article has originally been published in the journal Development

---

About the manuscript
My contributions to this paper comprised organization of mouse breeding as well as dissection, sectioning, immunofluorescent staining, microscopy and respective evaluations of embryonic mice for the analysis of apoptosis and interneuron distribution in the ganglionic eminence. Moreover, I contributed to live imaging of slice and primary cultures.

17

A crucial role for polysialic acid in developmental interneuron migration and the establishment of interneuron densities in the mouse prefrontal cortex

2.1 Abstract

Polysialic acid (polySia) is a unique glycan modification of the neural cell adhesion molecule NCAM and a major determinant of brain development. Polysialylation of NCAM is implemented by the two polysialyltransferases (polySTs) ST8SIA2 and ST8SIA4. Dysregulation of the polySia-NCAM system and variation in *ST8SIA2* has been linked to schizophrenia and other psychiatric disorders. Here, we show reduced interneuron densities in the medial prefrontal cortex (mPFC) of mice with either a partial or a complete loss of polySia synthesizing capacity by ablation of *St8sia2*, *St8sia4*, or both polySTs. Parvalbumin- and perineuronal net-positive cells as well as somatostatin-positive cells were reduced in the mPFC of all polyST-deficient lines, while calretinin-positive and the parvalbumin-negative fraction of calbindin-positive cells were unaffected. Lower interneuron numbers were corroborated by analyzing polyST-deficient GAD67-GFP knock-in mice. Searching for mechanisms that may cause these alterations, accumulation of precursors in the ganglionic eminences and reduced numbers of tangentially migrating interneurons in the pallium were observed in polyST-deficient embryos. Removal of polySia by endosialidase treatment of organotypic slice cultures led to decreased entry of GAD67-GFP-positive interneurons from the ganglionic eminences into the pallium. Moreover, the acute loss of polySia caused significant reductions of interneuron velocity and leading process length. Thus, attenuation of polySia interferes with

the developmental migration of cortical interneurons and causes pathological changes of specific interneuron subtypes. This provides a possible link between genetic variation in polyST genes, neurodevelopmental alterations and interneuron dysfunction in neuropsychiatric disease.

2.2 Introduction

The sugar polymer polysialic acid (polySia[1]) is a major regulator of cellular plasticity in brain development (Rutishauser 2008; Schnaar *et al.* 2014). PolySia modulates cell interactions by multiple mechanisms including the attenuation of homo- and heterophilic cell-cell and cell-matrix adhesion, adjustment of receptor functions and, possibly, membrane dynamics. Two independently regulated polysialyltransferases (polySTs), ST8SIA2 and ST8SIA4, are able to produce polySia and, as shown in the developing mouse brain, the vast majority of polySia is attached to the neural cell adhesion molecule NCAM (Mühlenhoff *et al.* 2013). In humans, several studies suggest a link between dysregulation of the polySia-NCAM system and variation in *ST8SIA2* with schizophrenia and other psychiatric disorders (Anney *et al.* 2010; Brennaman and Maness 2010; McAuley *et al.* 2012; Gilabert-Juan *et al.* 2012). In rodents, expression of the two polySTs shows considerable overlap, but ST8SIA2 is predominantly involved in polySia biosynthesis during brain development, whereas ST8SIA4 seems to be the major polyST of the adult brain (Hildebrandt *et al.* 2010). Accordingly, ST8SIA2-deficient mice were originally described to have neurodevelopmental defects manifesting in the aberrant topology of hippocampal mossy fiber projections, which may be linked to altered fear behavior (Angata *et al.* 2004). In contrast, and consistent with the prevalent expression of *St8sia4* in the adult, the lack of ST8SIA4 gives rise to mice with no detectable morphological defects but impaired synaptic plasticity in the CA1 subregion of the hippocampus (Eckhardt *et al.* 2000). Simultaneous ablation of *St8sia2* and *St8sia4* ($2^{-/-}4^{-/-}$) yielded entirely polySia-negative mice. These animals show a number of additional, severe defects, like postnatal growth retardation and precocious death, a high incidence of hydrocephalus as well as malformation of major brain axon tracts (Weinhold *et al.* 2005; Hildebrandt *et al.* 2009). In addition, $2^{-/-}4^{-/-}$ mice show a size reduction of the olfactory bulb caused by a migration deficit of subventricular zone-derived interneurons (Weinhold *et al.* 2005) and altered migration of neural precursors during cortical development of $2^{-/-}4^{-/-}$ mice has been suggested (Angata *et al.* 2007).

---

[1] the most commonly used abbreviation for polysialic acid in neuroscience is PSA but in tumor biology, PSA stands for prostate specific antigen. To avoid confusion, we therefore prefer to use polySia to abbreviate polysialic acid.

Immunohistochemical detection of the calcium-binding proteins parvalbumin (PV), calbindin (CB) and calretinin (CR) as well as the neuropeptide somatostatin (Sst) has proven a powerful tool for the identification and evaluation of GABAergic interneuron subtypes (Gabbott *et al.* 1997; Gonchar and Burkhalter 1997; Kawaguchi and Kubota 1997; Gelman and Marín 2010; Anastasiades and Butt 2011). Reminiscent to clinical studies reporting interneuron alterations in the prefrontal cortex (PFC) of schizophrenic patients (Lewis *et al.* 2012; Marín 2012), loss-of-function mouse models of major schizophrenia risk genes, like *NRG1* and *DISC1*, display defects of cortical interneuron development or altered interneuron numbers in the medial prefrontal cortex (mPFC) (Flames *et al.* 2004; Hikida *et al.* 2007; Shen *et al.* 2008; Steinecke *et al.* 2012). Motivated by these findings, and based on the well-known role of polySia in the migration of olfactory bulb interneurons (Ono *et al.* 1994; Chazal *et al.* 2000; Weinhold *et al.* 2005) we asked, if cortical interneurons, particularly those of the mPFC, would be affected by polySia-deficiency. The results indicate that even a moderate interference with NCAM-based polySia during brain development leads to reduced densities of PV- and Sst-positive interneuron populations. Aberrant allocation of migratory interneurons between the medial and lateral ganglionic eminences (MGE, LGE) and the pallium in $2^{-/-}$ and $4^{-/-}$ embryos as well as slower migration of GAD67-GFP labeled interneurons after acute enzymatic removal of polySia in slice cultures suggest that disturbed tangential migration accounts at least in part for the observed interneuron phenotype in the mPFC of polyST-deficient mice.

2.3 Results

Altered densities of PV-immunoreactive cells in the mPFC of polysialyltransferase-decient mice

Due to the high mortality of $2^{-/-}4^{-/-}$ mice after 4 weeks of age (Weinhold *et al.* 2005), all comparative analyses involving mice of this genotype were restricted to young, one-month-old animals. For analyses of $2^{-/-}4^{-/-}$ mice, which have a high incidence of hydrocephalus (Weinhold *et al.* 2005), only specimen with moderate ventricular dilatation and no cortical thinning were used. Compared to the control group, the densities of PV-positive cells (PV$^+$) in the upper and deep layers of the mPFC were significantly lower in both polyST single knockout lines ($2^{-/-}$ and $4^{-/-}$) as well as in the double knockout ($2^{-/-}4^{-/-}$) (Fig. 2.1). The most prominent effects were observed in the upper and deep layers of cingulate cortex area 1 (Cg1) harboring the highest densities of PV$^+$ cells in the wildtype (supplementary material Fig. S1A,B). Significant reductions or at least a trend were detected in the upper and deep layers of the infralimbic as well as in the deep layers of the prelimbic
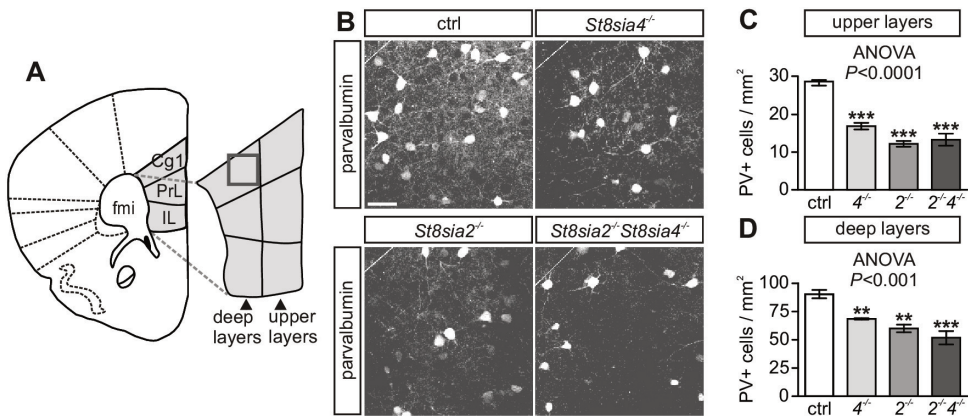
Figure 2.1: Parvalbumin (PV) immunoreactivity in the medial prefrontal cortex (mPFC) at P30. (A) Schematic illustration of the mPFC, consisting of cingulate cortex, area 1 (Cg1), prelimbic cortex (PrL) and infralimbic cortex (IL), and of the division into upper and deep layers (modified from Paxinos and Franklin, 2001; see Materials and Methods for details). The position of micrographs in (B) is marked (square). fmi, forceps minor of the corpus callosum. (B) PV-positive cells in the Cg1 of different genotypes. Scale bar: 50 μm. (C,D) Densities of PV-positive cells (PV^+) in the upper layers (C, cortical layers 1-3) and deep layers (D, cortical layers 5-6) of the mPFC of *St8sia4*$^{-/-}$ ($4^{-/-}$), *St8sia2*$^{-/-}$ ($2^{-/-}$) and $2^{-/-}4^{-/-}$ mice compared to a control group (ctrl) consisting of one $2^{+/-}4^{+/-}$ and two $2^{+/+}4^{+/+}$ mice. Per group, mean values ± s.e.m. from *n* = **3** animals are plotted. Results from one-way ANOVA and Newman-Keuls post hoc test are indicated. *** P < **0.001**, ** P < **0.01**.

cortex (IL, PrL; supplementary material Fig. S1A,B). Evaluation of PV and CB double immunofluorescence revealed reduced densities of PV^+CB^- cells in the mPFC of all polyST-deficient lines (supplementary material Fig. S1C,D) and of PV^+CB^+ cells in the upper but not in the deep layers (supplementary material Fig. S2A,B). Densities of PV^-CB^+ (supplementary material Fig. S2C,D) and CR^+ cells were not affected (mean densities of CR^+ cells per mm^2 mPFC ± s.e.m.: 59.1 ± 2.5, 49.36 ± 4.4, 43.52 ± 5.6, and 51.9 ± 1.8 for control, $4^{-/-}$, $2^{-/-}$, and $2^{-/-}4^{-/-}$ mice, n=3, each; one-way ANOVA, P > 0.1).

Expression of PV starts around P7 and throughout the next weeks these neurons slowly mature (Powell *et al.* 2012). Therefore, a developmental delay may cause reductions of PV^+ cells in 4-week-old mice. However, in older, 3-month-old $4^{-/-}$ and $2^{-/-}$ mice PV^+ cells were still significantly reduced in upper and deep layers of the mPFC (Fig. 2.2), as well as in all subdivisions, except for the IL (supplementary material Fig. S3A,B). This excludes a developmental delay or transient reduction but leaves the possibility of a permanent downregulation of PV expression, or either loss or agenesis of the respective interneuron populations during development. To assess if the observed effects were confined to the expression of PV as a marker we

analyzed the abundance of perineuronal nets (PNNs). PNNs are formed around mature basket cells and can be labeled with Wisteria floribunda agglutinin (WFA) (Härtig *et al.* 1992). In the mPFC of 3-month-old mice, WFA marked a subpopulation of PV$^+$ interneurons (Fig. 2.2C). In upper and deep layers, densities of PV$^+$ cells with PNNs were significantly reduced in $4^{-/-}$ and $2^{-/-}$ mice (Fig. 2.2D,E) and, except for the deep layers of IL, all subdivisions were affected (supplementary material Fig. S3C,D). In contrast, numbers of PV-negative cells with PNNs (PV$^-$PNN$^+$) were unaffected (mean densities of PV$^-$PNN$^+$ cells per mm^2 mPFC ± s.e.m.: 16.4 ± 1.6, 20.7 ± 0.3, and 20.6 ± 4.3 for control, $4^{-/-}$, and $2^{-/-}$ mice, n = 3, each; one-way ANOVA P > 0.1). These results argue against a specific loss of PV expression in polyST-deficient mice. Moreover, significantly reduced densities of somatostatin-positive interneurons (Sst$^+$) were found in the upper layers of the mPFC of 3-month-old $4^{-/-}$ and $2^{-/-}$ mice and in all of its subdivisions (Fig. 2.2F and supplementary material Fig. S3E), while a trend towards lower numbers of Sst$^+$ cells was observed for the deep layers, significantly affecting PrL and IL (Fig. 2.2G and supplementary material Fig. S3F).

Interneuron deficits of polysialyltransferase-deficient mice establish during development

GAD67-GFP knock-in mice were used to address the entire population of GABAergic interneurons (Tamamaki *et al.* 2003). Together with reductions of PV$^+$ cells, lower densities of GFP$^+$ interneurons were detected in the Cg1 of 3-month-old $4^{-/-}$- and $2^{-/-}$-GAD67-GFP mice (Fig. 2.3A-C). Densities of GFP$^+$ interneurons in the mPFC of both polyST-deficient lines were already reduced at postnatal day 1 (P1), but not at embryonic day 16.5 (E16.5) (Fig. 2.3D,E). Analyses of TUNEL stain at P1 or E16.5 yielded no signs of increased apoptotic cell death in the mPFC (Fig. 2.3F,G). Together these data suggest that the interneuron deficit of polyST-deficient mice develops between E16.5 and P1 but is not caused by lower survival rates in the mPFC.

Less migratory interneurons in the pallium of polysialyltransferase-deficient embryos

The large majority of the Sst$^+$ and PV$^+$ interneurons originates in the medial ganglionic eminence (MGE) (Gelman and Marín 2010). Thus, compromised migration from the MGE into the developing neocortex may account for the observed deficits in polyST-deficient mice. In the mouse, interneuron migration from the MGE starts at E12.5 and migrating precursors transiently express CB while entering the dorsal telencephalon and during their tangential migration through the marginal and intermediate zone (Anderson *et al.* 1997; Polleux *et al.* 2002). CB-immunoreactive
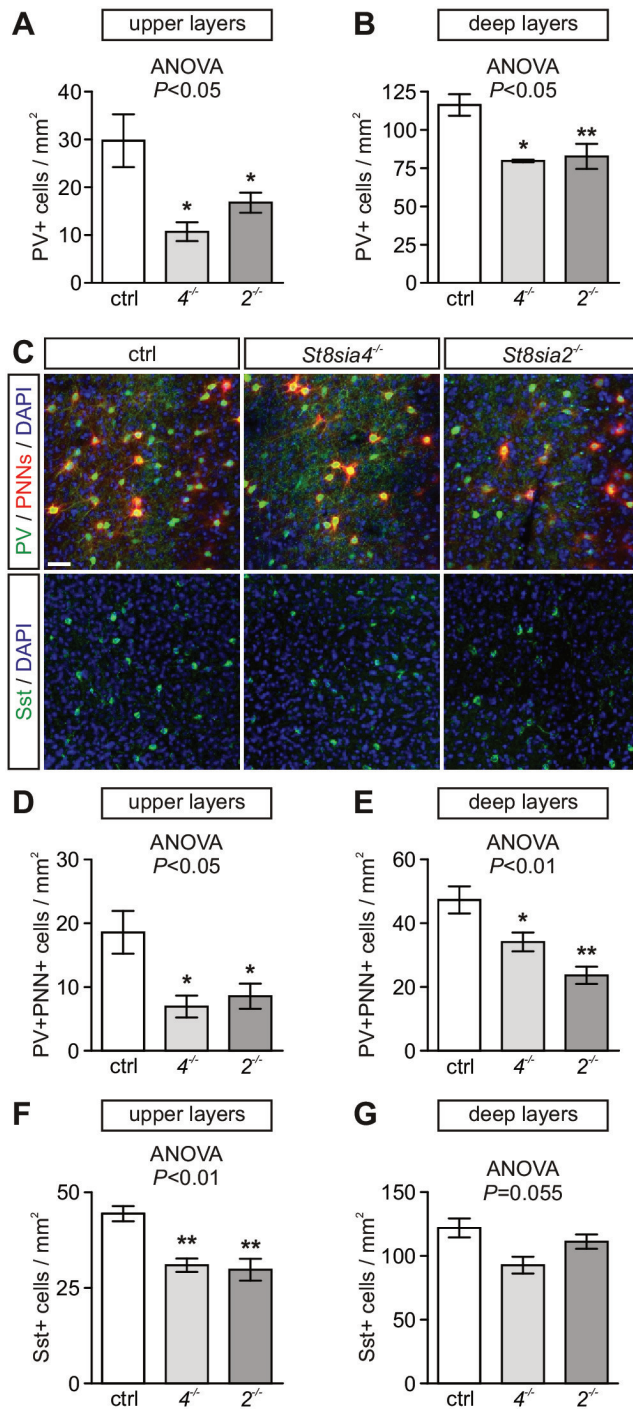
Figure 2.2: Caption on next page.

Figure 2.2: From previous page. Parvalbumin (PV)-, perineuronal net (PNN)-, and somato-statin (Sst)-positive cells in the medial prefrontal cortex (mPFC) of 3-month-old $St8sia4^{-/-}$ ($4^{-/-}$), $St8sia2^{-/-}$ ($2^{-/-}$) and wildtype control mice (ctrl, $2^{+/+}$ and $4^{+/+}$). (A,B) Densities of PV-positive (PV^+) interneurons in the upper and deep layers of the mPFC. (C) PV (green) and PNN (red) double-positive cells (upper panel) and Sst-positive cells (lower panel) of the mPFC. Nuclei: DAPI (blue). Scale bar: 50 μm (D,E) Densities of PV^+PNN^+ interneurons in the upper and deep layers of the mPFC. (F,G) Densities of Sst^+ interneurons in the upper and deep layers of the mPFC. Per group, mean values ± s.e.m. from $n = 3$ animals are plotted. Results from one-way ANOVA and Newman-Keuls post hoc test are indicated. ** $P < 0.01$, * $P < 0.05$, n.s., not significant ($P > 0.05$).

cells with typical morphologies of migrating interneurons were detected in sec-tions of control, $4^{-/-}$, and $2^{-/-}$ brains at E13.5 (Fig. 2.4A). Double labeling with polySia-specific antibody revealed that polySia is present on the migratory neurons as well as on structures in close contact (Fig. 2.4B). Densitometric analysis in the area of the intermediate zone indicated a clear reduction of polySia signal intensity in $4^{-/-}$ and, slightly more prominent, in $2^{-/-}$ embryos (Fig. 2.4C).

Concomitantly, migratory streams formed by CB-positive cells in the intermedi-ate zone were significantly shorter in $4^{-/-}$ and $2^{-/-}$ mice as compared to controls and numbers of CB-positive cells were reduced in the pallium at E13.5 (Fig. 2.4D,E). As a distinct population of interneurons, we sought to analyze tangentially mi-grating CR-positive precursors in the pallium, which are born between E14.5 and E16.5 and derive mainly from the caudal ganglionic eminence (CGE) (Xu *et al.* 2004). Thus, E16.5 was chosen for analysis and because counting was hampered by the abundance of CR-positive fibers entering the cortex at this stage (Fonseca *et al.* 1995), GAD67-GFP embryos were used to reliably identify interneurons. As shown in Fig. 2.4E (lower right) numbers of CR and GFP double-positive cells were unaffected in the pallium of $4^{-/-}$ and $2^{-/-}$ embryos.

CB-positive cells accumulate in the dorsal MGE and LGE of polysialyltransferase-deficient embryos

Interneurons born in the MGE migrate towards the LGE, which they pass to reach the cortex. In the subventricular zone of the MGE and the LGE of E13.5 $4^{-/-}$ and $2^{-/-}$ embryos, polySia immunoreactivity was reduced, and CB-positive cells accumulated mainly in the dorsal MGE (Fig. 2.5A-C). Accordingly, CB immunoreactivity was significantly increased in the MGE of both knockout lines (Fig. 2.5B) and a slight increase was also observed in the LGE (Fig. 2.5C). In addition, the numbers of TUNEL-positive apoptotic cells were increased in the MGE of $4^{-/-}$ and $2^{-/-}$ embryos at E13.5 (Fig. 2.5D,E). However, the TUNEL-positive cells were not perceivably enriched in the dorsal MGE, where the accumulation of CB-positive cells was
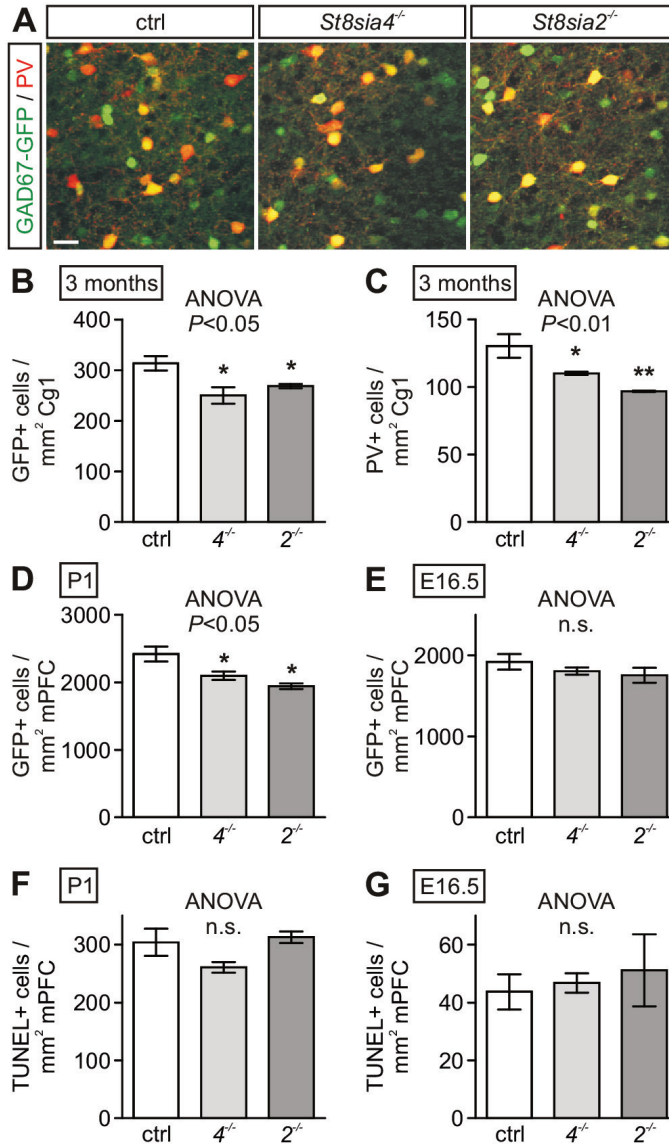
Figure 2.3: Reduced interneuron densities, but no increase in cell death in the medial prefrontal cortex (mPFC) of *St8sia4*$^{-/-}$ (*4*$^{-/-}$) and *St8sia2*$^{-/-}$ (*2*$^{-/-}$) mice compared to wildtype GAD67-GFPmice (ctrl). (A) GFP positive cells (green) and colocalization of GFP and PV (red) in the cingulate cortex area 1 (Cg1) of the mPFC of 3-month-old mice. Scale bar: 25 μm. (B-E) Densities of GFP-positive (GFP$^+$) and PV$^+$ cells in Cg1 (B,C) or mPFC (D,E) at the indicated age. (F,G) Densities of apoptotic cells (TUNEL$^+$) in the mPFC. Per group, mean values ± s.e.m. from *n* = 3 animals are plotted. Results from one-way ANOVA and Newman-Keuls post hoc test are indicated. ** P < **0.01**, * P < **0.05**, n.s., not significant (P > **0.05**).
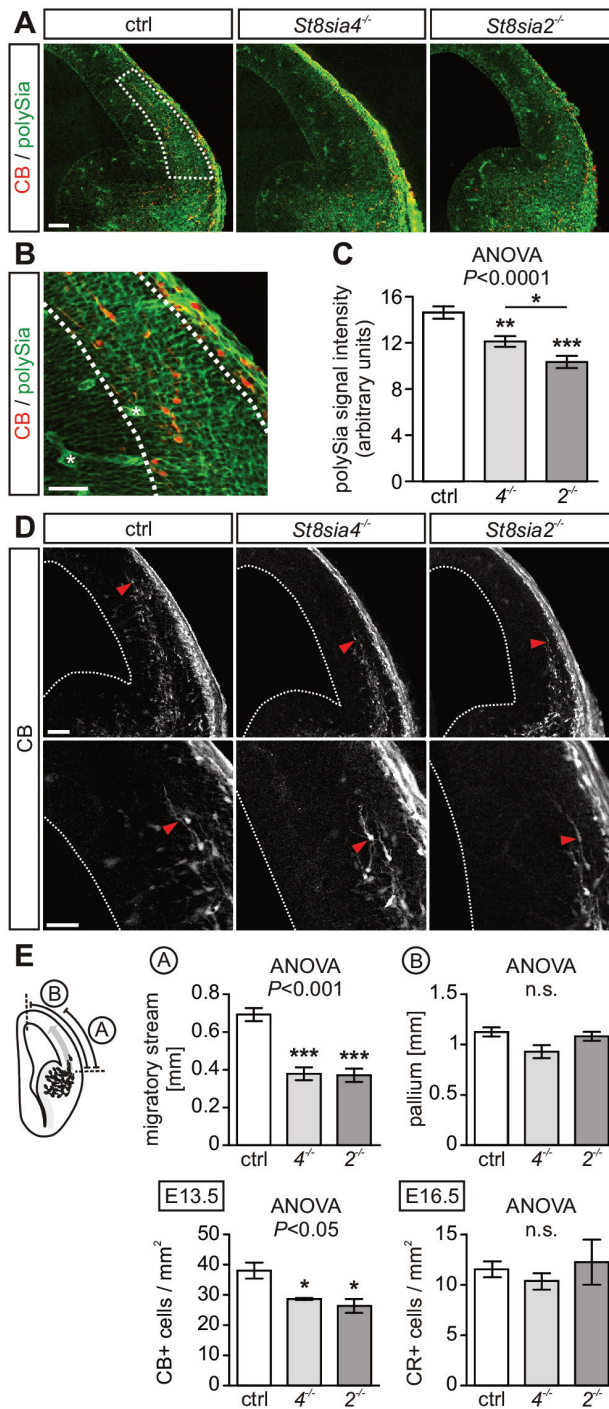
Figure 2.4: Caption on next page.

Figure 2.4: From previous page. Quantification of polySia and assessment of tangential interneuron migration in the pallium of E13.5 *St8sia4*$^{-/-}$ (*4*$^{-/-}$) and *St8sia2*$^{-/-}$ (*2*$^{-/-}$) embryos compared to littermate controls (ctrl, *2*$^{+/-}$ and *4*$^{+/-}$). (A) Immunostaining of polySia (green) and calbindin (CB, red), labeling migrating interneurons. The area of the migratory stream as evaluated in (C) is delineated (ctrl, dashed line). (B) Detail from (A), ctrl, illustrating partial colocalization of polySia and CB. Asterisks mark examples of strongly labeled blood vessels, which were excluded from evaluation in (C). (C) Quantification of polySia signal intensity in the area of tangential interneuron migration. Mean values from *n = 7 − 8* sections per group (1 animal per group). The experiment was repeated with comparative results (not shown). (D) Streams of CB-positive migrating interneurons. Cells at the end of each migratory stream (arrowheads) are shown at higher magnification. The lateral ventricle is delineated. (E) Lengths of the migratory streams and extent of the neocortex as depicted in the scheme, and numbers of CB- and CR-positive cells in the pallium at E13.5 and E16.5 respectively (cell counts per mm of neocortex). GAD67-GFP embryos were used to identify CR-positive interneurons (see text for details). Mean values ± s.e.m. from *n = 6* (E13.5 ctrl) or *n = 3* embryos (all other groups). In (C) and (E), results from one-way ANOVA with Newman-Keuls post hoc test are indicated. *** P < **0.001**, ** P < **0.01**, * P < **0.05**. n.s., not significant (P > **0.05**). Scale bars: 100 μm (A and D, upper panels), 50 μm (B and D, lower panels).

detected. Apoptosis was not significantly altered in LGE, CGE and in the pallium of E13.5 embryos (mean densities of TUNEL-positive cells per mm^2 ± s.e.m.: 44.1 ± 3.7, 61.4 ± 11.6, 59.8 ± 8.8 for LGE, 69.9 ± 6.1, 82.6 ± 3.6, 84.6 ± 5.3 for CGE, and 70.9 ± 8.3, 77.1 ± 4.7, 73.1 ± 3.7 for the pallium of control, *4*$^{-/-}$, and *2*$^{-/-}$ mice, n= 6, 4, 6 and one-way ANOVA P > 0.1, each).

To assess overall changes of MGE interneurons, protein levels of GAD65/67, CB and LHX6, a characteristic marker of MGE-derived interneuron populations (Lavdas *et al.* 1999; Liodis *et al.* 2007), were analyzed in E13.5 forebrain lysates by Western blot. No changes in any of these proteins could be detected (supplementary material, Fig. S4). These findings argue against drastic changes of MGE-derived interneuron numbers and are consistent with the immunohistological results demonstrating an accumulation of migratory interneurons in the ganglionic eminences and a corresponding reduction in the pallium of polyST-deficient mice.

Acute loss of polySia leads to reduced velocities of migrating interneurons in slice cultures

Interneuron migration was further studied in coronal slice cultures obtained from E12.5 or E13.5 GAD67-GFP embryos treated with endosialidase (endo) to remove polySia (supplementary material Fig. S5). Western blot analysis of E13.5 forebrain lysates (supplementary material Fig. S6) substantiates that polySia at this developmental stage is attached to NCAM. PolySia appeared as a broad band above 200 kDa
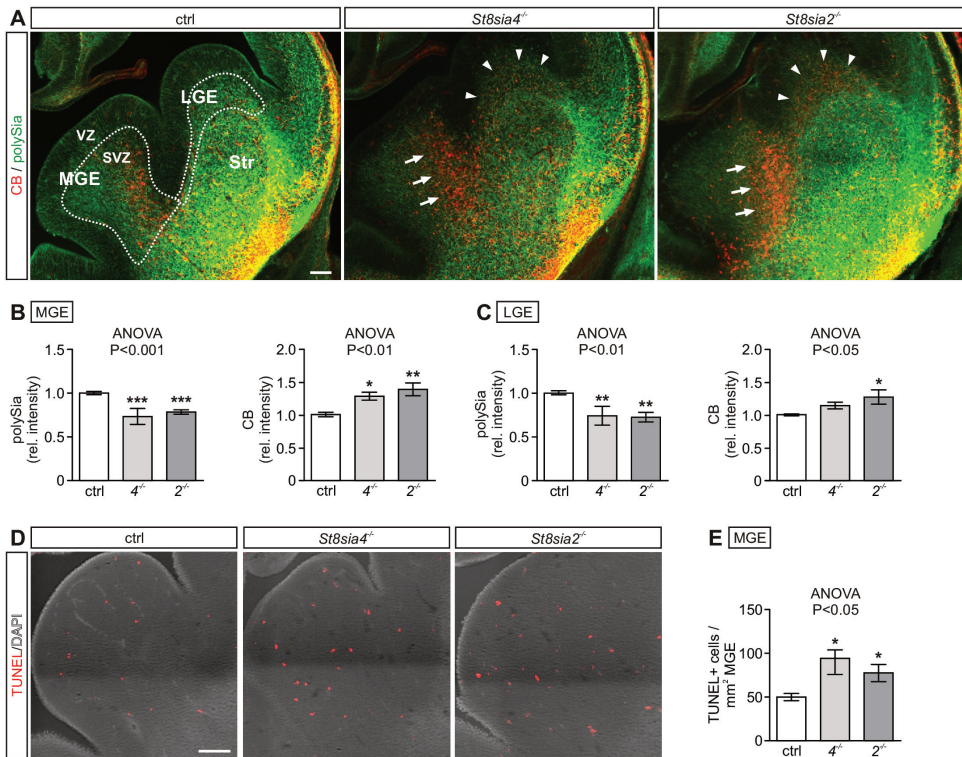
Figure 2.5: Reduced polySia, accumulation of calbindin-positive interneurons and increased apoptosis in the ganglionic eminences of E13.5 *St8sia4*$^{-/-}$ (*4*$^{-/-}$) and *St8sia2*$^{-/-}$ (*2*$^{-/-}$) embryos compared to wildtype controls (ctrl). (A-C) Immunostaining and densitometric quantification of polySia (green) and calbindin (CB, red). Compared to wildtype controls, accumulations of CB-positive cells in the SVZ of the dorsal MGE were more pronounced in *4*$^{-/-}$ and *2*$^{-/-}$ (arrows). In *2*$^{-/-}$ a slight increase was also detected in the SVZ of the LGE (arrowheads). Dashed lines denote the areas in the subventricular zone (SVZ) of the medial and lateral ganglionic eminence (MGE, LGE) as evaluated in (B) and (C), respectively. CB-positive cells were often too dense for reliable counting and therefore immunoreactivity was evaluated densitometrically. Str, striatum, VZ, ventricular zone. (D) TUNEL-positive cells in the MGE (red) and nuclear counterstain to illustrate tissue boundaries (DAPI, white). (E) Densities of TUNEL-positive cells in the MGE. Mean values ± s.e.m. from *n* = 8 (ctrl), *n* = 4 (*4*$^{-/-}$) and *n* = 6 embryos (*2*$^{-/-}$). Results from one-way ANOVA with Newman-Keuls post hoc test are indicated. *** P < **0.001**, ** P < **0.01**, * P < **0.05**. Scale bars: 100 µm.

Chapter 2

typical for polySia-NCAM (Galuska *et al.* 2006) and clearly exceeding the apparent molecular weights of polysialylated SynCAM 1 and neuropilin-2 as other possible carriers of polySia (Curreli *et al.* 2007; Galuska *et al.* 2010). After incubation of E12.5 slices with endo for 1 day the number of GFP$^+$ cells was significantly reduced in the pallium close to the pallial-subpallial boundary, while more distant cells were not affected (Fig. 2.6A,B). Consistent with the lower numbers of CB-positive cells in the pallium and their accumulation in the GE of $4^{-/-}$ and $2^{-/-}$ embryos at E13.5, these results argue for a decreased entry of interneurons into the pallium.

Thus, lower interneuron numbers in the PFC of polyST-deficient mice may arise from a reduced ability to cross the subpallial-pallial boundary or from deficits in the migratory process itself. To test for the latter, we sought to directly determine the impact of polySia on the process of interneuron migration by live imaging of GAD67-GFP-positive cells in slice cultures, which were treated with endo for 2h to acutely remove polySia prior to a 3h observation period. Due to the high density of GAD67-GFP-positive cells analysis of migration within the ganglionic eminences was not feasible. Live imaging of interneurons in the intermediate zone migratory stream of the pallium in E13.5 slices revealed migration at vastly different velocities (Fig. 2.6C). In the presence of endo, the mean velocity of all GFP$^+$ cells was significantly reduced (Fig. 2.6D; supplementary material Movies 1 and 2). Grouping into different velocity bins highlights a significant increase in the fraction of cells moving slower than 30 μm/hour at the expense of cells migrating with an intermediate velocity (30 to 60 μm/hour) upon removal of polySia with endo (Fig. 2.6E). Cells migrating faster than 60 μm/hour were not affected. Relative to their starting position interneurons migrated in all directions with a slight preference for dorsomedial orientation. This is consistent with previous reports (Britto *et al.* 2006; Tanaka *et al.* 2006) and was not altered by endo treatment (Fig. 2.6F,G).

Acute loss of polySia leads to decreased lengths of interneuron leading processes

Cortical interneurons migrate by extending a dynamic leading process followed by saltatory translocation of the nucleus (Bellion *et al.* 2005; for review see Marín *et al.* 2010). Alterations of leading process morphology have been repeatedly linked to migration deficits (Nasrallah *et al.* 2006; Friocourt *et al.* 2007; Wang *et al.* 2011; Steinecke *et al.* 2012; Luccardini *et al.* 2013) . To study the potential impact of polySia on the morphology of the leading process, coronal slices of E12.5 GAD67-GFP mice were cultured in the presence or absence of endo and the lengths of leading processes were evaluated after 1 day *in vitro*. Leading processes of GFP-positive interneurons were significantly shorter after endo treatment (Fig. 2.7A,B). To analyze whether this effect depends on cues provided by the cortical environment,
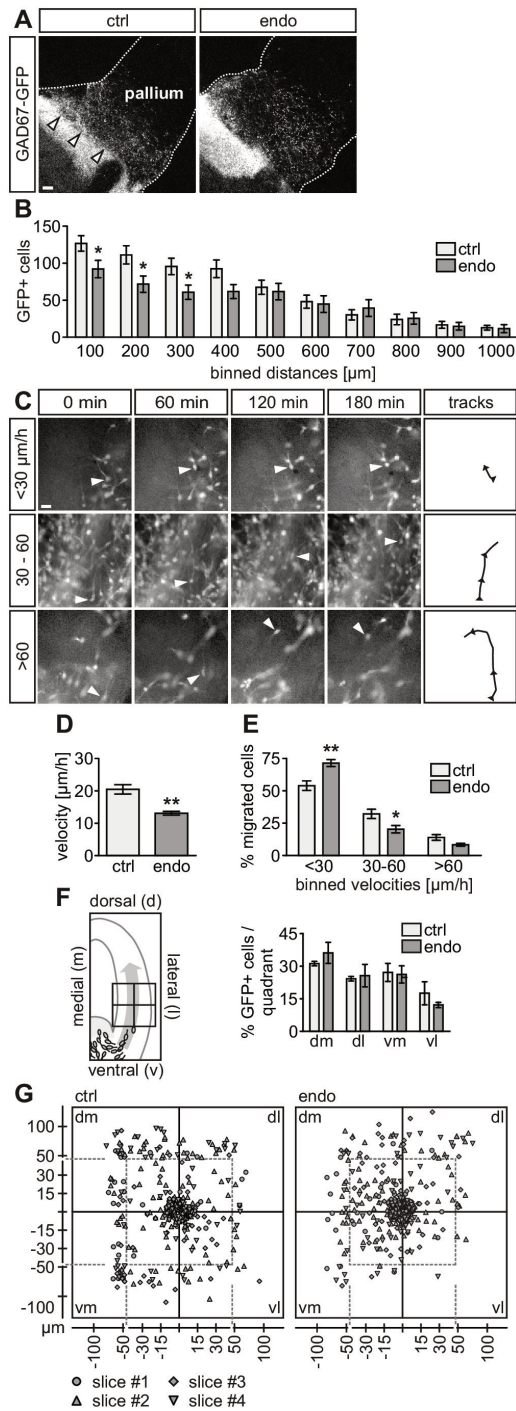
Figure 2.6: Caption on next page.

Figure 2.6: From previous page. Interneuron migration in embryonic GAD67-GFP slice cultures in the presence (ctrl) or after removal of polySia with endosialidase (endo). (A,B) E12.5 slices after 1 day *in vitro* (A). Distances between GFP-positive cells (GFP$^+$) in the pallium and the border of the ganglionic eminence (arrowheads) were determined and grouped in distance bins. Per bin, mean cell numbers ± s.e.m. from $n = 9$ slices per group are plotted (B). Tissue borders are outlined. (C) Live imaging of E13.5 slices revealed migration of GFP$^+$ interneurons at low (< 30μm/hour), intermediate ($30 - 60\mu$m/hour) and high velocities (> 60μm/hour). Frames at indicated time points and tracks of labeled cells (arrowheads) over a 3 hour observation period are shown. (D,E) Velocities of GFP$^+$ interneurons (D) and percent of GFP$^+$ interneurons falling into the indicated velocity bins (E). Means ± s.e.m. from $n = 4$ slices. A total of 385 cells for ctrl and 504 cells for endo were evaluated. (F,G) For each cell, the net direction of migration was determined and plotted as percentage of cells, migrating into the indicated quadrant (F; means ± s.e.m. from $n = 4$ slices) or for each cell individually (G). ** $P < 0.01$, * $P < 0.05$ (t test). Scale bars: $100\,\mu$m (A), $20\,\mu$m (C).

primary cultures of dissociated E13.5 MGE were prepared, which consisted of >80% GFP- and polySia-positive cells (Fig. 2.7D). Cultures were run for two days, but efficient migration was not observed on any of the substrates tested (poly-D-lysine, collagen, Matrigel, data not shown). Nevertheless, live cell imaging revealed a highly dynamic pro- and retraction of primary processes (Fig. 2.7C; supplementary material, Movie 3) and significantly shorter primary processes were detected after cultivation for 1 day in the presence of endo (Fig. 2.7D, E). These data indicate that loss of polySia perturbs migration of MGE-derived interneurons by interfering with leading process formation and/or stability.

2.4 Discussion

Based on the findings that PV- and Sst-positive interneuron populations are persistently reduced in the mPFC of polyST-deficient mice we tested the hypothesis that deficits in cortical interneuron migration might cause these alterations. Evaluation of genetically labeled interneurons in ST8SIA2- and ST8SIA4-deficient GAD67-GFP mice pointed towards a cell loss during embryonic development. Accumulation of precursors in the ganglionic eminences and reduced numbers of tangentially migrating interneurons in the pallium were observed in polyST-deficient embryos. Enzymatic removal of polySia in embryonic slice cultures revealed that acute loss of polySia hampered the entry of interneurons from the MGE into the pallium, reduced the speed of a fraction of cortical interneurons migrating at an intermediate velocity
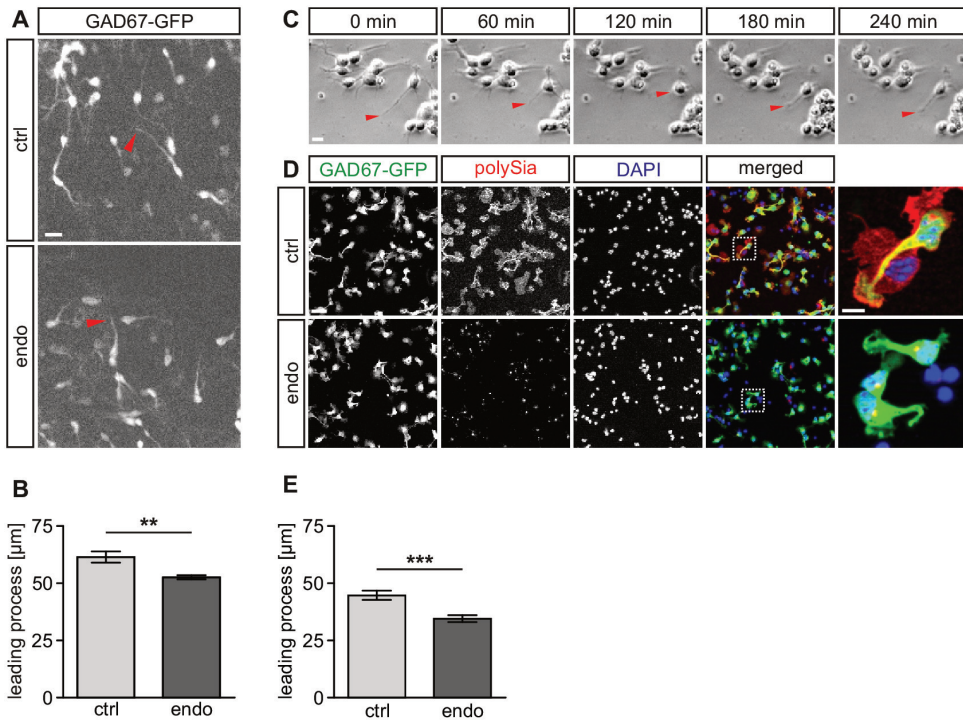
Figure 2.7: Removal of polySia leads to decreased lengths of interneuron leading processes in slice cultures and in MGE-derived primary cultures of embryonic GAD67-GFP mice. (A) Representative images of E12.5 slice cultures after 1 day *in vitro* in the absence (ctrl) or presence of endosialidase (endo). Arrowheads mark the end of one primary process, each. (B) Lengths of leading processes of GFP-positive cells. Means ± s.e.m. from *n* = 8 animals for each condition. A total of 186 cells for ctrl and 273 cells for endo were evaluated. (C) Selected frames of a time-lapse recording of an E13.5 MGE-primary culture illustrating the dynamics of leading processes of non-migrating interneurons. (D) Representative images of GFP-positive cells in E13.5 MGE primary cultures cultivated for 1 day in the absence (ctrl) or presence of endo and immunostained as indicated. Nuclei were counterstained with DAPI. The last image in each row shows a higher magnification of the area boxed in the merged image (GAD67-GFP, green; polySia, red; DAPI, blue). Residual polySia immunoreactivity after endo treatment was confined to an intracellular compartment close to the nucleus, most likely representing newly synthesized polySia in the Golgi. (E) Lengths of leading processes of GFP-positive cells. Mean values ± s.e.m. from *n* = 16 wells, each. A total of 321 cells for ctrl and 335 cells for endo were evaluated. ** $P < 0.01$, *** $P < 0001$ (t test). Scale bars: 20 μm (A, D upper left), 10 μm (C,D upper right).

and affected the lengths of their leading processes. Thus, polySia is essential for the migration of interneurons from the MGE into the cortex, suggesting that impaired tangential migration is a primary cause for the lack of mPFC interneurons in mice with compromised polySia synthesis.

PolySia is exclusively synthesized by the two polysialyltransferases ST8SIA2 and ST8SIA4 (Weinhold *et al.* 2005). ST8SIA2 is almost completely downregulated during postnatal development of the rodent and human cortex (Hildebrandt *et al.* 1998; Oltmann-Norden *et al.* 2008; McAuley *et al.* 2012), and ST8SIA4 is solely responsible for polySia expression in mature interneurons of the adult mouse cortex (Nacher *et al.* 2010). In contrast, and supportive of a common developmental origin of interneuron deficits in both polyST knockout lines, ST8SIA2 and ST8SIA4 are abundantly detected in the embryonic mouse brain and mRNA levels of both enzymes increase steeply between E12.5 and E14.5, a period of extensive interneuron precursor migration (Ong *et al.* 1998; Schiff *et al.* 2009).

As shown in the current study, acute removal of polySia in slice cultures leads to slower migration of cortical interneurons associated with shorter leading processes. Due to the high density of GAD67-GFP-positive interneurons in the ganglionic eminences these observations were restricted to the pallium. However, the accumulation of CB$^+$ interneuron precursors in the MGE as well as the lower numbers of interneurons invading the pallium at early stages of migration in polyST-deficient mice or after acute polySia removal in slice cultures suggest that polySia depletion impairs migration of MGE interneurons from the beginning. Furthermore, cultured MGE interneurons generated shorter processes after polySia removal indicating that the impact of polySia on leading process morphology is independent from factors provided by the cortical environment.

Previously, slower migration of interneurons has been found to be linked with either longer or shorter leading processes. For example, longer leading processes have been observed in LIS1- and DISC1-deficient mice in which impaired migration seems to be linked to altered nucleokinesis (Nasrallah *et al.* 2006; Steinecke *et al.* 2012). In contrast, ablation of the chemokine receptors CXCR4 or CXCR7 caused increased or reduced interneuron motility with longer or shorter leading processes, respectively (Wang *et al.* 2011). Of particular interest, perturbation of N-cadherin-mediated cell adhesion produced slower MGE-derived interneurons with shorter and less stable leading processes (Luccardini *et al.* 2013). Similarly, altered cell adhesion may be the primary mechanism, by which polySia affects leading process morphology and interneuron migration. However, other possibilities, such as altered interactions of cell surface receptors or different membrane dynamics in the presence or absence of polySia should be considered and explored in future studies. Reminiscent to the findings in polyST-deficient mice, altered precursor migration from the MGE and reduced numbers or loss of mainly PV-interneurons in the postnatal cortex were observed in mouse models with deficiencies of NRG1/ERBB4

(Flames *et al.* 2004; Fisahn *et al.* 2008) or DISC1 (Hikida *et al.* 2007; Shen *et al.* 2008; Steinecke *et al.* 2012), which are among the most compelling schizophrenia risk genes (Ross *et al.* 2006), and in mice lacking the brain-derived neurotrophic factor-receptor TrkB (Polleux *et al.* 2002), or the urokinase-type plasminogen activator receptor (uPAR) (Powell *et al.* 2001; Powell *et al.* 2003). Collectively, these results indicate that compromised migration into the pallium causes reductions of specific interneuron populations in the cortex.

The loss or a reduction of NCAM-bound polySia affects PV-positive interneurons comprising mainly basket and chandelier cells as well as Sst-positive interneurons, which are a heterogeneous population with many of the cells belonging to the PV-negative Martinotti cells (Kawaguchi and Kubota 1997; Gonchar and Burkhalter 1997; Markram *et al.* 2004; Gelman and Marín 2010). Fate mapping studies indicate that PV-, Sst- and CB-expressing interneurons of the adult cortex are preferentially generated from precursors of the central and ventral MGE characterized by the NKX2.1 and LHX6 transcription factors, while a CR and Sst double-positive fraction of Martinotti cells and the bipolar CR-expressing interneurons are generated from the dorsal MGE or outside the MGE, respectively (Xu *et al.* 2004; Fogarty *et al.* 2007; Anastasiades and Butt 2011). *Nkx2.1* knockout mice, which die at birth, lack Sst$^+$ cells at E19.0 (Anderson *et al.* 2001) and in the cortex of two-week-old *Lhx6* null mice dramatic reductions of PV$^+$ and Sst$^+$ cells were observed (Liodis *et al.* 2007). The latter study also established that these reductions were not due to a failure of GABAergic specification in the MGE but associated with delayed tangential migration and defective differentiation of MGE-derived progenitors into PV- and Sst-expressing interneurons. Together, these earlier studies support the assumption that the joint reduction of PV- and Sst-positive cells in the mPFC of polyST-deficient mice originates from deficits in tangential migration of central and ventral MGE-derived cortical interneuron precursors.

Assuming that defects of migration from the central and ventral MGE are the primary cause of altered PV$^+$ and Sst$^+$ densities it is surprising that PV$^-$CB$^+$ interneurons were not affected in the mPFC or its subdivisions in any of the polyST-deficient genotypes studied. Most, if not all MGE-derived interneurons seem to express CB in the embryonic and early postnatal phase (Anderson *et al.* 1997; Polleux *et al.* 2002) before undergoing a phenotypic shift as shown for the postnatal development of PV-positive interneurons of the rat cortex (Alcántara *et al.* 1996). Together with recent evidence for a common clonal origin of at least some of the PV- and Sst-positive interneurons (Brown *et al.* 2011), the available data seem compatible with the possibility that such a transition, i.e. the differentiation of CB-positive MGE-derived progenitors into PV- or Sst-expressing interneurons, is impaired by the inappropriate timing of the slower migrating interneurons and/or affected by the reduced numbers of cells arriving in the mPFC of polyST-deficient mice. Such

a scenario would also be consistent with earlier data indicating that the definite expression profiles of PV and CB as well as other parameters such as the laminar position can be influenced by environmental cues within the cortex (Mione *et al.* 1994; Valcanis and Tan 2003).

The persistent reduction of PV-expressing interneurons includes but was not confined to cells with WFA-positive PNNs. This special type of extracellular matrix is formed at the end of the critical period of cortical plasticity (Rhodes and Fawcett 2004) and is characteristic for a subpopulation of basket cells (Ojima 1993; Wegner *et al.* 2003). Notably, changes in basket cells have been found in other mouse models with altered polySia or NCAM levels. Transgenic mice overexpressing the extracellular domain of NCAM show reduced perisomatic innervation from basket cells and impaired synaptic plasticity in the PFC (Neeta *et al.* 2005; Brennaman and Maness 2008; Brennaman *et al.* 2011). Premature removal of polySia induced untimely maturation of perisomatic innervation and onset of critical period plasticity in the visual cortex (Di Cristo 2007). The balanced regulation of polySia and NCAM, therefore, has sequential functions during development of PV-positive basket cells.

It remains open if and how the reduced interneuron densities affect synaptic connectivity and network functions or if they lead to compensatory mechanisms in one or both of the polyST-deficient lines. However, altered mPFC interneuron functions may well contribute to some of the previously described behavioral changes common to $St8sia4^{-/-}$ and $St8sia2^{-/-}$ mice, such as decreased motivation of social interaction or impaired recognition memory, or even to the deficits of working memory, prepulse inhibition and other traits observed only in the absence of ST8SIA2 (Angata *et al.* 2004; Calandreau *et al.* 2010; Kröcher *et al.* 2015). Developmental defects of specific cortical interneuron subtypes can also be epileptogenic (Powell *et al.* 2003; Cobos *et al.* 2005), but so far, spontaneous seizures have not been observed in any of the polyST-deficient lines (Weinhold, unpublished observations). As studied in $St8sia4^{-/-}$ mice thresholds for pentylenetetrazole-induced seizures were unchanged and the anticonvulsant efficacy of the AMPA antagonist NBQX was even enhanced (Potschka *et al.* 2008). This effect may depend on the loss of direct modulation of AMPA receptors by polySia (Vaithianathan *et al.* 2004), but could also be linked to altered network activity such as feed forward disinhibition, which may play a role in the development of epileptic seizures (Birjandian *et al.* 2013).

In summary, our study demonstrates that polySia is essential for cortical interneuron development and provides a possible link between neurodevelopmental deficits and the emerging evidence that genetic variation of the polySia-NCAM system may be associated with schizophrenia (Arai *et al.* 2006; Tao *et al.* 2007; Brennaman and Maness 2010; McAuley *et al.* 2012). Reporter assays with a risk haplotype for *ST8SIA2* suggested higher expression (Arai *et al.* 2006), while another risk variant is associated with lower ST8SIA2 mRNA levels in post mortem PFC

samples (McAuley *et al.* 2012). Accordingly, the phenotype of *St8sia2*$^{-/-}$ mice can give clues on how reduced ST8SIA2 expression may actually lead to an increased risk for schizophrenia. Future work should focus on analyzing common or distinct alterations of synaptic and network activities in the mPFC of *St8sia2*$^{-/-}$ and *St8sia4*$^{-/-}$ mice and explore whether the interneuron deficits of polyST-deficient mice are necessary or sufficient to explain altered behavior.

2.5 Materials and Methods

Mice

All protocols for animal use were in accordance with the guidelines for animal experiments established by the European Union and approved by the local authorities. *St8sia2* and *St8sia4* knockout strains, backcrossed with C57BL/6J mice for six generations, were intercrossed to obtain $2^{-/-}4^{-/-}$ double knockout animals (Weinhold *et al.* 2005) or cross-bred with GAD67-GFP knock-in mice (Tamamaki *et al.* 2003) to obtain $2^{-/-}$ or $4^{-/-}$ mice heterozygous for the transgene ($2^{-/-}$-GAD67-GFP, $4^{-/-}$-GAD67-GFP). Genotyping was performed by PCR as previously described (Tamamaki *et al.* 2003; Weinhold *et al.* 2005). For staging of embryos, the morning of the vaginal plug was considered as embryonic day (E) 0.5. To ensure that embryos were matched for developmental stage, heterozygous (+/-) and homozygous (-/-) littermates were used and staging was controlled by external features such as the separation of digits (Kaufman and Kaufman 1992).

Immunofluorescence and terminal deoxynucleotidyl transferase-mediated dUTP nick end labeling

Sectioning, immunofluorescence staining, detection of perineuronal nets and terminal deoxynucleotidyl transferase-mediated digoxigenin-dUTP nick end labeling (TUNEL) was performed as described previously (Schiff *et al.* 2011). Specificity of TUNEL signals was controlled by omitting either the dioxigenin-conjugated dUTP or the terminal deoxynucleotidyl transferase. Both controls never gave any signal. The following monoclonal (mAb) or polyclonal antibodies (pAb) were applied according to the manufacturers' instructions: CR- and CB D-28k-specific rabbit pAb, PV-specific mouse mAb (IgG$_1$; all from Swant, Bellinzona, Switzerland), Sst-specific rat mAb (IgG$_{2b}$, Chemicon, Temecula, CA, USA), and respective Cy3- (Chemicon), Alexa488-, Alexa568- or, Alexa647-conjugated secondary antibodies (Invitrogen/Molecular Probes, Karlsruhe, Germany). PolySia-specific mouse mAb 735 (IgG$_{2a}$) (Frosch *et al.* 1985) was used at 5 µg/ml. All immunostaining procedures were controlled by omission of primary antibody. In double stained

samples, cross-reactivity of secondary antibodies was controlled by omitting either of the two primary antibodies. For nuclear counterstain, sections were mounted in Vectashield mounting medium with 4',6-diamidino-2-phenylindole (DAPI; Vector Laboratories, Burlingame, CA, USA).

Western blotting

Embryonic forebrains were dissected, lysed and extracts were subjected to SDS-PAGE and Western blotting with 20 or 40 µg of total protein per lane as described previously (Hildebrandt *et al.* 2009). Detection and densitometric evaluation was performed with the Odyssey Infrared Imaging System (LI-Cor Biosystems, Homburg, Germany). The following antibodies were used: polySia-specific mAb 735 (1 µg/ml), NCAM-specific rat mAb H28 (0.4 µg/ml) (Hirn *et al.* 1983), GAD56/67-specific rabbit pAb (3 µg/ml; Sigma-Aldrich, Taufkirchen, Germany), 0.4 µg/ml Lhx6-specific rabbit pAb (Santa Cruz Biotechnology Inc., Santa Cruz, CA, USA), and calbindin (CB) D-28-k-specific rabbit pAb (1:4000; Swant). As loading control, membranes were stripped and reacted with GAPDH-specific mouse mAb (0.4 µg/ml; Life Technologies, Darmstadt, Germany). Primary pAbs were detected with 25 ng/ml IgG-specific IRDye-680 and -800 conjugated antibodies (LI-COR Biosciences, Bad Homburg, Germany), whereas mAbs were detected with 100 ng/ml IgG-subtype-specific IRDye-680 and -800 conjugated antibodies (Rockland, Gilbertsville, PA, USA).

Cortical slice preparation and culture

E12.5 or E13.5 brains obtained from GAD67-GFP embryos were dissected in ice-cold dissection buffer composed of 126 mM NaCl, 2.5 mM KCl, 2.5 mM $CaCl_2$, 1.2 mM NaH_2PO_4, 1.2 mM $MgCl_2$, 11 mM D-glucose and 25 mM $NaHCO_3$ in ddH_2O and embedded in 4% low-gelling agarose (AppliChem, Darmstadt, Germany) in PBS, pH 7.4. Per embryo, 2-3 225 µm-thick coronal slices were obtained with a vibrating microtome. Slices were preincubated for 30 minutes on ice in dissection buffer 1 containing 10 mM HEPES, 1x penicillin/streptomycin (Biochrom, Berlin, Germany), 50 µg/ml gentamycin (Sigma-Aldrich). Where indicated, slices were incubated with endosialidase (Stummeyer *et al.* 2005) (endo; 4 µg/ml), which reliably and with high specificity removes polySia from the surface of living cells in culture and in tissues (Jakobsson *et al.* 2015). After transfer to Millicell cell culture inserts (PICM0RG50, Merck-Millipore, Darmstadt, Germany) in six-well-plates, slices were cultured for one day at 37℃ and 5% CO_2 in growth medium 1 consisting of Neurobasal medium (Life Technologies) containing 1x B27 supplement (Life Technologies), 32 mM D-glucose, 2 mM L-glutamine, 1x penicillin/streptomycin and 4 µg/ml endo, where indicated. For live imaging, slices of E13.5 embryos were prepared as described

above, but cultivation was carried out in 8-well imaging slides (μ-slide 8 well, ibidi, Martinsried, Germany) and slices were embedded in rat-tail collagen type I (BD Biosciences, Heidelberg, Germany) at a concentration of 1.3 mg per ml of PBS containing 32 mM D-glucose and 2 mM L-glutamine. After gelling of the collagen matrix, growth medium 1 was added with or without 4 μg/ml endo, and slices were incubated for 2 hours before starting image acquisition.

Time-lapse imaging

Live imaging was performed at 37℃ and 5% CO_2 using a microscope incubator (Pecon, Erbach, Germany). Time lapse sequences were generated by acquiring images with a 10x objective at an interval of 2 minutes for up to 14 hours using an Axiovert 200 M microscope equipped with an AxioCam MRm digital camera and AxioVision software (Carl Zeiss Microscopy, Göttingen, Germany). Pairs of endo-treated and control slices were recorded simultaneously using the microscope's automated stage controlled by the 'Mark and Find' feature of AxioVision software. For the quantification of interneuron precursor velocity, a sequence of 180 minutes (90 images) starting 4 hours after the onset of image acquisition was analyzed. Only cells visible throughout the entire sequence were used for analysis and migratory paths were reconstructed by manual tracking assisted by the AxioVision software. In order to summarize the direction of migration, all obtained paths were centered to a common starting point.

MGE primary culture

MGEs of E13.5 GAD67-GFP mice were dissected in ice-cold dissection buffer 2 consisting of PBS, pH 7.4 containing 0.6% D-glucose, centrifuged and digested with 0.25% trypsine (Biochrom) in dissection buffer 2 for 30 min at 37℃. After addition of 25% horse serum (Biochrom) and 100 μg/ml DNaseI (Roche, Mannheim, Germany) cells were dissociated by gentle trituration with a 1000 μl pipette. Cells were pelleted at 200 x g for 10 min, washed three times with dissection buffer 2 and resuspended in growth medium 2, consisting of Neurobasal medium with 2 mM Glutamax (Life Technologies), 1x B27 supplement, 1x penicillin/streptomycin, with or without the addition of 4 μg/ml endo. For live imaging, 6.6 x 105 cells per ml were seeded in 8-well imaging slides (ibidi) coated with 6 μg/cm^2 rat tail collagen type I (BD Biosciences), 25 μg/cm^2 poly-D-lysine (Sigma-Aldrich) or Matrigel (BD Biosciences, diluted 1:60 in Neurobasal Medium). For immunofluorescence, 106 cells per ml were plated on cover slips coated with 25 μg/cm^2 poly-D-lysine (Sigma-Aldrich) and contained in 12-well-plates. Cells were cultured at 37℃ and 5%CO_2. For immunofluorescence, cells were fixed after 1 div. For live imaging, cells were incubated for 2 h under standard conditions, prior to image acquisition in an Axiovert 200 M microscope with live imaging equipment (see above).

Image acquisition, cell counting, area and lengths measurements

For analyses of postnatal stages 3-6 sections per brain from at least three mice were analyzed per experimental group. Pairs of consecutive, 50 μm thick vibratome sections equally spaced between bregma level 1.9 mm and 1.54 mm were selected. PV was labeled together with either CR or CB (3 sections, each) or with Sst or Wisteria floribunda agglutinin (WFA; 6 sections, each). Near confocal images of 5.1 μm thick optical sections were acquired with structured illumination (ApoTome technology) using an Axiovert 200 M microscope and a 10x Plan-Apochromat objective with 0.45 numerical aperture (Carl Zeiss Microscopy, Göttingen, Germany). Micrographs of entire sections were acquired by the MosaiX image montage module of the AxioVision software. Identical microscope settings were used among different specimen. For evaluation, micrographs were coded and randomized to ensure that the observer was blind to experimental conditions. Always both hemispheres were evaluated. On each image the mPFC was lined out by use of anatomical landmarks, such as the characteristic shape of the forceps minor of the corpus callosum (fmi in Fig. 2.1A). The mPFC was subdivided into infralimbic (IL), prelimbic (PrL) and cingulate cortex area 1 (Cg1) according to Paxinos and Franklin 2001 and partitioned into upper and deep layers corresponding to layers 1 to 3 and 5 to 6 of the mPFC (lacking a distinct layer 4). The border between upper and deep layers was determined on each section by inspection of nuclear counterstain with DAPI. Cell counting and area measurements were performed as described before (Schiff *et al.* 2011). Briefly, areas were measured for each region of interest and the total numbers of labeled cells were counted by visual inspection assisted by the interactive event counting tool of the AxioVision software. To avoid bias by the slight reduction of overall cortex size in $2^{-/-}4^{-/-}$ mice (Hildebrandt *et al.* 2009), cell counts for each evaluated region were normalized to the respective area.

For analyses of embryonic stages, 2-4 coronal sections at the level of the MGE/LGE, the CGE or the mPFC from at least three E13.5 or E16.5 embryos per genotype were double-stained for polySia and CB or CR, or subjected to TUNEL, respectively. Acquired micrographs were blinded and evaluated either by cell counting as described above or by densitometry (see below). Leading processes of GAD67-GFP-positive interneurons were tracked on images of slice or MGE primary cultures and track lengths were evaluated with AxioVision software.

Densitometric quantification and assessment of migratory stream lengths

Densitometric quantification of polySia immunoreactivity in the pallium was carried out using ImageJ software (Schneider *et al.* 2012). Ten consecutive optical sections in a Z-stack were merged into one image using AxioVision software, exported to ImageJ in TIFF format and mean grey values of the intermediate zone

migratory stream were determined. Two independent sets of experiments were analyzed, each set consisting of 4-6 sections obtained from one animal per genotype. Tangential interneuron migration was assessed on coronal sections of E13.5 brains by measuring the length of the intermediate zone migratory stream and the extent of the dorsal telencephalon to the maximal dorsal expansion of the lateral ventricle beginning at the pallial/subpallial boundary. Per animal, four consecutive sections were evaluated. Densitometric quantification of polySia and CB immunoreactivity in the MGE or LGE was performed at E13.5 on at least four coronal sections per structure and embryo. Structures were outlined on double-stained sections and mean intensities of polySia and CB signals were determined from the same region of interest using ZEN 2012 software (Carl Zeiss Microscopy).

Statistical analysis

All data are given as mean ± s.e.m. Statistical analyses were performed with Graphpad Prism 4 software (GraphPad Software Inc., La Jolla, CA) using unpaired Student's t test and ANOVA with Newman-Keuls multiple comparison post hoc test, as indicated.

2.6 Others

Author contributions   T.K., I.R., U.D. and H.B. performed all experiments, B.W. organized breeding of polyST-deficient mice, Y.Y. provided GAD67-GFP mice, R.G.S. critically revised the manuscript, T.K., I.R., and H.H. designed experiments, analyzed the data and wrote the manuscript.

Competing interests statement   The authors declare no competing financial interests.

Supplementary material   Supplementary material is available online.

2.7 Supplement
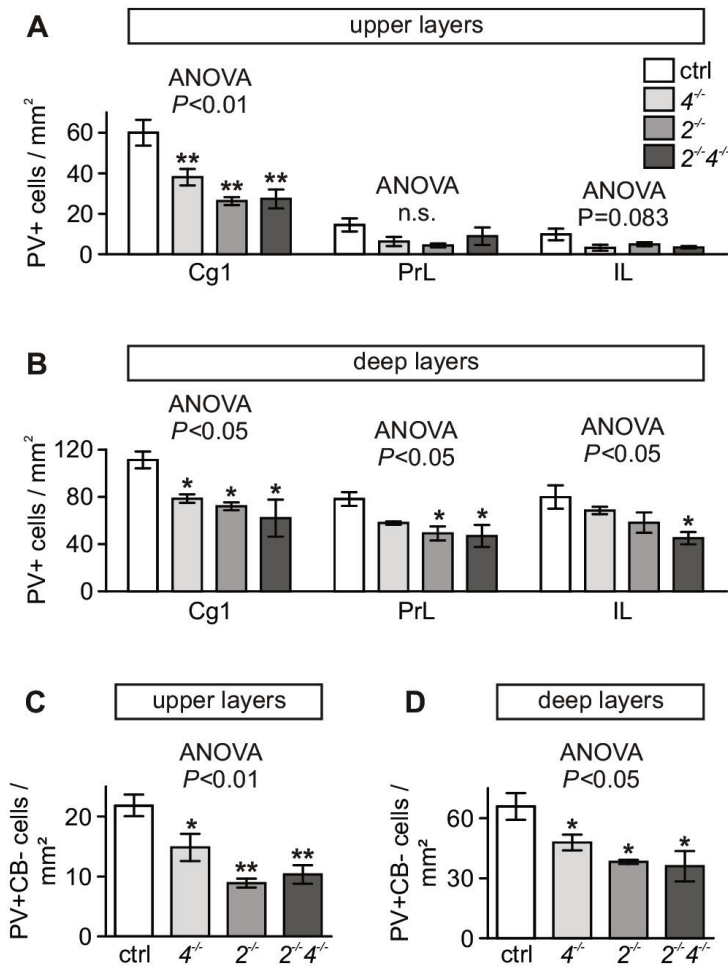
Figure S1: Densities of parvalbumin-positive interneurons (PV$^+$) in the medial prefrontal cortex (mPFC) of P30 *St8sia4$^{-/-}$* (*4$^{-/-}$*), *St8sia2$^{-/-}$* (*2$^{-/-}$*) and *2$^{-/-}$ 4$^{-/-}$* mice compared to a control group (ctrl, *2$^{+/+}$4$^{+/+}$* and *2$^{+/-}$ 4$^{+/-}$*). (A) Results for upper layers (cortical layers 1-3) of cingulate cortex, area 1 (Cg1), prelimbic cortex (PrL) and infralimbic cortex (IL) are shown. (B) Results for deep layers (cortical layers 5-6) are shown. (C,D) Densities of PV$^+$ interneurons negative for calbindin (CB$^-$) were analyzed. (A-D) For analyses of *2$^{-/-}$ 4$^{-/-}$* mice, which have a high incidence of hydrocephalus (13) only specimen with moderate ventricular dilatation and no cortical thinning were used. Per group, mean values ± s.e.m. from *n* = **3** animals are plotted. Results from one-way ANOVA and Newman-Keuls post hoc test are indicated. ** P < **0.01**, * P < **0.05**, n.s., not significant.
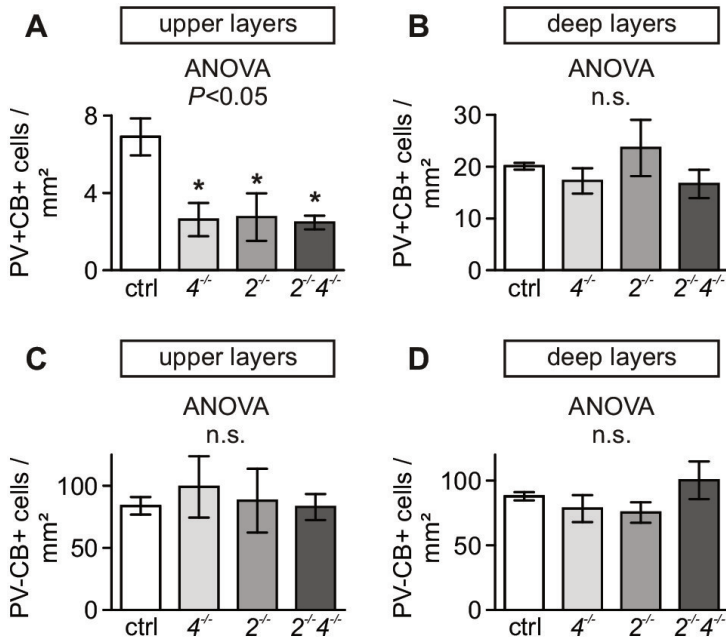
Figure S2: Densities of calbindin-positive interneurons (CB$^+$) in the medial prefrontal cortex (mPFC) of P30 *St8sia4*$^{-/-}$ (*4*$^{-/-}$), *St8sia2*$^{-/-}$ (*2*$^{-/-}$) and *2*$^{-/-}$ *4*$^{-/-}$ mice compared to a control group (ctrl, *2*$^{+/+}$*4*$^{+/+}$ and *2*$^{+/-}$*4*$^{+/-}$). (A,B) Densities of CB$^+$ cells positive for parvalbumin (PV$^+$) were estimated in the upper layers (A, cortical layers 1-3) and deep layers (B, cortical layers 5-6) of the mPFC. (C,D)Densities of CB$^+$ cells negative for parvalbumin (PV$^-$). (A-D) For analyses of *2*$^{-/-}$ *4*$^{-/-}$ mice, which have a high incidence of hydrocephalus (13) only specimen with moderate ventricular dilatation and no cortical thinning were used. Per group, mean values ±s.e.m. from *n* = **3** animals are plotted. Results from one-way ANOVA and Newman-Keulspost hoc test are indicated. * P < **0.05**, n.s., not significant.
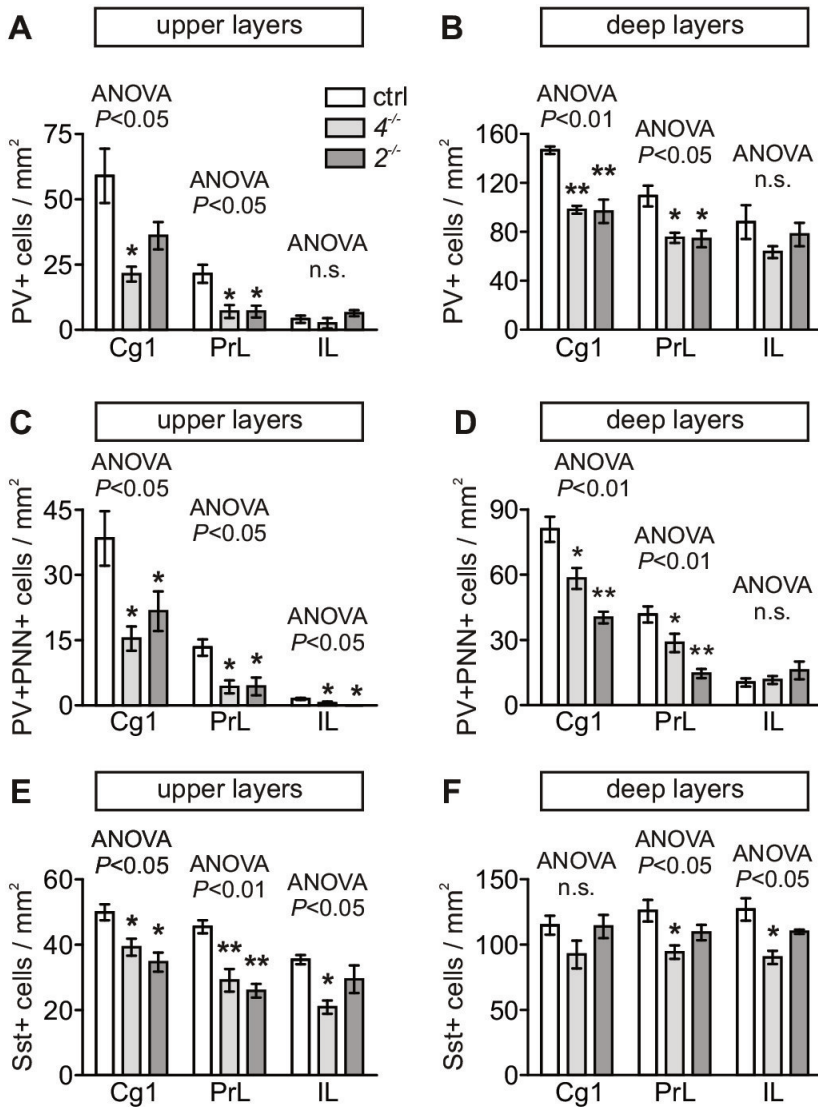
Figure S3: Densities of parvalbumin-positive (PV[+]) and somatostatin-positive (Sst[+]) interneurons of the medial prefrontal cortex (mPFC) of 3-month-old *St8sia4^{-/-}* (*4^{-/-}*), *St8sia2^{-/-}* (*2^{-/-}*) and wildtype control (ctrl, *2^{+/+}4^{+/+}*) mice. (A,B) Densities of PV^{+} cells were estimated in the upper (A, cortical layers 1-3) and deep layers (B, cortical layers 5-6) of cingulate cortex, area 1 (Cg1), prelimbic cortex (PrL) and infralimbic cortex (IL). (C,D) Densities of PV[+] interneurons with perineuronal nets (PNN[+]). (E,F) Densities of Sst[+] interneurons. (A-F) Per group, mean values ± s.e.m. from *n* = 3 animals are plotted. Results from one-way ANOVA and Newman-Keuls post hoc test are indicated. ** P < **0.01**, * P < **0.05**, n.s., not significant (P > **0.05**).

Chapter 2

A

GAD65/67 — ctrl $4^{-/-}$ $2^{-/-}$
— 72
Lhx6 — — 55
CB — — 26
GAPDH — — 34

B   ANOVA n.s.

rel. GAD65/67 protein level

1.5

1.0

0.5

0   ctrl $4^{-/-}$ $2^{-/-}$

C   ANOVA n.s.

rel. Lhx6 protein level

1.5

1.0

0.5

0   ctrl $4^{-/-}$ $2^{-/-}$

D   ANOVA n.s.

rel. CB protein level

1.5

1.0

0.5

0   ctrl $4^{-/-}$ $2^{-/-}$
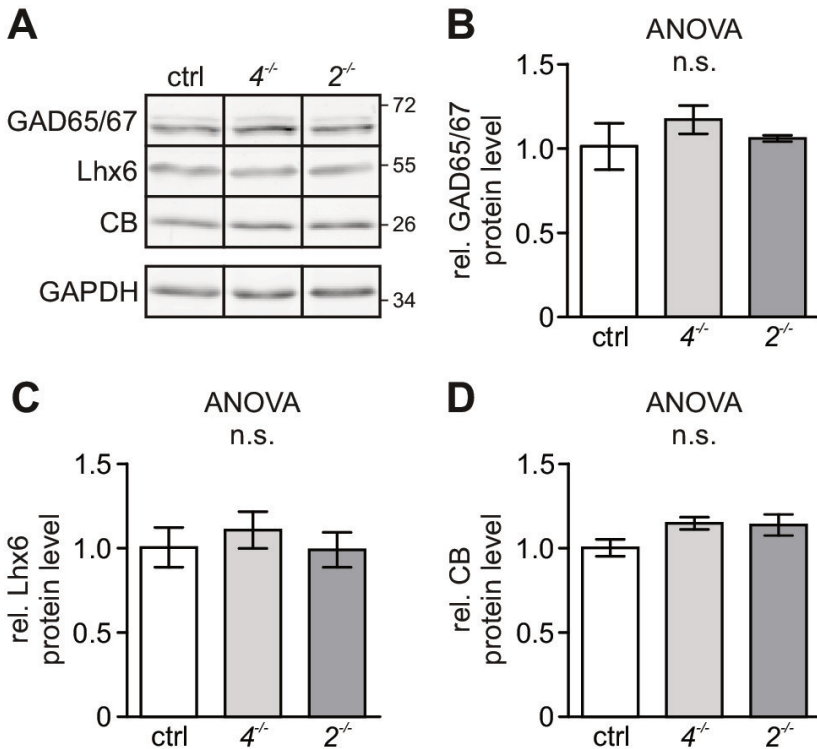
Figure S4: Quantification of glutamic acid decarboxylase 65/67 (GAD65/67), Lhx6, and calbindin (CB) in the forebrain of *St8sia4*$^{-/-}$ ($4^{-/-}$), *St8sia2*$^{-/-}$ ($2^{-/-}$) and control (ctrl) mice at E13.5. (A) Representative Western blots illustrating the levels of GAD65/67,Lhx6 and CB. GAPDH was used as loading control. Blots were scanned with the Odyssey Infrared Imaging System. Bands for each antigen were cropped from the same blot scan. (B-D) Densitometric quantification of GAD65/67,Lhx6, and CB.Mean values ± s.e.m. from *n* = **3** animals per group normalized to the mean value of the control group. Results from one-way ANOVA are indicated. n.s., not significant (P < **0.05**).
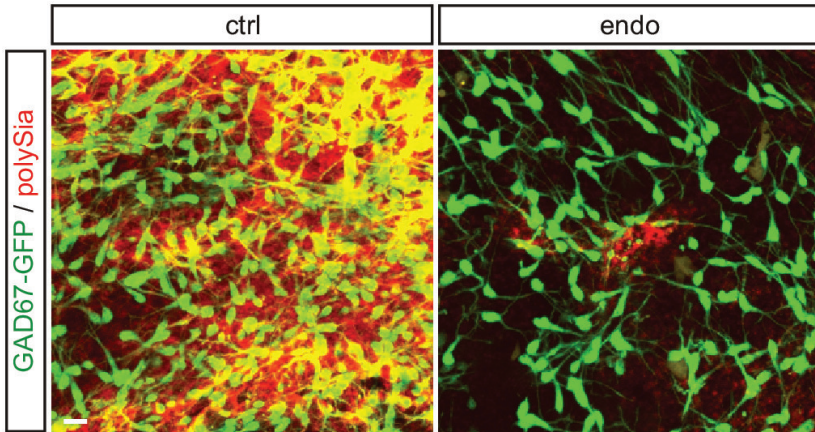
Figure S5: Incubation with endosialidase (endo) efficiently removes polysialic acid (polySia) from slice cultures. Coronal slices of E12.5 GAD67-GFP (GFP, green) brains were cultured for 1div in the absence (ctrl) or presence of 4 µg/ml endo. After fixation, slices were stained with polySia-specific antibody (red). Scale bar: **20** µm.
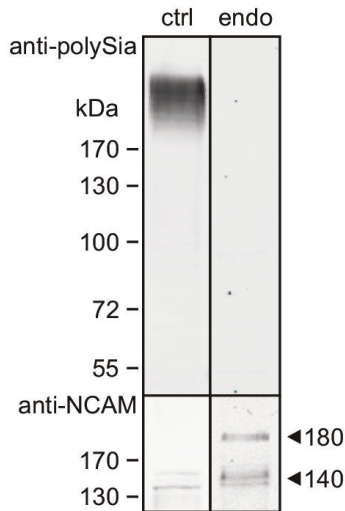
Figure S6: NCAM is the predominant carrier of polysialic acid (polySia) in the forebrain of E13.5 mice. Representative Western blots illustrating the levels of polySia and NCAM in forebrain lysates, incubated in the absence (ctrl, left lane) or presence of 40 µg/ml endosialidase (endo, right lane, see text for details). Note that after removal of polySia with endo, the major NCAM isoforms 180 and 140 become detectable.

2.8 Bibliography

Alcántara S, Lecea L, Río J, and Ferrer I (1996) Transient colocalization of par-
valbumin and calbindin D28k in the postnatal cerebral cortex: evidence for a
phenotypic shift in developing nonpyramidal neurons. Eur. J. Neurosci. 8:1329–
1339.

Anastasiades P G and Butt S J (2011) Decoding the transcriptional basis for GABAer-
gic interneuron diversity in the mouse neocortex. Eur. J. Neurosci. 34:1542–1552.

Anderson S, Eisenstat D, Shi L, and Rubenstein J (1997) Interneuron migration from
basal forebrain to neocortex: dependence on Dlx genes. Science 278:474–6.

Anderson S, Marín O, Horn C, Jennings K, and Rubenstein J (2001) Distinct cortical
migrations from the medial and lateral ganglionic eminences. Development
128:353–363.

Angata K, Huckaby V, Ranscht B, Terskikh A, Marth J, and Fukuda M (2007)
Polysialic acid-directed migration and differentiation of neural precursors are
essential for mouse brain development. Mol. Cell. Biol. 27:6659–68.

Angata K, Long J M, Bukalo O, Lee W, Dityatev A, Wynshaw-Boris A, Schachner M,
Fukuda M, and Marth J D (2004) Sialyltransferase ST8Sia-II assembles a subset
of polysialic acid that directs hippocampal axonal targeting and promotes fear
behavior. J. Biol. Chem. 279:32603–32613.

Anney R, Klei L, Pinto D, Regan R, Conroy J, Magalhaes T R, Correia C, Abrahams
B S, Sykes N, Pagnamenta A T, *et al.* (2010) A genome-wide scan for common
alleles affecting risk for autism. Hum. Mol. Genet. 19:4072–4082.

Arai M, Yamada K, Toyota T, Obata N, Haga S, Yoshida Y, Nakamura K, Minabe Y,
Ujike H, Sora I, Ikeda K, Mori N, Yoshikawa T, and Itokawa M (2006) Associa-
tion between polymorphisms in the promoter region of the sialyltransferase 8B
(SIAT8B) gene and schizophrenia. Biol. Psychiatry 59:652–659.

Bellion A, Baudoin J P, Alvarez C, Bornens M, and Métin C (2005) Nucleokinesis
in tangentially migrating neurons comprises two alternating phases: forward
migration of the Golgi/centrosome associated with centrosome splitting and
myosin contraction at the rear. J. Neurosci. 25:5691–5699.

Birjandian Z, Narla C, and Poulter M O (2013) Gain control of γ frequency activation
by a novel feed forward disinhibitory loop: implications for normal and epileptic
neural activity. Front. Neural Circuits 7:183.

Brennaman L, Kochlamazashvili G, Stoenica L, Nonneman R J, Moy S S, Schachner
M, Dityatev A, and Maness P F (2011) Transgenic mice overexpressing the extra-
cellular domain of NCAM are impaired in working memory and cortical plasticity.
Neurobiol. Dis. 43:372–378.

Brennaman L and Maness P (2008) Developmental regulation of GABAergic in-
terneuron branching and synaptic development in the prefrontal cortex by soluble
neural cell adhesion molecule. Mol. Cell. Neurosci. 37:781–93.

Chapter 2

Brennaman L and Maness P F (2010) NCAM in neuropsychiatric and neurodegenerative disorders. Adv. Exp. Med. Biol. 663:299–317.

Britto J M, Obata K, Yanagawa Y, and Tan S S (2006) Migratory response of interneurons to different regions of the developing neocortex. Cereb. Cortex 16:i57–i63.

Brown K N, Chen S, Han Z, Lu C, Tan X, Zhang X, Ding L, Alejandro L, Saur D, Anderson S A, Huang K, and Shi S (2011) Clonal production and organization of inhibitory interneurons in the neocortex. Science 334:480–486.

Calandreau L, Márquez C, Bisaz R, Fantin M, and Sandi C (2010) Differential impact of polysialyltransferase ST8SiaII and ST8SiaIV knockout on social interaction and aggression. Genes Brain Behav. 9:958–967.

Chazal G, Durbec P, Jankovski A, Rougon G, and Cremer H (2000) Consequences of neural cell adhesion molecule deficiency on cell migration in the rostral migratory stream of the mouse. J. Neurosci. 20:1446–1457.

Cobos I, Calcagnotto M, Vilaythong A, Thwin M, Noebels J, Baraban S, and Rubenstein J (2005) Mice lacking Dlx1 show subtype-specific loss of interneurons, reduced inhibition and epilepsy. Nat. Neurosci. 8:1059–1068.

Curreli S, Arany Z, Rita G, Mann D, and Stamatos N (2007) Polysialylated neuropilin-2 Is expressed on the surface of human dendritic cells and modulates dendritic Cell-T lymphocyte interactions. J. Biol. Chem. 282:30346–30356.

Di Cristo G (2007) Development of cortical GABAergic circuits and its implications for neurodevelopmental disorders. Clin. Genet. 72:1–8.

Eckhardt M, Bukalo O, Chazal G, Wang L, Goridis C, Schachner M, R G, Cremer H, and Dityatev A (2000) Mice deficient in the polysialyltransferase ST8SiaIV/PST-1 allow discrimination of the roles of neural cell adhesion molecule protein and polysialic acid in neural development and synaptic plasticity. J. Neurosci. 20:5234–44.

Fisahn A, Neddens J, Yan L, and Buonanno A (2008) Neuregulin-1 modulates hippocampal gamma oscillations: implications for schizophrenia. Cereb. Cortex 19:612–618.

Flames N, Long J E, Garratt A N, Fischer T M, Gassmann M, Birchmeier C, Lai C, Rubenstein J L, and Marın O (2004) Short-and long-range attraction of cortical GABAergic interneurons by neuregulin-1. Neuron 44:251–261.

Fogarty M, Grist M, Gelman D, Marín O, Pachnis V, and Kessaris N (2007) Spatial genetic patterning of the embryonic neuroepithelium generates GABAergic interneuron diversity in the adult cortex. J. Neurosci. 27:10935–46.

Fonseca M, Del Rio J A, Martinez A, Gómez S, and Soriano E (1995) Development of cairetinin immunoreactivity in the neocortex of the rat. J. Comp. Neurol. 361:177–192.

Friocourt G, Liu J S, Antypa M, Rakić S, Walsh C A, and Parnavelas J G (2007) Both doublecortin and doublecortin-like kinase play a role in cortical interneuron migration. J. Neurosci. 27:3875–3883.

Frosch M, Görgen I, Boulnois G, Timmis K, and D B (1985) NZB mouse system for production of monoclonal antibodies to weak bacterial antigens: isolation of an IgG antibody to the polysaccharide capsules of Escherichia coli K1 and group B meningococci. Proc. Natl. Acad. Sci. U.S.A. 82:1194–1198.

Gabbott P L, Dickie B G, Vaid R R, Headlam A J, and Bacon S J (1997) Local-circuit neurones in the medial prefrontal cortex (areas 25, 32 and 24b) in the rat: Morphology and quantitative distribution. J. Comp. Neurol. 377:465–499.

Galuska S, Imke O, Geyer H, Weinhold B, Kuchelmeister K, Hildebrandt H, Rita G, Geyer R, and Mühlenhoff M (2006) Polysialic acid profiles of mice expressing variant allelic combinations of the polysialyltransferases ST8SiaII and ST8SiaIV. J. Biol. Chem. 281:31605–31615.

Galuska S, Rollenhagen M, Kaup M, Eggers K, Imke O, Schiff M, Hartmann M, Weinhold B, Hildebrandt H, Geyer R, Mühlenhoff M, and Geyer H (2010) Synaptic cell adhesion molecule SynCAM 1 is a target for polysialylation in postnatal mouse brain. Proc. Natl. Acad. Sci. U.S.A. 107:10250–10255.

Gelman D M and Marín O (2010) Generation of interneuron diversity in the mouse cerebral cortex. Eur. J. Neurosci. 31:2136–2141.

Gilabert-Juan J, Varea E, Guirado R, Blasco-Ibáñez J M, Crespo C, and Nácher J (2012) Alterations in the expression of PSA-NCAM and synaptic proteins in the dorsolateral prefrontal cortex of psychiatric disorder patients. Neurosci. Lett. 530:97–102.

Gonchar Y and Burkhalter A (1997) Three distinct families of GABAergic neurons in rat visual cortex. Cereb. Cortex 7:347–358.

Härtig W, Brauer K, and Brückner G (1992) Wisteria floribunda agglutinin-labelled nets surround parvalbumin-containing neurons. Neuroreport 3:869–872.

Hikida T, Jaaro-Peled H, Seshadri S, Oishi K, Hookway C, Kong S, Wu D, Xue R, Andradé M, Tankou S, *et al.* (2007) Dominant-negative DISC1 transgenic mice display schizophrenia-associated phenotypes detected by measures translatable to humans. Proc. Natl. Acad. Sci. U.S.A. 104:14501–14506.

Hildebrandt H, Becker C, Mürau M, Gerardy-Schahn R, and Rahmann H (1998) Heterogeneous expression of the polysialyltransferases ST8Sia II and ST8Sia IV during postnatal rat brain development. J. Neurochem. 71:2339–2348.

Hildebrandt H, Mühlenhoff M, and Gerardy-Schahn R (2010) Polysialylation of NCAM. Adv. Exp. Med. Biol. 663:95–109.

Hildebrandt H, Mühlenhoff M, Imke O, Röckle I, Burkhardt H, Weinhold B, and Rita G (2009) Imbalance of neural cell adhesion molecule and polysialyltransferase alleles causes defective brain connectivity. Brain 132:2831–8.

Chapter 2

Hirn M, Ghandour M, Hermine D, and Goridis C (1983) Molecular heterogeneity and structural evolution during cerebellar ontogeny detected by monoclonal antibody of the mouse cell surface antigen BSP-2. Brain Res. 265:87–100.

Jakobsson E, Schwarzer D, Jokilammi A, and Finne J (2015) Endosialidases: versatile tools for the study of polysialic acid. Top. Curr. Chem. 367:29–73.

Kaufman M H and Kaufman M H (1992) *The atlas of mouse development.* Vol. 428. Academic press London.

Kawaguchi Y and Kubota Y (1997) GABAergic cell subtypes and their synaptic connections in rat frontal cortex. Cereb. Cortex 7:476–486.

Kröcher T, Malinovskaja K, Jürgenson M, Aonurm-Helm A, Zharkovskaya T, Kalda A, Röckle I, Schiff M, Weinhold B, Gerardy-Schahn R, *et al.* (2015) Schizophrenia-like phenotype of polysialyltransferase ST8SIA2-deficient mice. Brain Struct. Funct. 220:71–83.

Lavdas A, Grigoriou M, Pachnis V, and Parnavelas J (1999) The medial ganglionic eminence gives rise to a population of early neurons in the developing cerebral cortex. J. Neurosci. 19:7881–8.

Lewis D A, Curley A A, Glausier J R, and Volk D W (2012) Cortical parvalbumin interneurons and cognitive dysfunction in schizophrenia. Trends Neurosci. 35:57–67.

Liodis P, Denaxa M, Grigoriou M, Cynthia A, Yanagawa Y, and Pachnis V (2007) Lhx6 activity is required for the normal migration and specification of cortical interneuron subtypes. J. Neurosci. 27:3078–89.

Luccardini C, Hennekinne L, Viou L, Yanagida M, Murakami F, Kessaris N, Ma X, Adelstein R S, Mège R M, and Métin C (2013) N-cadherin sustains motility and polarity of future cortical interneurons during tangential migration. J. Neurosci. 33:18149–18160.

Marín O (2012) Interneuron dysfunction in psychiatric disorders. Nat. Rev. Neurosci. 13:107.

Marín O, Valiente M, Ge X, and Tsai L H (2010) Guiding neuronal cell migrations. Cold Spring Harb. Perspect. Biol. 2:a001834.

Markram H, Toledo-Rodriguez M, Wang Y, Gupta A, Silberberg G, and Wu C (2004) Interneurons of the neocortical inhibitory system. Nat. Rev. Neurosci. 5:793.

McAuley E, Scimone A, Tiwari Y, Agahi G, Mowry B, Holliday E, Donald J, Weickert C, Mitchell P, Schofield P, and Fullerton J (2012) Identification of sialyltransferase 8B as a generalized susceptibility gene for psychotic and mood disorders on chromosome 15q25-26. PLoS One 7:e38172.

Mione M, Danevic C, Boardman P, Harris B, and Parnavelas J (1994) Lineage analysis reveals neurotransmitter (GABA or glutamate) but not calcium-binding protein homogeneity in clonally related cortical neurons. J. Neurosci. 14:107–123.

Mühlenhoff M, Rollenhagen M, Werneburg S, Gerardy-Schahn R, and Hildebrandt H (2013) Polysialic acid: versatile modification of NCAM, SynCAM 1 and neuropilin-2. Neurochem. Res. 38:1134–1143.

Nacher J, Guirado R, Varea E, G. A, Röckle I, and Hildebrandt H (2010) Divergent impact of the polysialyltransferases ST8SiaII and ST8SiaIV on polysialic acid expression in immature neurons and interneurons of the adult cerebral cortex. Neuroscience 167:825–837.

Nasrallah I M, McManus M F, Pancoast M M, Wynshaw-Boris A, and Golden J A (2006) Analysis of non-radial interneuron migration dynamics and its disruption in Lis1+/- mice. J. Comp. Neurol. 496:847–858.

Neeta P, Panicker A, Rodriguiz R, Gilmore K, Demyanenko G, Huang J, Wetsel W, and Maness P (2005) Neural cell adhesion molecule-secreting transgenic mice display abnormalities in GABAergic interneurons and alterations in behavior. J. Neurosci. 25:4659–4671.

Ojima H (1993) Dendritic arborization patterns of cortical interneurons labeled with the lectin, Vicia villosa, and injected intracellularly with lucifer yellow in aldehyde-fixed rat slices. J. Chem. Neuroanat. 6:311–321.

Oltmann-Norden I, Galuska S P, Hildebrandt H, Geyer R, Gerardy-Schahn R, Geyer H, and Mühlenhoff M (2008) Impact of the polysialyltransferases ST8SiaII and ST8SiaIV on polysialic acid synthesis during postnatal mouse brain development. J. Biol. Chem. 283:1463–1471.

Ong E, Nakayama J, Angata K, Reyes L, Katsuyama T, Arai Y, and Fukuda M (1998) Developmental regulation of polysialic acid synthesis in mouse directed by two polysialyltransferases, PST and STX. Glycobiology 8:415–24.

Ono K, Tomasiewicz H, Magnuson T, and Rutishauser U (1994) N-CAM mutation inhibits tangential neuronal migration and is phenocopied by enzymatic removal of polysialic acid. Neuron 13:595–609.

Paxinos G and Franklin K B J (2001) *The mouse brain in stereotaxic coordinates.* Academic press San Diego, CA.

Polleux F, Whitford K L, Dijkhuizen P A, Vitalis T, and Ghosh A (2002) Control of cortical interneuron migration by neurotrophins and PI3-kinase signaling. Development 129:3147–3160.

Potschka H, Pekcec A, Weinhold B, and Gerardy-Schahn R (2008) Deficiency of neural cell adhesion molecule or its polysialylation modulates pharmacological effects of the AMPA receptor antagonist NBQX. Neuroscience 152:1093–1098.

Powell E, Mars W, and Levitt P (2001) Hepatocyte growth factor/scatter factor is a motogen for interneurons migrating from the ventral to dorsal telencephalon. Neuron 30:79–89.

Powell E, Campbell D B, Stanwood G D, Davis C, Noebels J L, and Levitt P (2003) Genetic disruption of cortical interneuron development causes region-and GABA cell type-specific deficits, epilepsy, and behavioral dysfunction. J. Neurosci. 23:622–631.

Powell S, Sejnowski T J, and Behrens M M (2012) Behavioral and neurochemical consequences of cortical oxidative stress on parvalbumin-interneuron maturation in rodent models of schizophrenia. Neuropharmacology 62:1322–1331.

Rhodes K and Fawcett J (2004) Chondroitin sulphate proteoglycans: preventing plasticity or protecting the CNS? J. Anat. 204:33–48.

Ross C A, Margolis R L, Reading S A, Pletnikov M, and Coyle J T (2006) Neurobiology of schizophrenia. Neuron 52:139–153.

Rutishauser U (2008) Polysialic acid in the plasticity of the developing and adult vertebrate nervous system. Nat. Rev. Neurosci. 9:26–35.

Schiff M, Röckle I, Burkhardt H, Weinhold B, and Hildebrandt H (2011) Thalamocortical pathfinding defects precede degeneration of the reticular thalamic nucleus in polysialic acid-deficient mice. J. Neurosci. 31:1302–1312.

Schiff M, Weinhold B, Grothe C, and Hildebrandt H (2009) NCAM and polysialyltransferase profiles match dopaminergic marker gene expression but polysialic acid is dispensable for development of the midbrain dopamine system. J. Neurochem. 110:1661–73.

Schnaar R L, Gerardy-Schahn R, and Hildebrandt H (2014) Sialic acids in the brain: gangliosides and polysialic acid in nervous system development, stability, disease, and regeneration. Physiol. Rev. 94:461–518.

Schneider C A, Rasband W S, and Eliceiri K W (2012) NIH Image to ImageJ: 25 years of image analysis. Nat. Methods 9:671–675.

Shen S, Lang B, Nakamoto C, Zhang F, Pu J, Kuan S L, Chatzi C, He S, Mackie I, Brandon N J, *et al.* (2008) Schizophrenia-related neural and behavioral phenotypes in transgenic mice expressing truncated Disc1. J. Neurosci. 28:10893–10904.

Steinecke A, Gampe C, Valkova C, Kaether C, and Bolz J (2012) Disrupted-in-Schizophrenia 1 (DISC1) is necessary for the correct migration of cortical interneurons. J. Neurosci. 32:738–745.

Stummeyer K, Dickmanns A, Mühlenhoff M, Gerardy-Schahn R, and Ficner R (2005) Crystal structure of the polysialic acid-degrading endosialidase of bacteriophage K1F. Nat. Struct. Mol. Biol. 12:90.

Tamamaki N, Yanagawa Y, Tomioka R, Miyazaki J, Obata K, and Kaneko T (2003) Green fluorescent protein expression and colocalization with calretinin, parvalbumin, and somatostatin in the GAD67-GFP knock-in mouse. J. Comp. Neurol. 467:60–79.

Tanaka D H, Maekawa K, Yanagawa Y, Obata K, and Murakami F (2006) Multidirectional and multizonal tangential migration of GABAergic interneurons in the developing cerebral cortex. Development 133:2167–2176.

Tao R, Li C, Zheng Y, Qin W, Zhang J, Li X, Xu Y, Shi Y, Feng G, and He L (2007) Positive association between SIAT8B and schizophrenia in the Chinese Han population. Schizophr. Res. 90:108–114.

Vaithianathan T, Matthias K, Bahr B, Schachner M, Suppiramaniam V, Dityatev A, and Steinhaüser C (2004) Neural cell adhesion molecule-associated polysialic acid potentiates α-amino-3-hydroxy-5-methylisoxazole-4-propionic acid receptor currents. J. Biol. Chem. 279:47975–47984.

Valcanis H and Tan S (2003) Layer specification of transplanted interneurons in developing mouse neocortex. J. Neurosci. 23:5113–22.

Wang Y, Li G, Stanco A, Long J E, Crawford D, Potter G B, Pleasure S J, Behrens T, and Rubenstein J L (2011) CXCR4 and CXCR7 have distinct functions in regulating interneuron migration. Neuron 69:61–76.

Wegner F, Härtig W, Bringmann A, Grosche J, Wohlfarth K, Zuschratter W, and Brückner G (2003) Diffuse perineuronal nets and modified pyramidal cells immunoreactive for glutamate and the GABA(A) receptor alpha1 subunit form a unique entity in rat cerebral cortex. Exp. Neurol. 184:705–14.

Weinhold B, Seidenfaden R, Röckle I, Mühlenhoff M, Schertzinger F, Conzelmann S, Marth J, Rita G, and Hildebrandt H (2005) Genetic ablation of polysialic acid causes severe neurodevelopmental defects rescued by deletion of the neural cell adhesion molecule. J. Biol. Chem. 280:42971–7.

Xu Q, Cobos I, De La Cruz E, Rubenstein J L, and Anderson S A (2004) Origins of cortical interneuron subtypes. J. Neurosci. 24:2612–2622.

Chapter 2

53

Cell-autonomous impact of ST8SIA2 on cortical interneuron distribution and BDNF-mediated migration

Ute Schuster[1], Charlotte Rossdam[1], Miriam Schiff[1], Isabel Meyer[1], Herbert Hildebrandt[1,2,#]

[1] *Institute of Clinical Biochemistry, Hannover Medical School, Carl-Neuberg-Str. 1, 30625 Hannover, Germany*
[2] *Center for Systems Neuroscience Hannover (ZSN), Hannover, Germany*
[#] *Corresponding author: Herbert Hildebrandt*

Institute of Clinical Biochemistry (4340), Hannover Medical School,
Carl-Neuberg-Str. 1, 30625 Hannover, Germany
Phone: +49 511 532 9808, Fax: +49 511 532 8801
e-mail: hildebrandt.herbert@mh-hannover.de

About the manuscript

My contributions to this manuscript comprised organization of mouse breeding as well as dissection, sectioning, immunofluorescent staining of embryonic and adult mice and microscopy. Validation of the conditional knockout by *in-situ* hybridization and genomic PCR was performed during my master thesis. Coculture assays were performed together with C.R. as part of her master thesis that I supervised. I wrote the MATLAB script for determination of shortest distances between cell coordinates and defined landmarks. I performed all live imaging experiments and analyzed migration parameters in slice cultures of *St8sia2*-knockout and -wildtype mice. Analysis of migration parameters in slice cultures of *Lhx6-Cre;St8sia2$^{f/f}$;-GAD67$^{GFP/+}$* mice was performed together with I.M. as part of her master thesis under my supervision. I analyzed all data and together with H.H. designed all experiments and wrote the manuscript.

<div style="text-align: right; font-size: 3em;">3</div>

Cell-autonomous impact of ST8SIA2 on cortical interneuron distribution and BDNF-mediated migration

<div style="text-align: right;">**Chapter 3**</div>

3.1 Abstract

Variations in *ST8SIA2* and in *BDNF* are associated with inhibitory dysregulation and neurodevelopmental psychiatric disorders. In mice, the ST8SIA2-dependent formation of polysialic acid is crucial for cortical interneuron development. Here, we used conditional knockout models to demonstrate a major cell-autonomous impact of ST8SIA2 on cortical interneuron distribution. Coculture assays and live imaging experiments revealed that ST8SIA2 in interneurons is essential for developmental migration and for the motogenic response of interneurons to BDNF. Based on the observation that deficits of mice with an interneuron-specific knockout of *St8sia2* were partially reversed by additional ablation of *St8sia2* in the cortex, we propose a model of polySia-dependent competition for BDNF between migratory interneurons and their cortical environment. These data provide a mechanism for converging functions of ST8SIA2 and BDNF in cortical interneuron migration with implications for neurodevelopmental psychiatric disorders.

3.2 Introduction

Polysialic acid (polySia) is a unique posttranslational modification, occurring mainly on the neural cell adhesion molecule NCAM. As a regulator of cell surface interactions, polySia is essential for proper brain development (Rutishauser 2008; Schnaar *et al.* 2014). Polysialylation of NCAM is implemented by the two polysialyltransferases ST8SIA2 and ST8SIA4 (Hildebrandt *et al.* 2010). Expression of the two

polysialyltransferases is differentially regulated. ST8SIA2-expression dominates during embryonic development, whereas ST8SIA4-expression persists into adulthood (Oltmann-Norden *et al.* 2008; Schiff *et al.* 2009; Hildebrandt *et al.* 2010). Both enzymes can at least partially compensate the loss of the other enzyme (Galuska *et al.* 2006). Variations in *ST8SIA2* have been associated with neurodevelopmental psychiatric disorders such as schizophrenia or autism (Arai *et al.* 2006; Tao *et al.* 2007; Anney *et al.* 2010; McAuley *et al.* 2012; Gilabert-Juan *et al.* 2013). In both diseases, the loss of parvalbumin-positive interneurons in the prefrontal cortex is a frequently reported neuropathological finding (Benes and Berretta 2001; Lewis *et al.* 2012; Hashemi *et al.* 2016). Earlier, we demonstrated reduced densities of parvalbumin (PV) and somatostatin (Sst) -expressing interneurons in the medial prefrontal cortex (mPFC) of *St8sia2*-deficient mice. The loss of these two major interneuron populations seems to be caused by impaired migration of their precursors from the embryonic medial ganglionic eminence (MGE) towards and into the cortical anlage (Kröcher *et al.* 2014, see Chapter 2).

Cortical interneuron migration is influenced by a variety of factors (Guo and Anton 2014), including neurotrophin-4 (NT-4) and the brain-derived neurotrophic factor BDNF, both motogenic ligands of the neurotrophin receptor trkB (Polleux *et al.* 2002). Several studies indicate physiological interactions between polySia, BDNF and trkB. Impaired long-term potentiation and compromised differentiation of cortical neurons (Muller *et al.* 2000; Vutskits *et al.* 2001) caused by a loss of polySia are associated with reduced trkB-signaling and can be rescued by addition of exogenous BDNF. This indicates enhanced sensitivity towards BDNF mediated by polySia. In septal neurons however, polySia limits the BDNF response, suggesting competing interactions of polySia and the trkB-receptor for BDNF (Burgess and Aubert 2006). More recently, evidence for direct interactions of polySia with BDNF and NT-4 has been obtained *in vitro* (Kanato *et al.* 2008; Sumida *et al.* 2015). Hence, these interactions may be needed for an adequate sensitivity of neurons to BDNF. Notably, in the context of cortical interneuron migration, polySia is present on the migrating interneurons as well as in their cortical environment (Kröcher *et al.* 2014, see Chapter 2). So far it is not known, whether polySia impacts interneuron migration cell-autonomously or as an environmental cue, and if it interacts with BDNF to induce a motogenic response.

Here, we report marked alterations of interneuron numbers in the frontal cortex of mice with an MGE- but not a cortex-specific deletion of *St8sia2*, indicating a cell-autonomous impact of ST8SIA2. These findings match results obtained by migration assays also demonstrating a robust cell-autonomous impact of polySia on interneuron migration and reduced responses of *St8sia2*-deficient interneurons to BDNF. Of note, genetic variations or altered levels of BDNF have been frequently associated with schizophrenia or autism (Nieto *et al.* 2013; Qin *et al.* 2016; Saghaz-

adeh and Rezaei 2017) and alterations of BDNF or trkB result in loss of PV-positive interneurons (Hashimoto *et al.* 2005; Sakata *et al.* 2009; Zheng *et al.* 2011). Thus, dysregulation of BDNF may converge with variations in ST8SIA2 on the level of developmental interneuron migration.

3.3 Results

Interneuron-specific inactivation of ST8SIA2 leads to loss of PV$^+$CB$^-$ cells

To address the question whether ST8SIA2 impacts cortical interneuron populations cell-autonomously or non-cell-autonomously, we generated mice with an interneuron- or cortex-specific deletion of *St8sia2*. The fourth exon of the *St8sia2* gene was flanked with loxp-sequences (Fig 3.1a) and mice were crossbred with MGE-specific *Lhx6-Cre* (Fragkouli *et al.* 2009), with cortex-specific *Emx1-Cre* mice (Gorski *et al.* 2002) and with *Zp3-Cre* mice (Lewandoski *et al.* 1997) to generate mice with a complete knockout of *St8sia2* (*St8sia2$^{\Delta/\Delta}$*). Excision of exon 4, which is essential for the sialyltransferase activity (Datta and Paulson 1995), results in inactivation of ST8SIA2. This approach has been used before to generate mice with a constitutive knockout of *St8sia2* (Angata *et al.* 2004). Successful recombination of *St8sia2$^{f/f}$* alleles in *Cre*-expressing mice was confirmed by genomic PCR. Here, we focus on PV-and CB-expressing interneurons in deep layers of the anterior cortex, because major alterations of the PV$^+$CB$^-$ interneuron population have been detected in deep layers of the mPFC in *St8sia2*-deficient animals (Kröcher *et al.* 2014, see Chapter 2) and because all PV$^+$ interneurons in deep cortical layers are basket cells (Miyamae *et al.* 2017). To assess, whether interneurons in other regions than the mPFC are affected by loss of ST8SIA2, we evaluated not only the cingulate cortex area 1 (Cg1) but also the adjacent primary and secondary motorcortices (M2 and M1) as well as the primary somatosensory cortex (S1) on six equally spaced rostral to caudal sections (based on Paxinos and Franklin 2001, bregma 1.10 to 1.94mm). Heatplots were created to illustrate the three-dimensional distribution (Fig 3.1b-e). For statistical analyses, values of the three caudal and the three rostral sections were pooled (Fig 3.1f, g).

As expected, we observed a dramatic loss of PV$^+$CB$^-$ interneurons in Cg1 of *St8sia2$^{\Delta/\Delta}$* animals. Analysis of the adjacent M2, M1 and S1 revealed similar reductions of PV$^+$CB$^-$ cells, but only in rostral levels (Fig 3.1e-g). Although less pronounced, *Lhx6-Cre;St8sia2$^{f/f}$* animals displayed similar reductions of PV$^+$CB$^-$ cells (Fig 3.1c, f and g). In contrast, no major alterations were detected in *Emx1-Cre;-St8sia2$^{f/f}$* animals (Fig 3.1b, f and g). However, as illustrated by the heatplot (Fig 3.1b), the amount of PV$^+$CB$^-$ cells was slightly increased in almost each of the 24 analyzed regions. Paired comparison of respective values for each region revealed

a significant increase of PV$^+$CB$^-$ cells by 4±1.35 % (mean ± s.e.m., paired t-test P = 0.007, n = 24) in *Emx1-Cre;St8sia2$^{f/f}$* animals compared to *St8sia2$^{f/f}$* controls. Moreover, the observed reduction of PV$^+$CB$^-$ interneurons in *Lhx6-Cre;St8sia2$^{f/f}$* mice seemed to be partially reversed by knockout of ST8SIA2 in the cortical environment (Fig 3.1d, f and g). The laminar distribution of interneurons was analyzed in deep-layers of the most rostral section in *Lhx6-Cre;St8sia2$^{f/f}$* and *St8sia2$^{\Delta/\Delta}$* mice, respectively. As exemplarily shown for the M2, the observed loss of PV$^+$CB$^-$ interneurons was most prominent in the upper half of the analyzed bins (Fig 3.1h). A similar pattern was observed in the Cg1, M1 and S1 (data not shown). Again, this effect was more pronounced in *St8sia2$^{\Delta/\Delta}$* than in *Lhx6-Cre;St8sia2$^{f/f}$* mice. Because MGE-derived interneurons populate the cortex in an inside-out pattern (Ang *et al.* 2003; Guo and Anton 2014), this indicates that early-born basket-cells are unaffected by loss of *St8sia2.*

Analysis of cells expressing both PV and CB in *St8sia2$^{\Delta/\Delta}$* animals revealed a decrease of PV$^+$CB$^+$ cells in rostromedial regions (e.g. Cg1, level 1, see Fig 3.2d). In contrast, caudolateral regions displayed a marked increase (e.g. S1, level 6). The laminar distribution of PV$^+$CB$^+$ interneurons resembled the distribution of PV$^+$CB$^-$ cells and loss of interneurons was detectable in the upper half of the analyzed bins (Fig 3.2g). *Lhx6-Cre;St8sia2$^{f/f}$* and *Emx1-Cre;St8sia2$^{f/f}$* mice did not display significant changes of the interneuron distributions (Fig 3.2a, b). However, as highlighted by heatplots, alterations of interneuron distributions in *Lhx6-Cre;-St8sia2$^{f/f}$* mice, although much smaller, were strikingly similar to those observed in *St8sia2$^{\Delta/\Delta}$* mice (Fig 3.2b, d, please note the different scale bars). In clear contrast to *Lhx6-Cre;St8sia2$^{f/f}$* and *Emx1-Cre;St8sia2$^{f/f}$* animals, double mutant mice (*Lhx6-Cre;Emx1-Cre;St8sia2$^{f/f}$*) displayed strong reductions in PV$^+$CB$^+$ cell populations, predominantly in rostral parts of the brain (Fig 3.2c and e).

In contrast to the PV$^+$ cell populations, PV$^-$CB$^+$ interneurons were reduced in all of the analyzed regions of the anterior cortex of *St8sia2$^{\Delta/\Delta}$* animals and no rostrocaudal gradient was observed (Fig 3.3d, e and f). The laminar distribution of PV$^-$CB$^+$ interneurons, however, again indicated a more pronounced loss in the upper half of the analyzed bins (Fig 3.3g). No significant alterations of the PV$^-$CB$^+$ population were detected in *Emx1-Cre;St8sia2$^{f/f}$*, *Lhx6-Cre;St8sia2$^{f/f}$*, and *Lhx6-Cre;-Emx1-Cre;St8sia2$^{f/f}$* mice (Fig 3.3a-c, e, f), but the heatplot for *Lhx6-Cre;St8sia2$^{f/f}$* animals (Fig 3.3b) indicated uniform, yet small, reductions of interneurons in the four rostral sections. Paired comparison of respective values in these four most rostral sections revealed a significant reduction of interneurons by 5.9±0.99% (mean ± s.e.m., paired t-test P < 0.0001 n = 16) in *Lhx6-Cre;St8sia2$^{f/f}$* compared to control mice.

Figure 3.1: Distribution of PV$^+$CB$^-$ interneurons in the anterior cortex of different conditional knockout mice at P90. (a) Genomic map of *St8sia2* with loxp-sequences flanking exon 4 (b-e) Heatplots illustrating the distribution of PV$^+$CB$^-$ cells from rostral to caudal (bregma levels 1-6) and from medial to lateral (Cg1, M2 , M1 and S1). (f, g) For each region, the numbers of PV$^+$CB$^-$ cells were normalized to the values of the respective *St8sia2$^{f/f}$* controls (WT). Normalized values for the three rostral and three caudal sections are presented separately. (h) Laminar distribution of PV$^+$CB$^-$ interneurons in the M2 region of the most rostral sections (bregma level 1). Coordinates of cells were used to calculate the distance from the forceps minor of the corpus callosum (fmi) and grouped in 14 bins of 100 μm. Total amount of cells in all bins are presented in the inset. Data are means ± s.e.m. of *n* = **13** floxed controls, *n* = 5 *Emx1-Cre;St8sia2$^{f/f}$*, *n* = 6 *Lhx6-Cre;St8sia2$^{f/f}$*, *Lhx6-Cre;Emx1-Cre;St8sia2$^{f/f}$* and *St8sia2$^{\Delta/\Delta}$* animals each. One-way ANOVA indicated significant differences in the inset in h (P < **0.01**), two-way ANOVA indicated significant differences for genotypes (P < **0.001** in f, g and h) and the Bonferroni post-test was applied for comparisons to the control group (* P < **0.05**; ** P < **0.01**; *** P < **0.001**). Colored scale bar corresponds to the shading of the heatplots, indicating the number of interneurons compared to the control group.
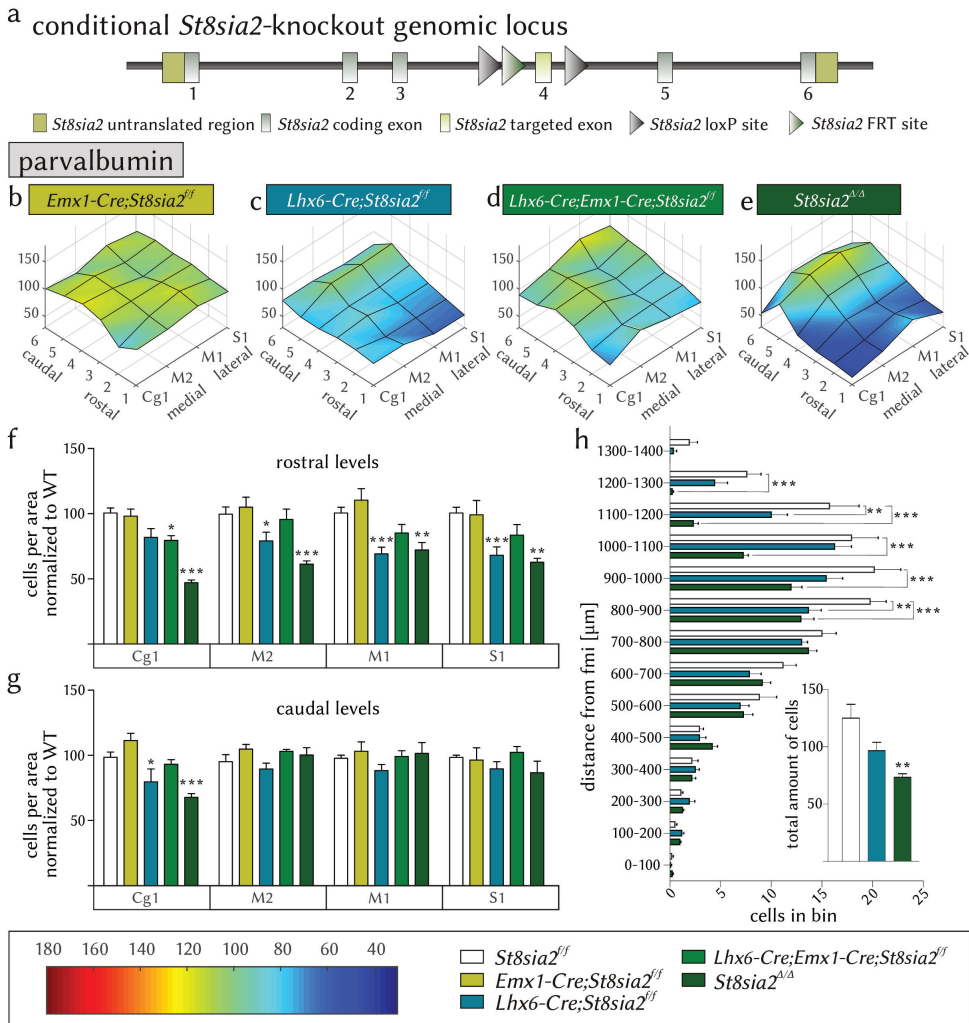
Figure 3.2: Distribution of PV$^+$CB$^+$ interneurons in the anterior cortex of different conditional knockout mice at P90. (a-d) Heatplots illustrating the distribution of PV$^+$CB$^+$ cells from rostral to caudal (bregma levels 1-6) and from medial to lateral (Cg1, M2 , M1 and S1). Note the different scale bars corresponding to the shading of the respective heatplots, indicating the number of interneurons compared to the control group. (e, f) For each region, the numbers of PV$^+$CB$^-$ cells were normalized to the values of the respective *St8sia2$^{f/f}$* controls (WT). Normalized values for the three rostral and three caudal sections are presented separately. (g) Laminar distribution of PV$^+$CB$^+$ interneurons in the M2 region of the most rostral sections (bregma level 1). Coordinates of cells were used to calculate the distance from the forceps minor of the corpus callosum (fmi) and grouped in 14 bins of 100 μm. Total amount of cells in all bins are presented in in the inset. Data are means ± s.e.m. of *n* = 13 floxed controls, *n* = 5 *Emx1-Cre;St8sia2$^{f/f}$*, *n* = 6 *Lhx6-Cre;St8sia2$^{f/f}$*, *Lhx6-Cre;Emx1-Cre;St8sia2$^{f/f}$* and *St8sia2$^{\Delta/\Delta}$* animals each. One-way ANOVA in the inset in g indicated no significant differences, two-way ANOVA indicated significant differences for genotypes (P < 0.001 in e and f, P < 0.05 in g) and the Bonferroni post-test was applied for comparisons to the control group (* P < 0.05; ** P < 0.01; *** P < 0.001).

Taken together, the pronounced alterations of PV$^+$CB$^-$ interneurons in *Lhx6-Cre;-St8sia2$^{f/f}$* mice demonstrate a clear cell-autonomous impact of ST8SIA2 on interneuron distributions. However, loss of *St8sia2* in the cortical environment partially reverses the reduction of PV$^+$CB$^-$ cells caused by *Lhx6-Cre*-dependent knockout, pointing towards a polySia-dependent interaction between cortical interneurons and their environment.

Cell-autonomous impact of ST8SIA2 on cortical interneuron migration

Since disturbed interneuron distributions in the cortex of polySia-deficient mice are already present at P1, these alterations arise from defects during embryonic development (Kröcher *et al.* 2014). To assess, whether loss of ST8SIA2 exerts a cell-autonomous or a non-cell-autonomous impact on cortical interneuron migration during development, we used cocultures of GAD67-GFP-positive MGEs with GFP-negative cortical tissue from E14.5 *St8sia2$^{-/-}$* or *St8sia2$^{+/+}$* embryos to monitor the invasion of GFP-labeled interneurons into the cortex (Fig 3.4a-c). Cocultures were performed in all possible combinations and the net migration distance of each interneuron was assessed by calculating its distance to the MGE-cortex boundary at the end of the cultivation period (48 hours). The maximal depth of infiltration into the cortical tissue was similar for all coculture combinations (Fig 3.4d), but significantly less *St8sia2$^{-/-}$* cells invaded *St8sia2$^{+/+}$* cortical tissue when compared to the numbers of either *St8sia2$^{+/+}$* or *St8sia2$^{-/-}$* cells that migrated into *St8sia2$^{-/-}$* cortical tissue (Fig 3.4e). On average, *St8sia2$^{-/-}$* interneurons invading *St8sia2$^{-/-}$* cortical tissue migrated significantly further when compared to the control situation (*St8sia2$^{+/+}$* into *St8sia2$^{+/+}$*) and compared to *St8sia2$^{-/-}$* interneurons invading an *St8sia2$^{+/+}$* wildtype environment (Fig 3.4f). Thus, significantly altered migration was observed for *St8sia2$^{-/-}$* cells invading either *St8sia2$^{+/+}$* or *St8sia2$^{-/-}$* cortical tissue. However, *St8sia2$^{+/+}$* and *St8sia2$^{-/-}$* cortical tissue had opposing effects on the migratory behavior, indicating that the state of polysialylation in the cortical environment had a decisive impact on the migration of *St8sia2$^{-/-}$* but not *St8sia2$^{+/+}$* interneurons. Analysis of the infiltration pattern revealed a cell-autonomous impact of ST8SIA2 on interneuron migration (Fig 3.4g). *St8sia2$^{-/-}$* interneurons accumulated in the first bins when migrating into *St8sia2$^{+/+}$* cortical tissue, whereas invasion of an *St8sia2$^{-/-}$* environment led to reduced interneuron densities in the first cortical bin and to increased densities in more distant bins. In contrast, comparable distributions were obtained for *St8sia2$^{+/+}$* interneurons invading *St8sia2$^{+/+}$* or *St8sia2$^{-/-}$* cortical tissues.
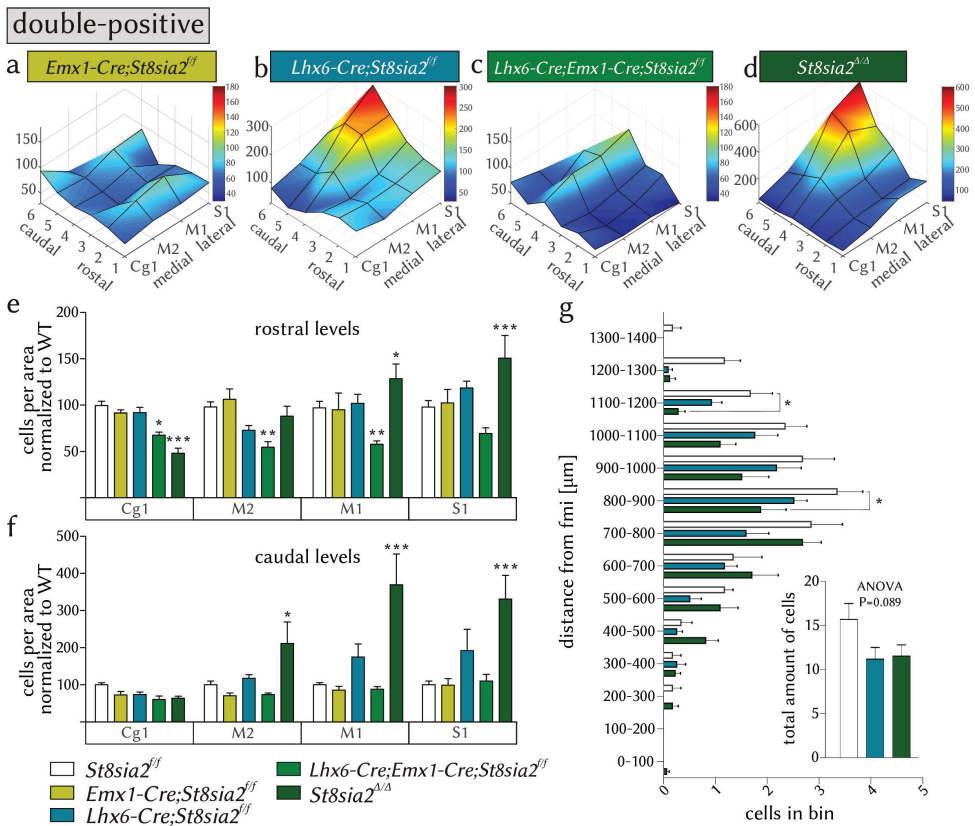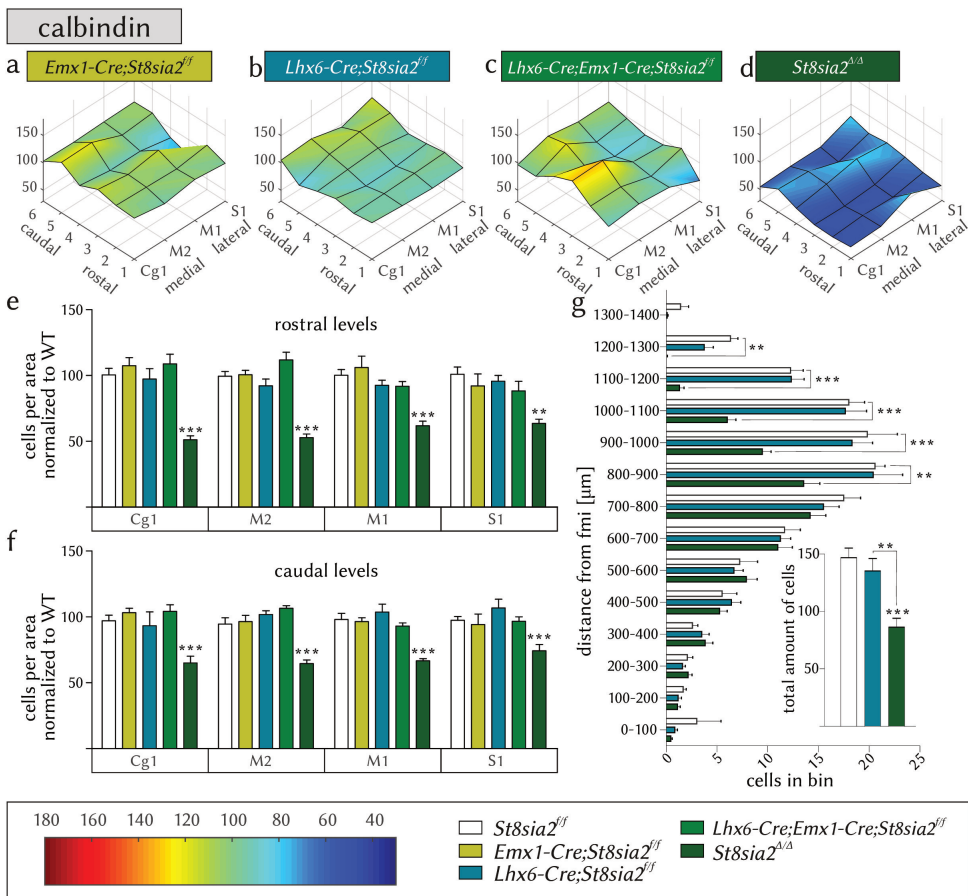
Figure 3.3: Distribution of PV⁻CB⁺-positive interneurons in the anterior cortex of different conditional knockout mice at P90. (a-d) Heatplots illustrating the distribution of PV⁻CB⁺ cells from rostral to caudal (bregma levels 1-6) and from medial to lateral (Cg1, M2 , M1 and S1). (e, f) For each region, the numbers of PV⁺CB⁻ cells were normalized to the values of the respective *St8sia2^{f/f}* controls (WT). Normalized values for the three rostral and three caudal sections are presented separately. (g) Laminar distribution of PV⁻CB⁺ interneurons in the M2 region of the most rostral sections (bregma level 1). Coordinates of cells were used to calculate the distance from the forceps minor of the corpus callosum (fmi) and grouped in 14 bins of 100 μm. Total amount of cells in all bins are presented in the inset. Data are means ± s.e.m. of $n = 13$ floxed controls, $n = 5$ *Emx1-Cre;St8sia2^{f/f}*, $n = 6$ *Lhx6-Cre;St8sia2^{f/f}*, *Lhx6-Cre;Emx1-Cre;St8sia2^{f/f}* and *St8sia2^{Δ/Δ}* animals each. One-way ANOVA revealed significant differences in the inset in g ($P < 0.001$), two-way ANOVA indicated significant differences for genotypes ($P < 0.001$ in e, f and g) and the Bonferroni post-test was applied for comparison to the control group (* $P < 0.05$; ** $P < 0.01$; *** $P < 0.001$). Colored scale bar corresponds to the shading of the heatplots, indicating the number of interneurons compared to the control group

These data demonstrate a clear cell-autonomous impact of ST8SIA2 on interneuron migration but also suggest that polysialylation of the cortical environment is relevant for the migration of ST8SIA2-negative cortical interneurons. Both findings are consistent with the divergent impact of *Lhx6-* and *Emx1-Cre* driven ST8SIA2-inactivation on cortical interneuron distributions in adult mice.

Inactivation of ST8SIA2 alters interneuron migration

Live cell imaging of interneuron migration in slice cultures of embryonic *St8sia2^{+/+};-GAD67^{GFP/+}* and *St8sia2^{−/−};GAD67^{GFP/+}* mice (Fig 3.5a-d) demonstrated that genetic ablation of *St8sia2* caused no significant alteration of the migration velocity (Fig 3.5e), but increased branching of the leading process (Fig 3.5f) and a reduced rate of nukleokinesis associated with an increased step width (Fig 3.5g-h). Unexpectedly, none of these defects could be detected in slice cultures of *Lhx6-Cre;St8sia2^{f/f};-GAD67^{GFP/+}* mice (data not shown). This is in stark contrast to the cell-autonomous impact of ST8SIA2 on interneuron migration detected in the coculture assays. We therefore investigated the possibility of an incomplete or delayed loss of polySia in *Lhx6-Cre;St8sia2^{f/f}* animals.

Late onset of ST8SIA2 and polySia-reduction by conditional inactivation in MGE-derived interneurons

Fig 3.6a illustrates the events from expression of *St8sia2* to the appearance of polySia on the cell surface. In order to evaluate the knockout of *St8sia2* in *Lhx6-*expressing interneurons, we first performed PCR analysis with genomic DNA obtained from E13.5 MGEs to confirm successful recombination of *St8sia2* by CRE-recombinase (Fig 3.6b). Bands indicating the presence of the recombined allele were obtained, but were relatively weak. This might be due to different efficacies of primer pairs or due to a delayed onset of *St8Sia2* recombination affecting only cells that already migrated out of the MGE. *In situ* hybridization demonstrated *Lhx6-*expression strictly confined to the SVZ of the MGE and also revealed strong expression of *St8sia2* in this region (Fig 3.6c). Loss of *St8sia2* transcripts in *Lhx6-Cre;-St8sia2^{f/f}* mice could not be analyzed by *in situ* hybridization, since generation of riboprobes able to distinguish between transcripts of floxed and recombined alleles was not possible. Evaluation of *St8sia2* transcripts was therefore conducted by qPCR. Analysis of mRNA isolated from MGEs of E14.5 *Lhx6-Cre;St8sia2^{f/f}* and *St8sia2^{f/f}* embryos was performed with primers binding to exon 4 of *St8sia2* or to the exon 3 to exon 5 boundary, obtained by CRE-mediated recombination. The levels of wildtype-transcripts in *Lhx6-Cre;St8sia2^{f/f}* animals and *St8sia2^{f/f}* controls were not significantly different. Detection of the truncated mRNA, however, proved

Chapter 3
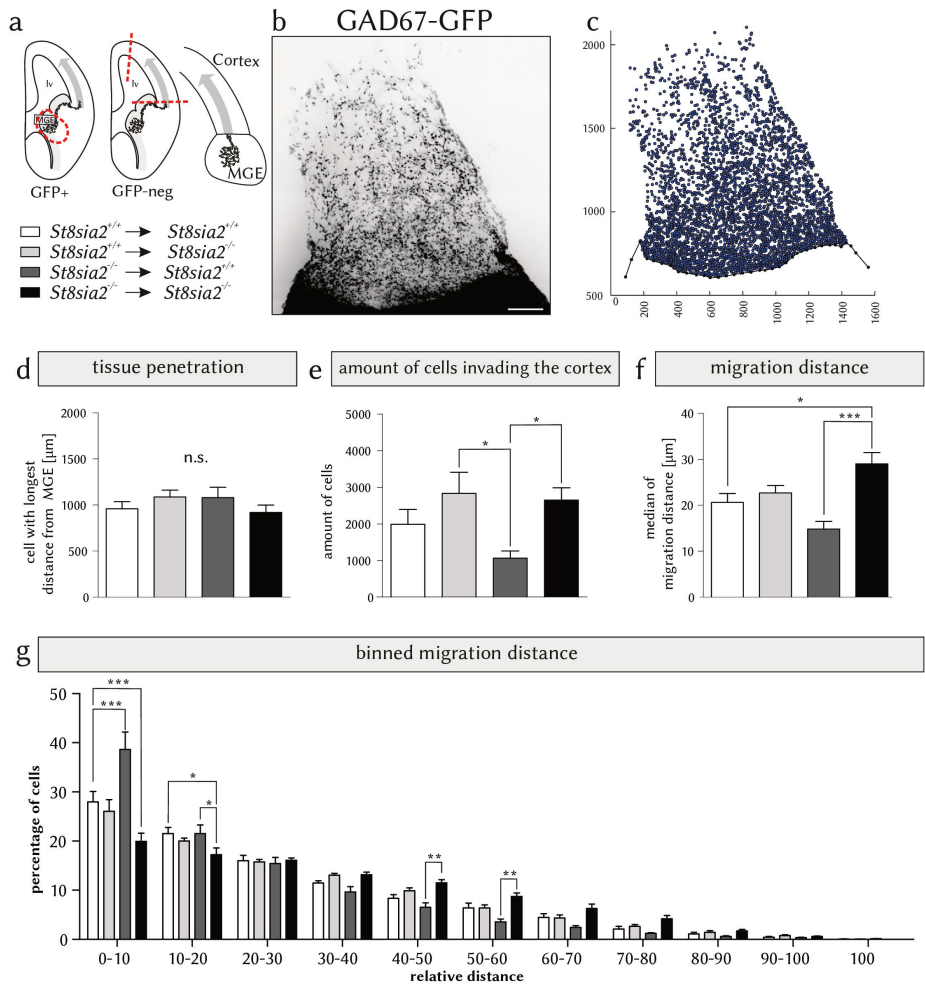
Figure 3.4: Coculture assays demonstrate a cell-autonomous role of ST8SIA2 in interneuron migration.
(a) Scheme of the coculture assay performed with all possible combinations of E13.5 *St8sia2*$^{+/+}$ and *St8sia2*$^{-/-}$ MGE and cortex tissue explants (see text for details). (b) Representative image and (c) determined coordinates of all infiltrated GFP-positive interneurons. For each cell, the shortest distance to the MGE-cortex boundary was calculated. (d) Depth of infiltration of host tissue, (e) comparison of cell amounts infiltrating host tissue and (f) analysis of the median of migrated distances. (g) Analysis of interneuron distribution by plotting of binned net migration distances. For each coculture, bins were defined in percent of the maximum net migration distance and the relative numbers of interneurons per bin were calculated in percent of all interneurons that invaded the cortex in a given coculture. A total of 100,752 cells were analyzed. Plotted values represent means ± s.e.m. of *n* = 7 or *n* = 8 cocultures of *St8sia2*$^{+/+}$ or *St8sia2*$^{-/-}$ MGE with *St8sia2*$^{+/+}$ cortices and *n* = 10 cocultures of *St8sia2*$^{+/+}$ or *St8sia2*$^{-/-}$ MGE with *St8sia2*$^{-/-}$ cortices, each. Analysis by one-way (d-f) or two-way ANOVA (g) indicated significant differences in e and f (P < 0.05 and P < 0.001, respectively) and a significant interaction between net migration and genotype in g (P < 0.001). Bonferroni post-hoc tests were applied for group comparisons (* P < 0.05; ** P < 0.01; *** P < 0.001, as indicated). Scale bar represents 200 µm.
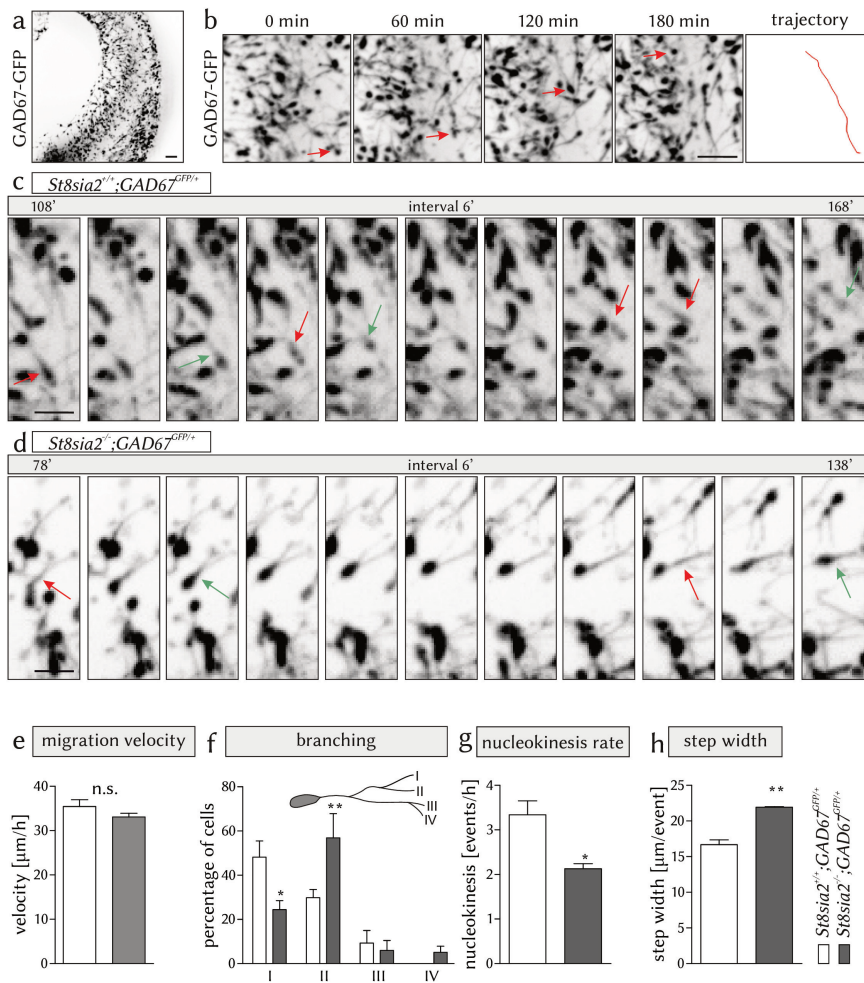
Figure 3.5: Live imaging reveals that ST8SIA2 impacts interneuron migration in slice culture. (a) First frame of a representative live imaging sequence of a GAD67-GFP embryo at E13.5. (b) Tracking of a migrating interneuron (red arrow) over 180 minutes of live imaging and corresponding trajectory. Scale bars correspond to 50 μm. Analysis of nukleokinesis in (c) $St8sia2^{+/+};GAD67^{GFP/+}$ and (d) $St8sia2^{-/-};GAD67^{GFP/+}$ mice is shown in a series of images acquired with an interval of 6 minutes. Red arrows indicate the translocation of the Golgi-apparatus into the swelling, green arrows indicate completed nukleokinesis. Wildtype interneurons in c complete 3-4 nukleokinesis steps in one hour, knockout interneurons in d only perform 2. Scale bars represent 25 μm. To determine the migration parameters, we analyzed (e) the migration velocity, (f) branching of the leading process, (g) nukleokinesis rate and (h) the nukleokinesis step width. Values are given as mean ± s.e.m. in n = 7 animals in e with a total of 790 analyzed cells in control and 1144 cells in $St8sia2^{-/-};GAD67^{GFP/+}$ slices and n = 3 in f-g with a total of 87 cells per genotype. In each case, one slice culture per embryo was analyzed. Statistical analysis by t-tests in e, g and h indicated no significant changes for e (P = 0.1412), but for g and h (* P < 0.05, ** P < 0.01). Two-way ANOVA revealed a significant interaction for f (P < 0.01) and a Bonferroni post-hoc test was applied (* P < 0.05, ** P < 0.01).
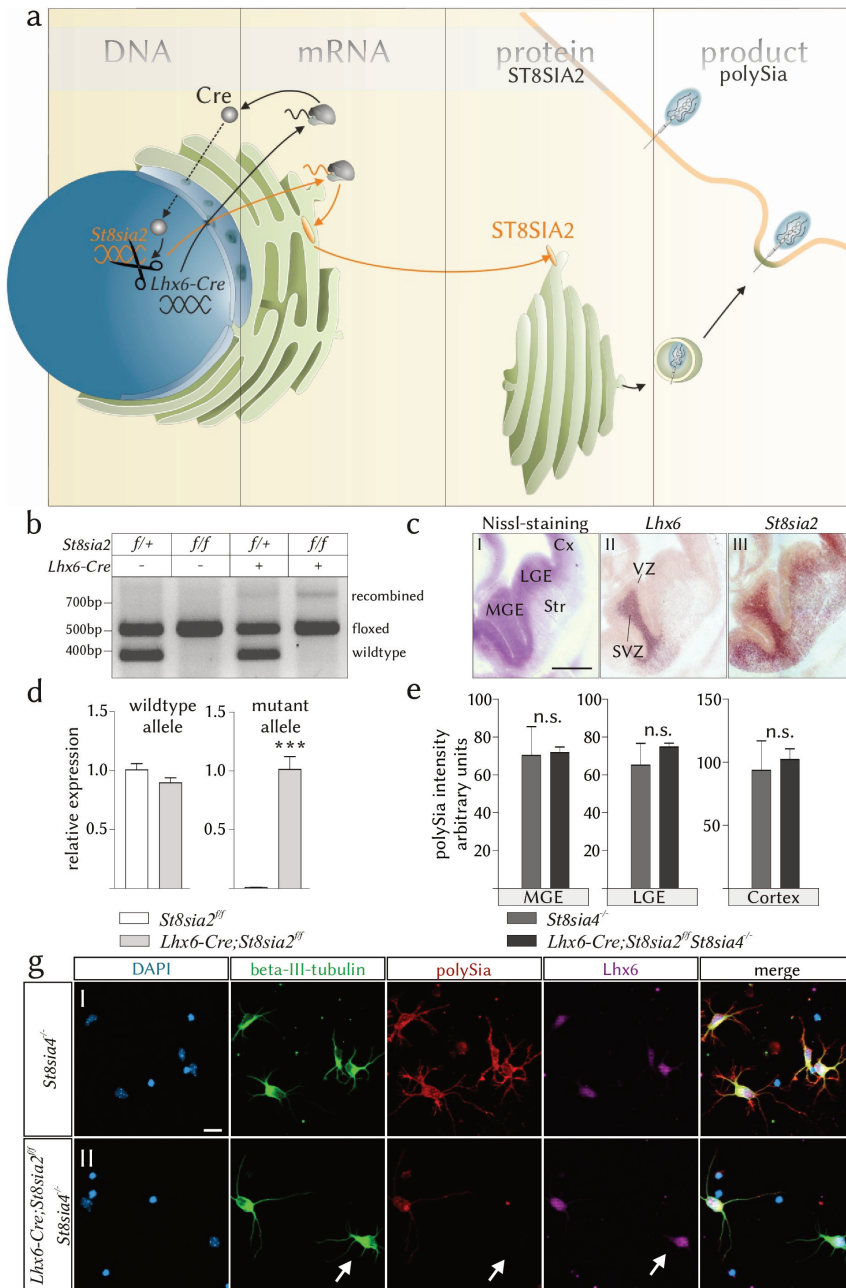
Figure 3.6: Caption on next page.

Figure 3.6: From previous page. Illustration of events from *St8sia2*-expression to altered polySia-levels. (a) Events from expression of *St8sia2* to the appearance of polySia on the cell surface. (b) Genomic PCR of DNA isolated from E13.5 MGEs of mice heterozygous (f/+) or homozygous (f/f) for the floxed allele and positive (+) or negative (-) for *Lhx6-Cre*. (c) Nissl-staining and in-situ hybridization of E13.5 coronal sections with riboprobes targeting *Lhx6* or *St8sia2*. (d) qPCR analysis of cDNA generated from E14.5 isolated MGEs detecting transcripts of wildtype (left) and mutant alleles (right) in *n* = 6 *St8sia2$^{f/f}$* and *n* = 3 *Lhx6-Cre;St8sia2$^{f/f}$* embryos. Values for each animal were obtained by three technical replicates and normalized to the relative expression of wildtype alleles in control animals (left) and to the relative expression of mutant alleles in *Lhx6-Cre;St8sia2$^{f/f}$* animals (right). (e) Densitometric evaluation of polySia immunoreactivity on E15.5 coronal sections of *Lhx6-Cre;St8sia2$^{f/f}$;St8sia4$^{-/-}$* and control mice in the MGE, LGE and the cortex. (g) Representative images of E14.5 primary MGE-cultures of *St8sia4$^{-/-}$* (I) and *Lhx6-Cre;St8sia2$^{f/f}$;St8sia4$^{-/-}$* (II) animals after 3 days *in vitro*. White arrows in II highlight a polySia-negative. Values are presented as mean ± s.e.m. and statistical analysis by t-test indicated significant differences in d (* P < **0.001**). Cx = cortex, MGE = medial ganglionic eminence, LGE = lateral ganglionic eminence, Str = striatum, VZ = ventricular zone, SVZ = subventricular zone. Scale bar represents 20 μm.

the presence of recombined *St8sia2* transcripts in the MGE of *Lhx6-Cre;St8sia2$^{f/f}$* embryos (Fig 3.6d). The inability to detect reduced mRNA expression of wildtype *St8sia2* is consistent with the weak bands obtained by genomic PCR for recombined *St8sia2* in the MGE.

Densitometric evaluation of polySia-levels in the MGE, LGE or the cortex performed on sections obtained from E13.5 *Lhx6-Cre;St8sia2$^{f/f}$* and *St8sia2$^{f/f}$* embryos yielded no significant differences (data not shown). Assuming that compensation of polySia synthesis by the remaining expression of ST8SIA4 precludes the detection of altered polySia-levels, we generated *St8sia4*-negative *Lhx6-Cre;St8sia2$^{f/f}$* animals (*Lhx6-Cre;St8sia2$^{f/f}$;St8sia4$^{-/-}$*). In the absence of ST8SIA4, inactivation of ST8SIA2 should result in a complete loss of polySia. However, detection of altered polySia levels in *Lhx6-Cre;St8sia2$^{f/f}$;St8sia4$^{-/-}$* compared to *St8sia2$^{f/f}$;St8sia4$^{-/-}$* animals was still not possible (Fig 3.6e). High magnification images of interneurons in the cortex of these animals revealed abundant polySia-signals on cells in the cortical environment and it was impossible to discriminate between polySia expressed in the direct vicinity of a migrating interneuron or by the interneuron itself (data not shown). Therefore, interneurons obtained from the MGE of *Lhx6-Cre;St8sia2$^{f/f}$;-St8sia4$^{-/-}$* and *St8sia2$^{f/f}$;St8sia4$^{-/-}$* animals were analyzed in primary culture to monitor the time-course of polySia-expression on interneurons independent of the

cortical environment. In contrast to cultivation for one or two days, first polySia-negative interneurons were detected in *Lhx6-Cre;St8sia2$^{f/f}$;St8sia4$^{-/-}$* cultures after three days *in vitro*. No polySia-negative cells were observed in control cultures (Fig 3.6g).

These results suggest that the conditional knockout of *St8sia2* is functional, but subject to a temporal delay, resulting in a loss of polySia only after exiting the MGE. This could result in a heterogenous population of polySia-positive and –negative MGE-derived interneurons in the cortex, explaining why altered interneuron migration could be detected in slice cultures of *St8sia2$^{-/-}$* but not *Lhx6-Cre;St8sia2$^{f/f}$;-GAD67$^{GFP/+}$* mice.

Interneurons with inactivation of ST8SIA2 display an impaired response to BDNF

The coculture assays revealed a robust cell-autonomous impact of ST8SIA2 on interneuron migration but also indicated polySia-dependent interactions between migrating interneurons and their environment. This would be compatible with the concept of polySia-dependent sensing of motogenic factors, such as BDNF (Polleux 2002). We therefore tested the effect of BDNF on interneuron migration by live imaging of slice cultures obtained from *Lhx6-Cre;St8sia2$^{f/f}$;GAD67$^{GFP/+}$* animals, in which *St8sia2*-deficiency is confined to MGE-derived interneurons in comparison to *St8sia2$^{f/f}$;GAD67$^{GFP/+}$* controls. To test for the BDNF effect, migration was monitored for three hours before slice cultures were transferred to medium without (mock) or with BDNF. Compared to the mock-treated controls, BDNF caused a significant increase in the migration velocity of *St8sia2$^{f/f}$;GAD67$^{GFP/+}$* controls (Fig 3.7a-c). *Lhx6-Cre;St8sia2$^{f/f}$;GAD67$^{GFP/+}$* interneurons still reacted to BDNF, but the BDNF-induced change in migration velocity was significantly reduced compared to control sections. Analysis of the nukleokinesis-rate displayed a similar reduction, but the difference between the genotypes was not significant (Fig 3.7d-f).

3.4 Discussion

Here, we provide a detailed analysis of the three-dimensional distribution of PV$^+$CB$^-$, PV$^-$CB$^+$ and double positive interneurons in the anterior cortex of mice with MGE- and cortex-specific deletions of *St8sia2*. The data demonstrate a strong cell-autonomous impact of ST8SIA2 on the distribution of PV$^+$ interneurons, but also provide evidence for a polySia-dependent interaction between interneurons and their cortical environment. Similarly, assessment of interneuron migration by coculture assays revealed a major cell-autonomous impact of ST8SIA2 but also indicated that the state of polysialylation in the cortical environment is important. Asking for a possible mechanism, we analyzed the migration of interneurons by
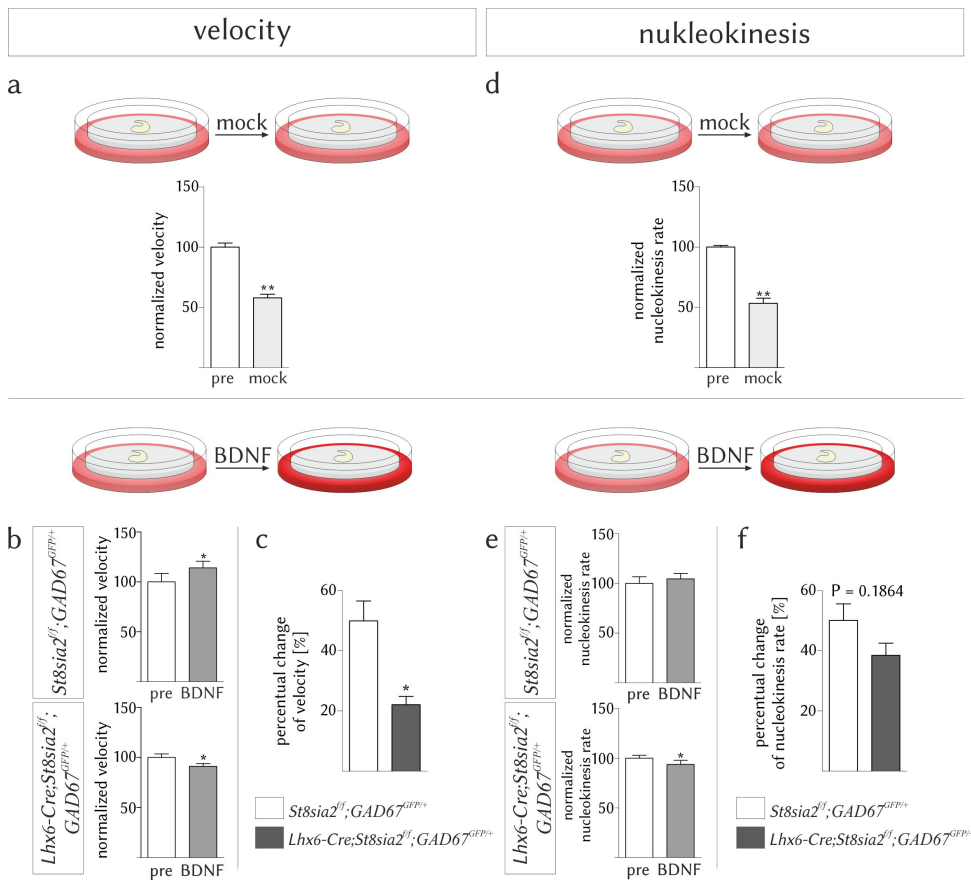
Figure 3.7: Inactivation of ST8SIA2 leads to an impaired response to BDNF. Live imaging experiments on E13.5 slice cultures obtained from *Lhx6-Cre;St8sia2$^{f/f}$;GAD67$^{GFP/+}$* and *St8sia2$^{f/f}$;GAD67$^{GFP/+}$* control mice. (a, b) Interneuron velocities in a 3h period before and after mock- (a) and BDNF-treatment (b). Values were normalized to the mean migration velocity in the first three hour period. (c) BDNF-induced change of velocities after correction for the decline of migration velocity in mock-treated cultures. (d, e) Nukleokinesis rate of interneurons in a 3h period before and after mock-treatment (d) and BDNF-treatment (e). Values were normalized to the mean nukleokinesis rate in the first three hour period. (f) BDNF-induced change of nukleokinesis after correction for the decrease of the nukleokinesis rate in mock-treated cultures. Data are presented as mean ± s.e.m. of *n* = 3 *St8sia2$^{f/f}$* control and *Lhx6-Cre;St8sia2$^{f/f}$* animals. Prior to incubation, 67 or 90 cells were analyzed in wildtype and knockout slices, respectively. Post-incubation, 90 cells were analyzed for each genotype.

live imaging and found that *Lhx6-Cre;St8sia2$^{f/f}$* mice displayed an impaired reaction to BDNF. This suggests that polySia produced by ST8SIA2 is essential for BDNF-mediated migration in the cortex and possibly affects the distribution of interneurons.

An interesting outcome of the coculture experiments was that migration of *St8sia2$^{-/-}$* interneurons into an *St8sia2$^{+/+}$* cortical environment was impaired, whereas invasion of an *St8sia2$^{-/-}$* environment was facilitated. The latter was unexpected, as acute removal of polySia by endosialidase (endo) in slice culture caused impaired entry of interneurons into the cortex (Kröcher *et al.* 2014, see Chapter 2). A similar discrepancy between *St8sia2$^{-/-}$* and endo-treated slice cultures was observed by live imaging. *St8sia2$^{-/-}$* interneurons displayed altered migration parameters but no change in the migration velocity, while acute removal of polySia by endo caused reduced migration velocities (Kröcher *et al.* 2014, see Chapter 2). One obvious explanation for these differences is that endo-treatment causes a complete loss of polySia, whereas *St8sia2$^{-/-}$* mice retain expression of ST8SIA4, which partially compensates for the loss of ST8SIA2 (Galuska *et al.* 2006). Moreover, accumulation and apoptosis of interneuron precursors in the MGE of *St8sia2$^{-/-}$* animals (Kröcher *et al.* 2014, see Chapter 2), indicates the loss of a subpopulation of MGE-derived interneurons in *St8sia2$^{-/-}$* mice. Due to this presorting, the interneuron population covered by live imaging of *St8sia2$^{-/-}$* slice cultures differs from the population affected by endo-treatment.

Differences between *Lhx6-Cre;St8sia2$^{f/f}$* and *St8sia2$^{-/-}$* mice became evident by live imaging and by evaluation of interneuron distributions. Interneurons in *St8sia2$^{-/-}$* slice cultures displayed altered nukleokinesis, which was not observed in *Lhx6-Cre;St8sia2$^{f/f}$* slices. Similarly, the altered distribution of interneurons in the anterior cortex of *St8sia2$^{\Delta/\Delta}$* animals was only partially recapitulated in *Lhx6-Cre;-St8sia2$^{f/f}$* mice. Both, the differences in migration and interneuron distribution can be explained by the late onset of polySia-reduction in *Lhx6-Cre;St8sia2$^{f/f}$* mice, which affects interneurons only after exiting the MGE. Therefore, the accumulation of CB-precursors and increased apoptosis inside the MGE observed in *St8sia2$^{-/-}$* animals could be circumvented in *Lhx6-Cre;St8sia2$^{f/f}$*. Nevertheless, as indicated by *in vitro* analysis, depletion of polySia in *Lhx6*-expressing interneurons starts after 48-72h. Assuming that MGE-derived interneurons need at least 48h to reach the cortex (Denaxa *et al.* 2005; Miyoshi and Fishell 2010), the *Lhx6-Cre* driven reduction of polySia should affect at least a subset of migrating interneurons in the cortex. Consequently, this late onset of polySia-reduction in *Lhx6-Cre;St8sia2$^{f/f}$* animals circumvents the early defects observed in the MGE of *St8sia2$^{-/-}$* mice and causes heterogeneous polySia-levels on interneurons in the developing neocortex. Both effects may explain why deficits in cortical interneuron migration and distribution observed in *St8sia2$^{\Delta/\Delta}$* are not fully recapitulated in *Lhx6-Cre;St8sia2$^{f/f}$* animals.

Another possible explanation for the differences in PV$^+$ interneuron distributions observed in the anterior cortex of *Lhx6-Cre;St8sia2$^{f/f}$* and *St8sia2$^{\Delta/\Delta}$* animals could be that inactivation of ST8SIA2 affects other than *Lhx6*-expressing cells. Since PV-positive interneurons are derived exclusively from *Lhx6*-expressing cells in the MGE (Fogarty *et al.* 2007; Rudy *et al.* 2011), loss of polySia in other regions of interneurogenesis should not account for these differences. Furthermore, *St8sia2*-expression in *Emx1*-positive cells cannot cause these differences, because *Emx1-Cre;-St8sia2$^{f/f}$* mice show no reduction, but a slight increase of PV$^+$ interneurons. Other structures that could affect the development of cortical interneurons in *St8sia2$^{\Delta/\Delta}$* but not in *Lhx6-Cre;St8sia2$^{f/f}$* animals are thalamocortical axons. These fibers traverse the subpallium and invade the cortex simultaneous with MGE-derived interneurons (López-Bendito *et al.* 2006). Therefore, as suggested for corticofugal fibers (Denaxa *et al.* 2001; Denaxa *et al.* 2005), cortical interneurons could depend on thalamocortical axons for their migration towards and inside the cortex.

Of note, the loss of PV$^-$CB$^+$ interneurons observed in the current study in *St8sia2$^{\Delta/\Delta}$* mice at P90 has not been detected in a previous study, which compared PV$^-$CB$^+$ cells in the mPFC of *St8sia2$^{-/-}$*, *St8sia4$^{-/-}$* and control mice at P30 (Kröcher *et al.* 2014, see Chapter 2). However, reevaluation of this data set by a direct comparison between *St8sia2$^{-/-}$* and control animals in a t-test indicated a significant reduction of PV$^-$CB$^+$ cells. This suggests that a loss of PV$^-$CB$^+$ cells is already present in *St8sia2*-negative mice at P30 but further aggravated until P90. In addition, this defect is observed only in *St8sia2$^{\Delta/\Delta}$* mice and not in any of the conditional knockout models. This indicates that the loss of CB-expressing interneurons arises from inactivation of ST8SIA2 in other than *Lhx6*- or *Emx1*-expressing cells. Unlike PV-expressing interneurons, CB$^+$ cells of the cortex are poorly characterized and not all of the CB-positive interneurons are derived from the MGE (Nery *et al.* 2002). Together, these data indicate that the loss of CB$^+$ and PV$^+$ interneurons are caused by different mechanisms. A possible reason for the late loss of CB$^+$ cells in *St8sia2*-negative mice could be reduced glutamatergic input into the cortex due to defective innervation by thalamocortical fibers (Kröcher *et al.* 2015). Most thalamocortical axons terminate in layer 4 of the granular neocortex, although some also terminate in layers 1, 2/3 and 6 (as reviewed in López-Bendito and Molnár 2003) and polySia seems to be essential for proper branching of these thalamocortical axons (Yamamoto *et al.* 2000). Hence, disturbed thalamocortical connectivity caused by loss of ST8SIA2 might have an impact on proper maturation and maintenance of the cortical inhibitory system. Inhibitory maturation is not completed before P35 (Gordon and Stryker 1996; Di Cristo 2007; Ueda *et al.* 2015). Likewise, the late formation of perineuronal nets argues for ongoing inhibitory

Chapter 3

maturation in the cortex after P30 (Rhodes and Fawcett 2004). Thus, altered thalamocortical input could influence interneuron maturation and therefore cause the late loss of CB$^+$ interneurons observed in *St8sia2*-negative mice. This should be investigated in future studies.

Another outcome of the analysis of interneurons in the anterior cortex is that loss of ST8SIA2 in *Lhx6*- and *Emx1*-expressing cells have opposing effects. *Emx1-Cre;-St8sia2$^{f/f}$* animals displayed a small increase of PV$^+$ cells, whereas PV-expressing interneurons in *Lhx6-Cre;St8sia2$^{f/f}$* mice were reduced. Double-mutant mice however (*Lhx6-Cre;Emx1-Cre;St8sia2$^{f/f}$*) displayed an intermediate phenotype. Assuming that the opposing effect of the *Lhx6*- and *Emx1*-driven inactivation of ST8SIA2 arise from independent mechanisms, the magnitude of the intermediate phenotype should correspond to the sum of the two individual contributing effects. In contrast, if both effects can be ascribed to a common mechanism, the intermediate phenotype should correspond to the mean. As shown in Fig. 3.8a, the actual change of PV$^+$ cells observed in *Lhx6-Cre;Emx1-Cre;St8sia2$^{f/f}$* corresponds almost perfectly to the value obtained by calculating the mean of the interneuron numbers determined separately for *Emx1-Cre;St8sia2$^{f/f}$* and *Lhx6-Cre;St8sia2$^{f/f}$* mice. This clearly argues for a common mechanism of how ST8SIA2 in *Lhx6*- and *Emx1*-expressing cells affects the distribution of cortical interneurons. This implies (i) a polySia-dependent interaction between interneurons and their cortical environment and (ii) that the state of the environment gains importance if interneurons lack ST8SIA2. Notably, both implications are consistent with the differential impact of ST8SIA2 on interneuron migration observed in coculture experiments.

PolySia has been implicated in recognition and presentation of soluble factors (for review see Schnaar *et al.* 2014). The motogenic factor BDNF (Polleux *et al.* 2002) was shown to directly bind to polySia (Kanato *et al.* 2008; Sumida *et al.* 2015). Indeed, analysis of the BDNF-response in live imaging experiments performed in the current study demonstrated a strong motogenic response of wildtype interneurons to BDNF. In contrast, the response to BDNF in *Lhx6-Cre;St8sia2$^{f/f}$* interneurons was impaired. A possible explanation for this finding is depicted in Fig 8b, proposing a model in which interneurons and their environment compete for BDNF by expression of polySia. In wildtype animals, a balance between polySia-positive interneurons and polySia in their environment is maintained, resulting in balanced levels of BDNF. Ablation of polySia in the cortical environment results in a disturbed balance, shifting towards a higher effective BDNF-concentration available to migrating interneurons. In contrast, ablation of polySia on migrating interneurons results in a decreased binding capacity and a lower effective BDNF-concentration available to the interneuron. Therefore, the simultaneous ablation of polySia on interneurons and the environment will not cause a more severe, but an intermediate phenotype.
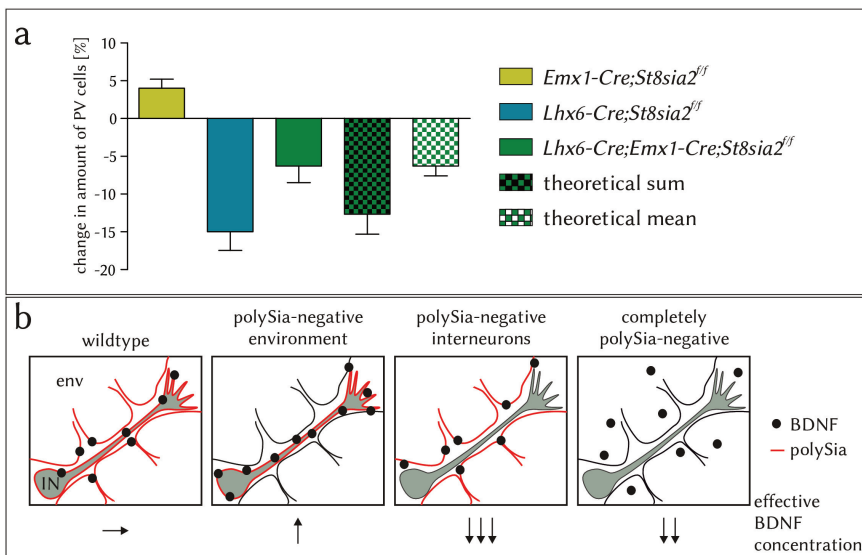
Figure 3.8: Working hypothesis for polySia-dependent sensing of BDNF. (a) Relative amounts of PV$^+$ interneurons in P90 old *Emx1-Cre;St8sia2$^{f/f}$*, *Lhx6-Cre;St8sia2$^{f/f}$*, *Lhx6-Cre;-Emx1-Cre;St8sia2$^{f/f}$* and mathematical approximations by calculation of the sum or the mean of the individual contributions observed in *Emx1-Cre;St8sia2$^{f/f}$* and *Lhx6-Cre;St8sia2$^{f/f}$* animals. (b) Model for the competition of environment (env) and interneurons (IN) for soluble factors (e.g. BDNF) via binding to polySia. The effective BDNF-concentration is indicated by black arrows.

Of note, genetic variations of *ST8SIA2* (Arai *et al.* 2006; Tao *et al.* 2007; Anney *et al.* 2010; McAuley *et al.* 2012; Gilabert-Juan *et al.* 2013) and *BDNF* as well as altered levels of BDNF have been linked to psychiatric disorders, such as schizophrenia and autism (Nieto *et al.* 2013; Qin *et al.* 2016; Saghazadeh and Rezaei 2017). Furthermore, loss of PV$^+$ interneurons is another hallmark of both diseases (Benes and Berretta 2001; Lewis *et al.* 2012; Hashemi *et al.* 2016) and alterations of BDNF or trkB have been linked to the loss of PV-interneurons (Hashimoto *et al.* 2005; Sakata *et al.* 2009; Zheng *et al.* 2011). Thus, the proposed model could provide a connection between dysregulation of ST8SIA2-activity and BDNF on the level of developmental interneuron migration impacting cortical interneuron distributions.

In conclusion, this study reveals a strong cell-autonomous role for ST8SIA2 in interneuron migration and in the distribution of interneurons in the anterior cortex. Furthermore, we demonstrate that the lack of polySia produced by ST8SIA2 leads to impaired recognition of BDNF and propose a model for polySia-dependent sensing of BDNF, which may contribute to the altered distribution of cortical interneurons in mice deficient for ST8SIA2.

3.5 Methods

Mice

All mice used in this work were bred at the central animal facility of Hannover Medical School. Protocols for animal use were in compliance with the German Animal Welfare Act and approved by the local authorities (Niedersächsisches Landesamt für Verbraucherschutz und Lebensmittelsicherheit, permissions no. 33.9-42502-04-10-0169 and -15/1902). Mice with a loxp sequence-insertion flanking exon 4 of *St8sia2* (*St8sia2$^{f/f}$*) were generated by a commercial supplier (Taconic Biosciences GmbH). A targeting vector comprising loxp-sequences flanking exon 4 and a neomycin resistance flanked by FRT sites inserted into intron 3 was transfected into C57BL/6N Tac embryonic stem cells and positive clones were implanted in a surrogate mother. By Flp-mediated removal of the neomycin resistance mice with the conditional allele (*St8sia2$^{f/f}$*) were obtained. In these mice recombination by *Cre*-recombinase will result in the deletion of exon 4, encoding a significant portion of the sialyl motif L, which is essential for sialyltransferase activity (Datta and Paulson 1995). The same strategy has been applied for the generation of *St8sia2$^{-/-}$* mice (Angata *et al.* 2004). Mice with the conditional *St8sia2*-allele were then cross-bred with mice expressing *Cre*-recombinase under an MGE-specific (*Lhx6-Cre*; Fragkouli *et al.* 2009), or a cortex-specific promotor (*Emx1-Cre*; Gorski *et al.* 2002, The Jackson Laboratory, Stock #005628). *Zp3-Cre* mice (Lewandoski *et al.* 1997) were used to obtain a mouse line with constitutively recombined *St8sia2* (*St8sia2$^{\Delta/\Delta}$*). All mouse strains were backcrossed with C57BL/6J mice for at least six generations. *St8sia2$^{+/+}$*, *St8sia2$^{-/-}$* (Angata *et al.* 2004) and *Lhx6-Cre;St8sia2$^{f/f}$* mice were cross-bred with GAD67-GFP knock-in mice (Tamamaki *et al.* 2003) to obtain *St8sia2$^{+/+}$;GAD67$^{GFP/+}$*, *St8sia2$^{-/-}$;GAD67$^{GFP/+}$* and *Lhx6-Cre;St8sia2$^{f/f}$;GAD67$^{GFP/+}$* animals for coculture assays and live imaging experiments. *St8sia4$^{-/-}$* mice (Eckhardt *et al.* 2000) were crossbred with *Lhx6-Cre;St8sia2$^{f/f}$* mice to obtain *Lhx6-Cre;St8sia2$^{f/f}$;St8sia4$^{-/-}$* mice. Genotyping of *St8sia2$^{-/-}$*, *St8sia4$^{-/-}$* and GAD67$^{GFP/+}$ mice was performed by PCR as previously described (Tamamaki *et al.* 2003; Weinhold *et al.* 2005). Genotyping of the conditional allele, Lhx6- and *Emx1-Cre* was performed utilizing the following primers: cond-1b (5'-GAGACAGCAACTAGAGGAATAACA-3') cond-2 (5'-CCTAGATGGGTTGGTGTTGC-3') for the floxed *St8sia2* allele, and cond-1b with cond-4 (5'-ACAGTTAGAACACCACCTTC-3') for the recombined *St8sia2* allele; iCreF (5'-GAGGGACTACCTCCTGTACC-3'), iCreR (5'-TGCCCAGAGTCATCC-TTGGC-3'), ctrl-F (5'-ACTGGGATCTTCGAACTCTTTGG-3') and ctrl-R (5'-GAT-GTTGGGGCACTGCTCATTCA-3') for the *Lhx6-Cre* allele; Emx-s (5'-GCGGTC-TGGCAGTAAAAACTATC-3'), Emx-as (5'-GTGAAACAGCATTGCTGTCACTT-3'), EmxWT-s (5'-AAGGTGTGGTTCCAGAATCG-3'), EmxWT-as (5'-CTCTCCACC-AGAAGGCTGAG-3') for the *Emx1-Cre* allele. For staging of embryos, the morning

of the vaginal plug was considered as E0.5. For the phenotypic analyses, P90 old *Lhx6-Cre;St8sia2*$^{f/f}$, *Emx1-Cre;St8sia2*$^{f/f}$ and *Lhx6-Cre;Emx1-Cre;St8sia2*$^{f/f}$ mice and whenever possible, *St8sia2*$^{f/f}$ littermates were obtained. Results from *St8sia2*$^{f/f}$ animals of different genotype-groups did not display statistically significant differences and were grouped.

qPCR-analysis

RNA-extraction from trizol-stored probes was performed by adding acrylamide solution (1:1000) and chloroform (1:5) and incubation for 10 minutes on ice. After centrifugation (13000 rpm, 4℃, 15 min), isopropanol was added to the aqueous phase and RNA was precipitated for 10 minutes at room temperature, followed by centrifugation. The pellet was dissolved in diethylpyrocarbonate (DEPC)-treated water with 3 M sodiumacetate solution pH 5.2 (1:10) and 2.5 x volumes of ethanol. After precipitation over night at -20℃ and centrifugation, the pellet was washed with 70% ethanol and dried. RNA was reconstituted in DEPC-treated water. Residual DNA was digested for 30 min at 37℃ in a total volume of 25 µL (1.25 µg RNA, 50 U RiboLock RNase inhibitor (Thermo Scientific), 2.5 U RQ1 DNase in RQ1 DNase buffer (Promega)). Stretching of RNA was performed for 10 min at 70℃ by addition of 10% (V/V) STOP solution and random hexamer primers (Invitrogen), followed by cDNA synthesis in a total volume of 50 µL (0.5 mM dNTPs (Thermo Scientific), 250 U RevertAid Premium Reverse Transcriptase in RevertAid buffer (Thermo Scientific)). qPCR was performed in a final volume of 20 µL containing 0.25 µM primer pair solution (5'-GCCTGGAGACATTATTCATTA-3' and 5'-GGAGGAGTTCATAGA-GGTT-3' for detection of the floxed allele; 5'-TCTCTGAGGATCAGGTGC-3' and 5'-TTCATGGTCACTAGGTCTGT-3' for the recombined allele), 0.2 mM dNTPs, 2.25 mM MgCl$_2$, 1.6 µL SYBR Green (diluted 1:104; Invitrogen), 0.2 µL ROX reference dye (Invitrogen) and 4 µL cDNA (1:10) in Maxima Hot Start reaction buffer. Mixtures were preheated to 50℃ for 20s, then 95℃ for 10 minutes. qPCR was performed in 40 cycles of 95℃ for 15s and 60℃ for 1min (7500 Fast Real-time PCR system, Applied Biosystems).

In situ hybridization

In-situ hybridization was performed as described previously (Diederichs 2013).

Immunohistochemistry

Perfusion, generation of 50 µm vibratom sections and immunofluorescent staining on free-floating sections was performed as described previously (Schiff *et al.* 2011), but instead of fetal calf serum, 2% normal goat serum (Vector) was added to the blocking buffer. The following monoclonal (mAb) or polyclonal (pAb) antibodies

Chapter 3

were used: pAb rabbit anti-CB D28-k (Swant CB38a, 1:5000), mAb mouse anti-PV (Swant, 1:5000), mAb mouse anti-beta-III-Tubulin IgG_{2b} (Sigma # T-8660, 1:200), mAb mouse-anti-polySia IgG_{2a} (Genovac, 1:2000), pAb rabbit anti-LHX6 (Santa Cruz # sc-98607, 1:400) and respective Alexa Fluor 488 conjugated goat anti-mouse IgG (Molecular Probes # A 21141), Alexa Fluor 568 conjugated goat anti-mouse IgG (Molecular Probes # A 21134), Alexa Fluor 647 conjugated goat anti-rabbit IgG H+L (Molecular Probes # A 21245), Alexa Fluor 488 conjugated donkey anti-mouse IgG (H+L) (Molecular Probes # A 21202) and anti-mouse IgG Cy3 (SIGMA # C2181) secondary antibodies. Staining specificity was controlled by omission of primary antibodies.

Coculture assay and live imaging

E13.5 heads of $St8sia2^{-/-};GAD67^{GFP/+}$, $St8sia2^{+/+};GAD67^{GFP/+}$, GFP-negative litter-mates, $Lhx6$-$Cre;St8sia2^{f/f};GAD67^{GFP/+}$ and $St8sia2^{f/f};GAD67^{GFP/+}$ mice were ob-tained and transferred to ice-cold dissection buffer (126 mM NaCl, 25 mM $NaHCO_3$, 11 mM D-glucose, 2.5 mM KCl, 2.5 mM $CaCl_2$, 1.2 mM NaH_2PO_4 and 1.2 mM $MgCl_2$ in double-destilled water). After removal of the meninges, GFP-negative heads were embedded in 4% Plaque Genetic Pure Agarose (Biozym) and 220 μm thick coronal sections were obtained with a vibrating microtome. Sections on the level of the ganglionic eminences were kept in ice cold dissection buffer supplemented with 10 mM HEPES, 1x penicillin/streptomycin (Merck) and 50 μg/ml gentamycin (Gibco). MGEs of $St8sia2^{-/-};GAD67^{GFP/+}$ and $St8sia2^{+/+};GAD67^{GFP/+}$ brains were dissected and divided into three equal-sized pieces each. After removal of the subpallium, two to three cortex-slices per embryo were transferred to Millicell cell culture inserts (PICMORG50, Merck-Millipore) and MGE-tissue was placed with a slight overlap onto the pallial-subpallial boundary. Remaining buffer was removed and cocultures were kept for 48 h at 37℃ and 5% CO_2 in 1 mL Neurobasal medium (Gibco) supplemented with 1x B27 (Gibco), 32 mM D-glucose, 1x penicillin/strep-tomycin and 1x glutamax (Gibco). After transfer of the tissue to superfrost object slides (Menzel), the tissue was fixed in 4% PFA for 20 minutes and washed two times with PBS and once with water. Dried tissue was embedded with 80 μL VectaShield (Vector) for DAPI-costaining.

   For live imaging sequences, GFP-positive heads were embedded, cut and stored as described above. For analysis of $St8sia2$-wildtype and –knockout animals, one section per embryo was transferred to an eight-well imaging slide (μ-Slide 8 well, ibitreat, ibidi). Embedding was conducted by application of 10 μL PBS with 0.05 U thrombin (restriction grade, Merck) and 20 μL chicken plasma (Sigma). Cortical tissue was kept at 37℃ and 5% CO_2 for 30 minutes for crosslinking before ap-plication of 200 μL supplemented neurobasal medium (see above). Live imaging was performed over night with 25 z-stacks acquired every 2 minutes. For live

imaging of *Lhx6-Cre;St8sia2$^{f/f}$;GAD67$^{GFP/+}$* and respective *St8sia2$^{f/f}$;GAD67$^{GFP/+}$* control cortices were transferred to Millicell cell culture inserts (PICMORG50, Merck-Millipore), cultivated with supplemented neurobasal medium and z-stacks consisting of 20 individual frames were acquired every three minutes. In this case, after three hours of imaging, cell culture inserts were transferred to another 6-well plate containing equilibrated medium with or without 50 ng/mL BDNF (Peprotech) and slices were imaged for three more hours. Interneurons on the same slice were analyzed before and after BDNF-application. Live imaging sequences were obtained at an Axio Observer.Z1 (Zeiss) with a Yonogawa CSU-X1 spinning disc unit, an EMCCD camera (QuantEM:512SC) and an incubation chamber (Incubator XLmulti S1 and P-Set 2000, Pecon) with a 10x Plan-Apochromat objective with 0.45 numerical aperture (Zeiss). Z-stacks were subsequently superimposed by maximum projection. For analysis of migration parameters, image sequences representing a time-course of three hours were analyzed. Migration trajectories were measured, nuclear translocalizations were counted and for *St8sia2*-wildtype and –knockout animals, the highest degree of branching during the observation was noted.

MGE Primary Culture

MGE primary cultures from E14.5 *Lhx6-Cre;St8sia2$^{f/f}$;St8sia4$^{-/-}$* animals were obtained as previously described (Kröcher *et al.* 2014).

Image acquisition, cell counting and distance-calculations

For analysis of interneuron distributions in adult mice, at least six sections of *n* = 5 – 13 animals (dependent on the experimental group) were analyzed. Sections were distributed in six groups matching bregma levels 1.10 to 1.94 based on Paxinos and Franklin 2001. Double staining for PV and CB was conducted and images were acquired with an Axio Observer.Z1, equipped with an ApoTome device for near-confocal imaging by use of structured illumination and an AxioCam MRm digital camera. Optical sections of 5.11 μm (488 channel) and 5.54 μm (568 channel) were obtained using a 10x Plan-Apochromat objective with 0.45 numerical aperture (Zeiss). Single images were stitched with Zen2012 (Zeiss). Regions of interest were identified by fitting a template based on respective bregma layers (Paxinos and Franklin 2001) and blind analysis was subsequently performed. Upper and deep layers were separated by inspection of the DAPI immunostaining pattern. Cell countings of both hemisspheres were averaged and mean values of all animals were visualized in heatplots using MATLAB. Analysis of the laminar distribution of interneurons and the infiltration depth in coculture was conducted by calculation of the shortest distance of each cell to the forceps minor of the corpus callosum or the MGE-border, respectively, using MATLAB and subsequent binning.

Densitometric analysis

For densitometric analysis, at least three consecutive 50 μm sections were stained for polySia and optical sections were acquired as described above. Three equal-sized rectangles were placed in the SVZ of MGE and LGE and into the cortical plate of the neocortex using Zen 2012 Software (Zeiss). Mean gray values were obtained from both hemispheres and averaged. Mean values of at least three animals per group were compared.

Statistical analysis

All statistical comparisons were conducted with Prism 4.0 (GraphPad) and all values are given as mean ± s.e.m. Paired or unpaired t-tests, one- or two-way ANOVA with subsequent application of the Bonferroni post-tests were applied as indicated.

Acknowledgements

Competing interests

The authors declare no competing financial interests.

Author contributions

U.E.S. and C.R. performed all experiments. I.M. contributed to analysis of the BDNF-response in live imaging experiments. U.E.S. and M.S. organized breeding of mice. U.E.S. analyzed the data and together with H.H. planned all experiments and wrote the manuscript.

Funding

3.6 Bibliography

Ang E S, Haydar T F, Gluncic V, and Rakic P (2003) Four-dimensional migratory co-ordinates of GABAergic interneurons in the developing mouse cortex. J. Neurosci. 23:5805–15.

Angata K, Long J M, Bukalo O, Lee W, Dityatev A, Wynshaw-Boris A, Schachner M, Fukuda M, and Marth J D (2004) Sialyltransferase ST8Sia-II assembles a subset of polysialic acid that directs hippocampal axonal targeting and promotes fear behavior. J. Biol. Chem. 279:32603–32613.

Anney R, Klei L, Pinto D, Regan R, Conroy J, Magalhaes T R, Correia C, Abrahams B S, Sykes N, Pagnamenta A T, *et al.* (2010) A genome-wide scan for common alleles affecting risk for autism. Hum. Mol. Genet. 19:4072–4082.

Arai M, Yamada K, Toyota T, Obata N, Haga S, Yoshida Y, Nakamura K, Minabe Y, Ujike H, Sora I, Ikeda K, Mori N, Yoshikawa T, and Itokawa M (2006) Association between polymorphisms in the promoter region of the sialyltransferase 8B (SIAT8B) gene and schizophrenia. Biol. Psychiatry 59:652–659.

Benes F M and Berretta S (2001) GABAergic interneurons: implications for understanding schizophrenia and bipolar disorder. Neuropsychopharmacology 25:1.

Burgess A and Aubert I (2006) Polysialic acid limits choline acetyltransferase activity induced by brain-derived neurotrophic factor. J. Neurochem. 99.

Datta A K and Paulson J C (1995) The sialyltransferase sialylmotif participates in binding the donor substrate CMP-NeuAc. J. Biol. Chem. 270:1497–1500.

Denaxa M, Chan C, Schachner M, Parnavelas J, and Karagogeos D (2001) The adhesion molecule TAG-1 mediates the migration of cortical interneurons from the ganglionic eminence along the corticofugal fiber system. Development 128:4635–44.

Denaxa M, Kyriakopoulou K, Theodorakis K, Trichas G, Vidaki M, Takeda Y, Watanabe K, and Karagogeos D (2005) The adhesion molecule TAG-1 is required for proper migration of the superficial migratory stream in the medulla but not of cortical interneurons. Dev. Biol. 288:87–99.

Di Cristo G (2007) Development of cortical GABAergic circuits and its implications for neurodevelopmental disorders. Clin. Genet. 72:1–8.

Diederichs U (2013) *Expression der Polysialyltransferase ST8SIA2 und Analyse der Gehirnentwicklung bei Mäusen mit hirnregionsspezifischer Deletion der ST8SIA2*. Master Thesis. Hannover Medical School.

Eckhardt M, Bukalo O, Chazal G, Wang L, Goridis C, Schachner M, R G, Cremer H, and Dityatev A (2000) Mice deficient in the polysialyltransferase ST8SiaIV/PST-1 allow discrimination of the roles of neural cell adhesion molecule protein and polysialic acid in neural development and synaptic plasticity. J. Neurosci. 20:5234–44.

Fogarty M, Grist M, Gelman D, Marín O, Pachnis V, and Kessaris N (2007) Spatial genetic patterning of the embryonic neuroepithelium generates GABAergic interneuron diversity in the adult cortex. J. Neurosci. 27:10935–46.

Fragkouli A, Wijk N, Lopes R, Kessaris N, and Pachnis V (2009) LIM homeodomain transcription factor-dependent specification of bipotential MGE progenitors into cholinergic and GABAergic striatal interneurons. Development 136:3841–3851.

Galuska S, Imke O, Geyer H, Weinhold B, Kuchelmeister K, Hildebrandt H, Rita G, Geyer R, and Mühlenhoff M (2006) Polysialic acid profiles of mice expressing variant allelic combinations of the polysialyltransferases ST8SiaII and ST8SiaIV. J. Biol. Chem. 281:31605–31615.

Gilabert-Juan J, Nacher J, Sanjuán J, and Moltó M D (2013) Sex-specific association of the ST8SIAII gene with schizophrenia in a Spanish population. Psychiatry Res. 210:1293–1295.

Gordon J A and Stryker M P (1996) Experience-dependent plasticity of binocular responses in the primary visual cortex of the mouse. J. Neurosci. 16:3274–3286.

Gorski J, Talley T, Qiu M, Puelles L, Rubenstein J, and Jones K (2002) Cortical excitatory neurons and glia, but not GABAergic neurons, are produced in the Emx1-expressing lineage. J. Neurosci. 22:6309–14.

Guo J and Anton E (2014) Decision making during interneuron migration in the developing cerebral cortex. Trends Cell Biol. 24:342–351.

Hashemi E, Ariza J, Rogers H, Noctor S, and Verónica M (2016) The number of parvalbumin-expressing interneurons is decreased in the medial prefrontal cortex in autism. Cereb. Cortex 27:1931–1943.

Hashimoto T, Bergen S E, Nguyen Q L, Xu B, Monteggia L M, Pierri J N, Sun Z, Sampson A R, and Lewis D A (2005) Relationship of brain-derived neurotrophic factor and its receptor TrkB to altered inhibitory prefrontal circuitry in schizophrenia. J. Neurosci. 25:372–383.

Hildebrandt H, Mühlenhoff M, and Gerardy-Schahn R (2010) Polysialylation of NCAM. Adv. Exp. Med. Biol. 663:95–109.

Kanato Y, Kitajima K, and Sato C (2008) Direct binding of polysialic acid to a brain-derived neurotrophic factor depends on the degree of polymerization. Glycobiology 18:1044–53.

Kröcher T, Malinovskaja K, Jürgenson M, Anu A, Zharkovskaya T, Kalda A, Röckle I, Schiff M, Weinhold B, Rita G, Hildebrandt H, and Zharkovsky A (2015) Schizophrenia-like phenotype of polysialyltransferase ST8SIA2-deficient mice. Brain Struct. Funct. 220:71–83.

Kröcher T, Röckle I, Diederichs U, Weinhold B, Burkhardt H, Yanagawa Y, Gerardy-Schahn R, and Hildebrandt H (2014) A crucial role for polysialic acid in developmental interneuron migration and the establishment of interneuron densities in the mouse prefrontal cortex. Development 141:3022–3032.

Lewandoski M, Wassarman K, and Martin G (1997) Zp3-cre, a transgenic mouse line for the activation or inactivation of loxP-flanked target genes specifically in the female germ line. Curr. Biol. 7:148–51.

Lewis D A, Curley A A, Glausier J R, and Volk D W (2012) Cortical parvalbumin interneurons and cognitive dysfunction in schizophrenia. Trends Neurosci. 35:57–67.

López-Bendito G and Molnár Z (2003) Thalamocortical development: how are we going to get there? Nat. Rev. Neurosci. 4:276.

López-Bendito G, Cautinat A, Sánchez J A, Bielle F, Flames N, Garratt A N, Talmage D A, Role L W, Charnay P, Marín O, *et al.* (2006) Tangential neuronal migration controls axon guidance: a role for neuregulin-1 in thalamocortical axon navigation. Cell 125:127–142.

McAuley E, Scimone A, Tiwari Y, Agahi G, Mowry B, Holliday E, Donald J, Weickert C, Mitchell P, Schofield P, and Fullerton J (2012) Identification of sialyltransferase 8B as a generalized susceptibility gene for psychotic and mood disorders on chromosome 15q25-26. PLoS One 7:e38172.

Miyamae T, Chen K, Lewis D A, and Gonzalez-Burgos G (2017) Distinct physiological maturation of parvalbumin-positive neuron subtypes in mouse prefrontal cortex. J. Neurosci. 37:4883–4902.

Miyoshi G and Fishell G (2010) GABAergic interneuron lineages selectively sort into specific cortical layers during early postnatal development. Cereb. Cortex 21:845–52.

Muller D, Djebbara-Hannas Z, Jourdain P, Vutskits L, Durbec P, Rougon G, and Kiss J Z (2000) Brain-derived neurotrophic factor restores long-term potentiation in polysialic acid-neural cell adhesion molecule-deficient hippocampus. Proc. Natl. Acad. Sci. U.S.A. 97:4315–4320.

Nery S, Fishell G, and Corbin J G (2002) The caudal ganglionic eminence is a source of distinct cortical and subcortical cell populations. Nat. Neurosci. 5:1279.

Nieto R, Kukuljan M, and Silva H (2013) BDNF and schizophrenia: from neurodevelopment to neuronal plasticity, learning, and memory. Front. Psychiatry 4:45.

Oltmann-Norden I, Galuska S P, Hildebrandt H, Geyer R, Gerardy-Schahn R, Geyer H, and Mühlenhoff M (2008) Impact of the polysialyltransferases ST8SiaII and ST8SiaIV on polysialic acid synthesis during postnatal mouse brain development. J. Biol. Chem. 283:1463–1471.

Paxinos G and Franklin K B J (2001) *The mouse brain in stereotaxic coordinates.* Academic press San Diego, CA.

Polleux F, Whitford K L, Dijkhuizen P A, Vitalis T, and Ghosh A (2002) Control of cortical interneuron migration by neurotrophins and PI3-kinase signaling. Development 129:3147–3160.

Chapter 3

Qin X Y, Feng J C, Cao C, Wu H T, Loh Y P, and Cheng Y (2016) Association of peripheral blood levels of brain-derived neurotrophic factor with autism spectrum disorder in children: a systematic review and meta-analysis. JAMA Pediatr. 170:1079–1086.

Rhodes K and Fawcett J (2004) Chondroitin sulphate proteoglycans: preventing plasticity or protecting the CNS? J. Anat. 204:33–48.

Rudy B, Fishell G, Lee S, and Hjerling-Leffler J (2011) Three groups of interneurons account for nearly 100% of neocortical GABAergic neurons. Dev. Neurobiol. 71:45–61.

Rutishauser U (2008) Polysialic acid in the plasticity of the developing and adult vertebrate nervous system. Nat. Rev. Neurosci. 9:26–35.

Saghazadeh A and Rezaei N (2017) Brain-derived neurotrophic factor levels in autism: a systematic review and meta-analysis. J. Autism Dev. Disord. 47:1018–1029.

Sakata K, Woo N H, Martinowich K, Greene J S, Schloesser R J, Shen L, and Lu B (2009) Critical role of promoter IV-driven BDNF transcription in GABAergic transmission and synaptic plasticity in the prefrontal cortex. Proc. Natl. Acad. Sci. U.S.A. 106:5942–5947.

Schiff M, Röckle I, Burkhardt H, Weinhold B, and Hildebrandt H (2011) Thalamocortical pathfinding defects precede degeneration of the reticular thalamic nucleus in polysialic acid-deficient mice. J. Neurosci. 31:1302–1312.

Schiff M, Weinhold B, Grothe C, and Hildebrandt H (2009) NCAM and polysialyltransferase profiles match dopaminergic marker gene expression but polysialic acid is dispensable for development of the midbrain dopamine system. J. Neurochem. 110:1661–73.

Schnaar R L, Gerardy-Schahn R, and Hildebrandt H (2014) Sialic acids in the brain: gangliosides and polysialic acid in nervous system development, stability, disease, and regeneration. Physiol. Rev. 94:461–518.

Sumida M, Hane M, Yabe U, Shimoda Y, Pearce O M, Kiso M, Miyagi T, Sawada M, Varki A, Kitajima K, *et al.* (2015) Rapid trimming of cell surface polysialic acid (PolySia) by exovesicular sialidase triggers release of preexisting surface neurotrophin. J. Biol. Chem. 290:13202–13214.

Tamamaki N, Fujimori K, Nojyo Y, Kaneko T, and Takauji R (2003) Evidence that Sema3A and Sema3F regulate the migration of GABAergic neurons in the developing neocortex. J. Comp. Neurol. 455:238–48.

Tao R, Li C, Zheng Y, Qin W, Zhang J, Li X, Xu Y, Shi Y, Feng G, and He L (2007) Positive association between SIAT8B and schizophrenia in the Chinese Han population. Schizophr. Res. 90:108–114.

Ueda S, Niwa M, Hioki H, Sohn J, Kaneko T, Sawa A, and Sakurai T (2015) Sequence of molecular events during the maturation of the developing mouse prefrontal cortex. Mol. Neuropsychiatry 1:94–104.

Vutskits L, Djebbara-Hannas Z, Zhang H, Paccaud J, Durbec P, Rougon G, Muller D, and Kiss J (2001) PSA-NCAM modulates BDNF-dependent survival and differentiation of cortical neurons. Eur. J. Neurosci. 13:1391–402.

Weinhold B, Seidenfaden R, Röckle I, Mühlenhoff M, Schertzinger F, Conzelmann S, Marth J, Rita G, and Hildebrandt H (2005) Genetic ablation of polysialic acid causes severe neurodevelopmental defects rescued by deletion of the neural cell adhesion molecule. J. Biol. Chem. 280:42971–7.

Yamamoto N, Inui K, Matsuyama Y, Harada A, Hanamura K, Murakami F, Ruthazer E S, Rutishauser U, and Seki T (2000) Inhibitory mechanism by polysialic acid for lamina-specific branch formation of thalamocortical axons. J. Neurosci. 20:9145–9151.

Zheng K, An J J, Yang F, Xu W, Xu Z Q D, Wu J, Hökfelt T G, Fisahn A, Xu B, and Lu B (2011) TrkB signaling in parvalbumin-positive interneurons is critical for gamma-band network synchronization in hippocampus. Proc. Natl. Acad. Sci. U.S.A. 108:17201–17206.

Chapter 3

Impact of St8sia2 in Foxb1- and Emx1-expressing cells on long-range connectivity of the mammillary body

Ute E. Schuster[1], Herbert Hildebrandt[1,2,#]

[1] *Institute of Clinical Biochemistry, Hannover Medical School, Carl-Neuberg-Str. 1, 30625 Hannover, Germany*
[2] *Center for Systems Neuroscience Hannover (ZSN), Hannover, Germany*
[#] *Corresponding author: Herbert Hildebrandt*

Institute of Clinical Biochemistry (4340), Hannover Medical School,
Carl-Neuberg-Str. 1, 30625 Hannover, Germany
Phone: +49 511 532 9808, Fax: +49 511 532 8801
e-mail: hildebrandt.herbert@mh-hannover.de

About the manuscript
U.E.S. organized and performed all experiments, analyzed the data and created the figures. Validation of the conditional knockout by *in-situ* hybridization and genomic PCR was performed during my master thesis. U.E.S. and H.H. designed experiments and wrote the manuscript.

4

Impact of *St8sia2* in *Foxb1-* and *Emx1*-expressing cells on long-range connectivity of the mammillary body

Chapter 4

4.1 Abstract

ST8SIA2 is a key regulator of polysialic acid synthesis during embryonic development. Mice lacking ST8SIA2 show deficits of cortical interneurons and thalamus-cortex connectivity, which may be linked to impaired working memory and sensorimotor gating. Here, we compared mice with conventional or conditional knockout of *St8sia2*, targeting either the diencephalon (*Foxb1-Cre;St8sia2$^{f/f}$*) or the cortex (*Emx1-Cre;St8sia2$^{f/f}$*), to dissect the neuropathological consequences of ST8SIA2 deficiency for thalamic and cortical long-range connectivity as well as for cortical interneuron distribution. In contrast to the conventional knockout, deletion of *St8sia2* by *Foxb1-Cre* and/or *Emx1-Cre* caused no hypoplasia of the internal capsule in the adult and no defects of thalamocortical or corticofugal fibers in embryonic development. Amending previous findings for *Emx1-Cre;St8sia2$^{f/f}$*, *Foxb1-Cre;St8sia2$^{f/f}$* mice also lacked the marked reduction of parvalbumin-positive interneurons observed in *St8sia2$^{-/-}$* mice. However, size reductions of the mammillothalamic tract and the mammillary body were detected in *St8sia2*-negative mice and reproduced in the *Foxb1-Cre;St8sia2$^{f/f}$* line. In contrast, *Emx1-Cre;St8sia2$^{f/f}$* mice recapitulated deficits of the corpus callosum and hypoplasia of the postcommissural fornix caused by a complete loss of ST8SIA2. Unexpectedly, mild hypoplasia of the mammillothalamic tract or the fornix were also detected in *Emx1-Cre;St8sia2$^{f/f}$* or *Foxb1-Cre;St8sia2$^{f/f}$* mice, respectively, highlighting the close functional and

anatomical relation between these parts of the Papez circuit. Together these data reveal that *Foxb1-Cre;St8sia2$^{f/f}$* mice are a suitable animal model to study, whether any of the behavioral consequences of ST8SIA2-deficiency can be attributed to disturbed long-range connectivity of the mammillary body.

4.2 Introduction

Polysialylation of the neural cell adhesion molecule NCAM is a unique posttranslational modification that is essential for the regulation of cellular interactions (Rutishauser 2008; Schnaar *et al.* 2014). Synthesis of polysialic acid (polySia) is mediated by the two polysialyltransferases ST8SIA2 and ST8SIA4 (Hildebrandt *et al.* 2010). Analyses of polysialyltransferase-negative mice demonstrated that polySia is essential for proper brain development (Weinhold *et al.* 2005; Angata *et al.* 2007; Hildebrandt *et al.* 2009). Among other defects, these mice display hypoplasia of major brain axon tracts, like corpus callosum (cc), internal capsule (ic), and mammillothalamic tract (mth, Weinhold *et al.* 2005; Hildebrandt *et al.* 2009). Hypoplasia of the internal capsule is a result of defective pathfinding of thalamocortical and corticofugal axons, which also leads to reduced innervation and degeneration of the reticular thalamic nucleus (Rt, Schiff *et al.* 2011), an essential regulator of thalamus-cortex circuits. Forming a curved sheet around the thalamus, the reticular thalamic nucleus consists of GABAergic neurons that receive glutamatergic input from collaterals of thalamocortical and corticofugal axons and send inhibitory projections to the other thalamic nuclei (Sherman 2016).

Hypoplasia of the internal capsule has also been detected in mice deficient for ST8SIA2, but the defect was significantly smaller than in *St8sia2$^{-/-}$ St8sia4$^{-/-}$* double-knockout animals (Hildebrandt *et al.* 2009). Subsequently, it was found that adult *St8sia2$^{-/-}$* mice also display reduced thalamic input to the cortex and a marked disorganization of fibers traversing the reticular thalamic nucleus (Kröcher *et al.* 2015). In addition, these mice show several behavioral abnormalities like impaired working memory, deficits in prepulse inhibition and increased sensitivity to amphetamine-induced hyperlocomotion.

Apart from compromised thalamus-cortex connectivity, mice deficient for ST8SIA2 display reduced densities of parvalbumin- and somatostatin-positive interneuron populations in the prefrontal cortex and altered developmental migration of these interneurons from their region of origin, the medial ganglionic eminence (MGE), into the embryonic cortex (Kröcher *et al.* 2014, see Chapter 2). Moreover, reduced amounts of parvalbumin-positive interneurons were observed only in mice with a conditional knockout of *St8sia2* in MGE-derived interneurons (*Lhx6-Cre;St8sia2$^{f/f}$*) but not in mice with a loss of ST8SIA2 in the developing cortex (*Emx1-Cre;St8sia2$^{f/f}$*, Schuster et al in preparation, see Chapter 3). Nevertheless, defects in the consti-

tutively ST8SIA2-negative mice were more pronounced than those in *Lhx6-Cre;-St8sia2$^{f/f}$* (Schuster et al in preparation, see Chapter 3), indicating that other factors such as defective innervation by thalamocortical axons might contribute to the loss of cortical interneurons in *St8sia2$^{-/-}$* mice.

So far it is not known, if the behavioral deficits of *St8sia2$^{-/-}$* mice are linked to deficits of thalamus-cortex connectivity or interneurons or to other, yet undisclosed defects. Possibly, changes of the mammillothalamic tract, as observed in the *St8sia2$^{-/-}$ St8sia4$^{-/-}$* double-knockout animals, might be present in *St8sia2$^{-/-}$* mice. As part of the Papez circuit (Papez 1937), mammillothalamic fibers project from the mammillary body of the hypothalamus to nuclei of the thalamus. Ablation of the mammillary body or lesions of the mammillothalamic tract cause impaired spatial working memory (Vann and Aggleton 2003; Radyushkin *et al.* 2005; Vann *et al.* 2011; Vann 2013). This effect was not obtained by lesioning of the postcommissural fornix, providing excitatory input from the hippocampus to the mammillary bodies.

Here, we used *Foxb1-Cre* (Zhao *et al.* 2007) and *Emx1-Cre* mice (Gorski *et al.* 2002) for a targeted deletion of *St8sia2* in the diencephalon and the cortex and analyzed the consequences for thalamus-cortex and mammillary body connectivity. Furthermore, we screened adult *Foxb1-Cre;St8sia2$^{f/f}$* mice for alterations of cortical interneurons or impaired thalamic input to the cortex.

Chapter 4

4.3 Results

Functional inactivation of ST8SIA2 mediated by Foxb1-Cre

To validate the conditional recombination of *St8sia2* (Fig 4.1a) in *Foxb1-Cre;St8sia2$^{f/f}$* mice, the presence of the recombined allele in thalamic tissue at embryonic day 13.5 (E13.5) was confirmed by genomic PCR (Fig 4.1b). Expression of *St8sia2* in the dorsal thalamus was verified by *in situ* hybridization (Fig 4.1c). The loss of *St8sia2* in *Foxb1-Cre;St8sia2$^{f/f}$* mice could not be analyzed by *in situ* hybridization, because it was not possible to generate riboprobes that were able to distinguish between transcripts of floxed and recombined alleles. qPCR with primers targeting exon 4 of *St8sia2* or the exon 3 to exon 5 boundary obtained by CRE-mediated recombination revealed a significant reduction of wildtype mRNA and identified transcripts of the recombined allele in isolated thalamic tissue of E14.5 *Foxb1-Cre;St8sia2$^{f/f}$* embryos (Fig 4.1d). Together these results demonstrate that ST8SIA2 is expressed in the targeted brain region and that the conditional knockout is functional.
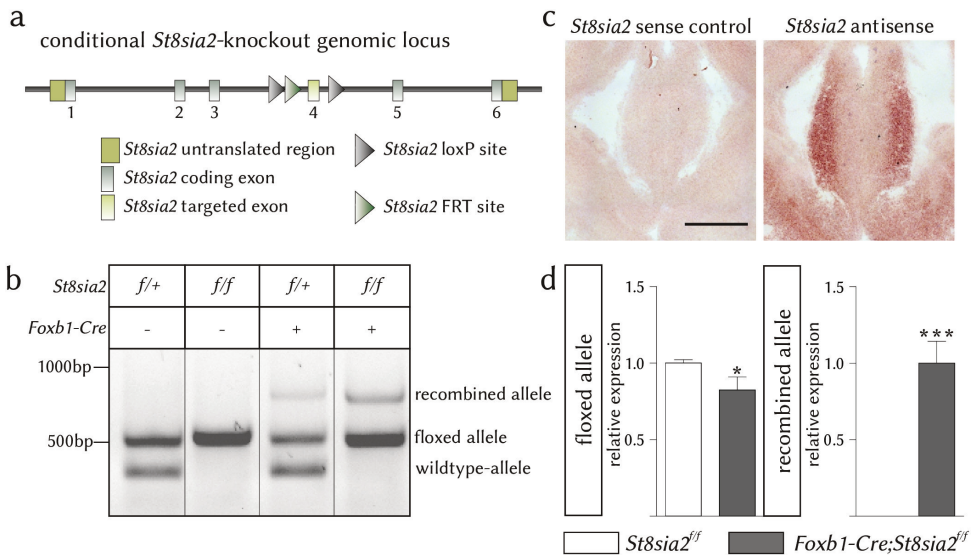
Figure 4.1: Validation of the *Foxb1-Cre* mediated conditional knockout of *St8sia2*. (a) Structure of the conditional *St8sia2* allele with loxp sequences flanking exon 4 (referred to as the 'floxed' allele). (b) Genomic PCR of thalamic tissue isolated from animals homozygous (*f/f*) or heterozygous (*f/+*) for the floxed allele with (+) or without (-) *Foxb1-Cre* expression at E13.5. (c) *In situ* hybridization of E13.5 coronal sections obtained from *St8sia2$^{f/f}$* embryos with sense and antisense riboprobes against *St8sia2*. Scale bar represent 500 μm. (d) qPCR analysis of E14.5 isolated thalamic tissue of *St8sia2$^{f/f}$* and *Foxb1-Cre;St8sia2$^{f/f}$* animals detecting transcripts of floxed (left) and recombined alleles (right). Values are mean ± s.e.m. of *n* = **6** wildtype and *n* = **3** knockout animals and values for each embryo were obtained by three technical replicates. Statistical analyses by t-tests indicated significant differences (* P < **0.05**, *** P < **0.0001**).

ST8SIA2 in Emx1-expressing cells causes hypoplasia of the corpus callosum but not of the internal capsule

In *St8sia2*-negative mice generated by cross-breeding of *Zp3-Cre* animals with *St8sia2$^{f/f}$* mice (*St8sia2$^{\Delta/\Delta}$*, Schuster et al in preparation, see Chapter 3) the rostrocaudal extent of the corpus callosum was significantly reduced at postnatal day 90 (P90; Fig 4.2b). This is consistent with a previous analysis of *St8sia2$^{-/-}$* mice at P30 (Hildebrandt *et al.* 2009), although the effect was not significant, which could be due to differences in age and/or a smaller sample size in the former study. The same reduction in the rostrocaudal extent of the corpus callosum was found in *Emx1-Cre;St8sia2$^{f/f}$* and, although not significant, in *Foxb1-Cre;Emx1-Cre;St8sia2$^{f/f}$*, but not in *Foxb1-Cre;St8sia2$^{f/f}$* or *Lhx6-Cre;St8sia2$^{f/f}$* animals, indicating that the hypoplasia of the corpus callosum is caused by loss of ST8SIA2 in the cortex.
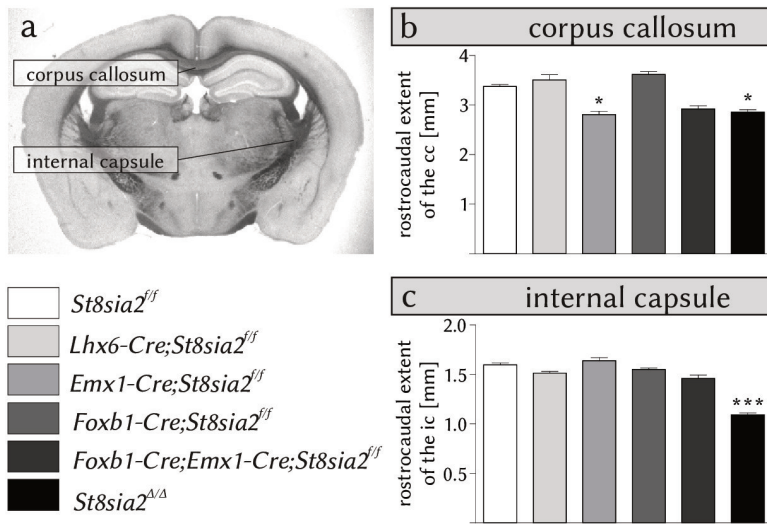
Figure 4.2: Hypoplasia of the corpus callosum is recapitulated by inactivation of ST8SIA2 in *Emx1*-expressing cells. (a) Representative image of a coronal brain section obtained from an *St8sia2$^{f/f}$* control at P90. The corpus callosum (cc) and the internal capsule (ic) are depicted. The rostrocaudal extent of the cc (b) and the ic (c) were determined in $n = 19$ controls, $n = 6$ *Lhx6-Cre;St8sia2$^{f/f}$*, $n = 5$ *Emx1-Cre;St8sia2$^{f/f}$*, $n = 6$ *Foxb1-Cre;St8sia2$^{f/f}$*, $n = 5$ *Foxb1-Cre;Emx1-Cre;St8sia2$^{f/f}$* and $n = 6$ *St8sia2$^{\Delta/\Delta}$* animals. Values are mean ± s.e.m. and analyses by non-parametric one-way ANOVA indicated significant differences ($P < 0.0001$ for b and c). The Kruskal-Wallis post-test was applied and statistical differences compared to the control group are depicted (*, $P < 0.05$; ***, $P < 0.001$).

Inactivation of ST8SIA2 in the thalamus or the cortex does not lead to impaired thalamus-cortex connectivity

Consistent with published results (Hildebrandt *et al.* 2009), the rostrocaudal extent of the internal capsule was strongly reduced in *St8sia2$^{\Delta/\Delta}$* mice (Fig 4.2c). This phenotype was not recapitulated in any of the conditional knockout lines, including *Foxb1-Cre;Emx1-Cre;St8sia2$^{f/f}$* mice, indicating that even the loss of ST8SIA2 in thalamocortical and corticofugal axons is not causing the hypoplasia of the internal capsule observed in *St8sia2$^{\Delta/\Delta}$* mice.

Even in the absence of severe anatomical changes a specific reduction of polySia on thalamocortical or corticofugal fibers during embryonic development could impact the maintenance of the reticular thalamic nucleus or lead to disorganized thalamus-cortex connectivity. However, analyses of adult *Emx1-Cre;St8sia2$^{f/f}$*, *Foxb1-Cre;St8sia2$^{f/f}$* and *Foxb1-Cre;Emx1-Cre;St8sia2$^{f/f}$* animals revealed a normally shaped reticular thalamic nucleus (Fig 4.3a-d') and traversing fibers displayed

the same organized patterning as in control mice (Fig 4.3a''-d'''). *St8sia2$^{\Delta/\Delta}$* mice, however, reproduced the overall deformation as well as the disorganization of fibers traversing the reticular thalamic nucleus described for *St8sia2$^{-/-}$* mice (Fig 4.3e-e'''; Kröcher et al. 2015).

To address the possibility that early developmental deficits occur in *Foxb1-Cre;-St8sia2$^{f/f}$* or *Emx1-Cre;St8sia2$^{f/f}$* animals, which then are compensated in adult mice, the pattern of thalamocortical and corticofugal fibers was analyzed at embryonic stage E14.5 (Fig 4.4). Staining with L1- and TAG1-specific antibodies in *St8sia2$^{f/f}$* embryos (Fig. 4a) revealed the normal pattern of thalamocortical and corticofugal fibers at E14.5 (Schiff *et al.* 2011). Thalamocortical axons traverse the internal capsule, turn dorsally towards the cortex and meet the corticofugal axons in the subpallium (the "handshake"). The same pattern was detected in *Lhx6-Cre;St8sia2$^{f/f}$* (data not shown), as well as in *Emx1-Cre;St8sia2$^{f/f}$*, *Foxb1-Cre;St8sia2$^{f/f}$* and *Foxb1-Cre;-Emx1-Cre;St8sia2$^{f/f}$* embryos (Fig 4.4b-d). For unknown reasons, however, TAG-1 immunostaining of *Emx1-Cre;St8sia2$^{f/f}$* embryos (Fig. 4c) yielded strong signals in the subpallium, which may be due to unspecific staining of blood vessels. In contrast, analysis of *St8sia2$^{\Delta/\Delta}$* embryos revealed that the L1-positive thalamocortical axons failed to turn dorsally and that the TAG-1 expressing corticofugal axons are virtually absent (Fig 4.4e). This defect in *St8sia2$^{\Delta/\Delta}$* mice is very similar to that observed in the completely polySia-negative *St8sia2$^{-/-}$St8sia4$^{-/-}$* double-knockout animals (Schiff *et al.* 2011).

Even though we were unable to detect severe anatomical defects, minor changes of thalamocortical innervation in *Foxb1-Cre;St8sia2$^{f/f}$* mice may cause altered glutamatergic input into the cortex. Axon terminals of thalamocortical fibers express the vesicular glutamate transporter VGLUT2, whereas corticofugal axons express VGLUT1 (Kaneko and Fujiyama 2002; Graziano *et al.* 2008). To evaluate glutamatergic thalamic input into the cortex, we analyzed levels of VGLUT2 in extracts of isolated thalamic and cortical tissue by Western blot relative to GAPDH and VGLUT1. An exemplary Western blot is shown in Fig 4.5a. Statistical analysis did not reveal any differences, indicating unaltered glutamatergic innervation of the cortex and the thalamus (Fig 4.5b).

We earlier reported a pronounced loss of parvalbumin- (PV) positive interneurons in the anterior cortex of *St8sia2*-deficient mice that was not fully reproduced by *St8sia2*-deletion in interneurons or their cortical environment (Schuster et al in preparation, see Chapter 3). This raised the possibility that cortical interneuron development could be affected by altered polySia-levels on thalamocortical fibers invading the cortex during the phase of interneuron migration, or by altered thalamocortical innervation. To assess, if loss of ST8SIA2 in the thalamus may contribute to the loss of interneurons in *St8sia2*-negative animals, interneuron populations in the cortex of adult *Foxb1-Cre;St8sia2$^{f/f}$* mice were analyzed. As presented by heatplots (Fig 4.6a-b) and corresponding bar diagrams (Fig 4.6c-h),
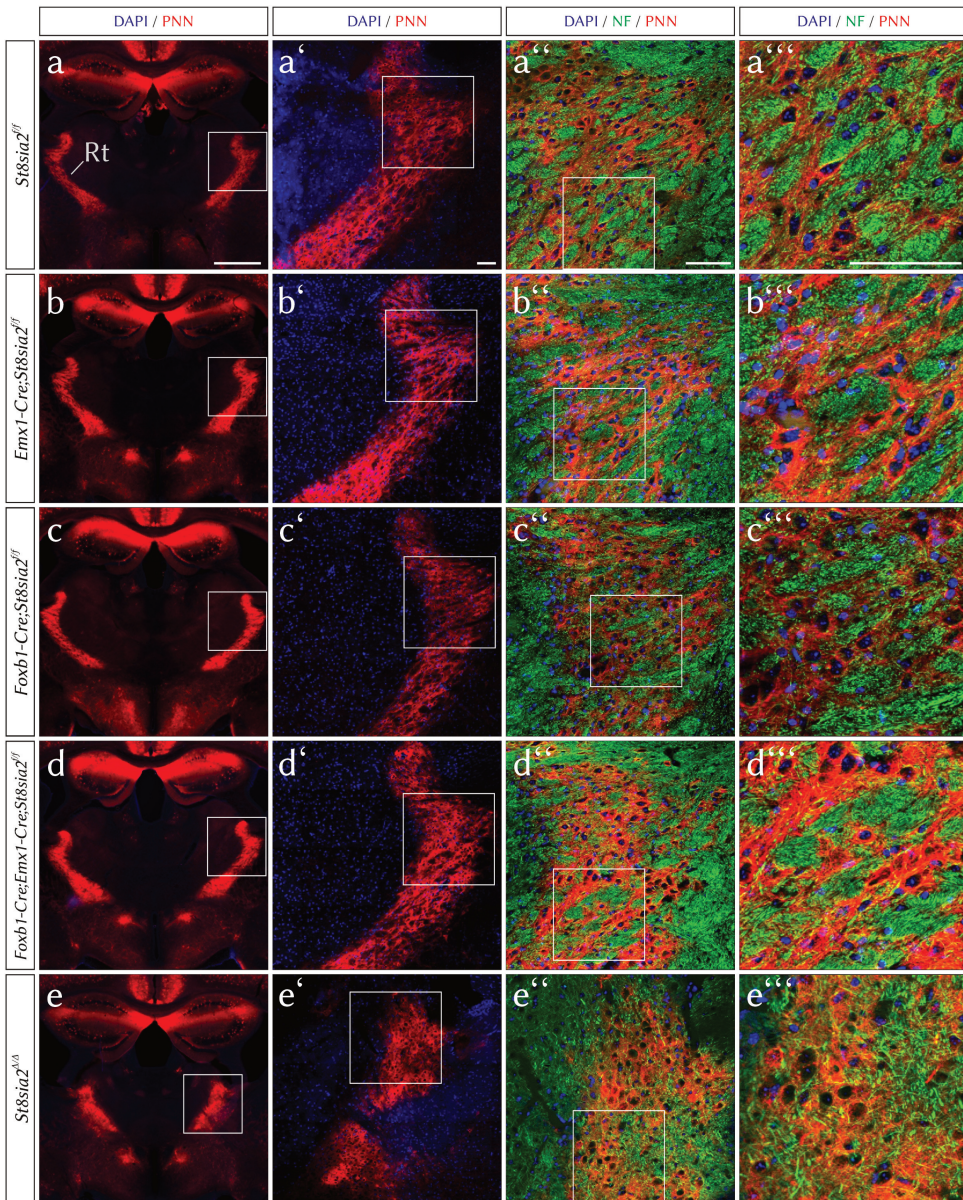
Figure 4.3: Organized patterning of fibers traversing the reticular thalamic nucleus in mice with conditional knockout of *St8sia2* driven by *Emx1-* and *Foxb1-Cre*. (a-e) Representative sections of P90 old *St8sia2^{f/f}*, *Emx1-Cre;St8sia2^{f/f}*, *Foxb1-Cre;St8sia2^{f/f}*, *Foxb1-Cre;Emx1-Cre;St8sia2^{f/f}* and *St8sia2^{Δ/Δ}* animals. The reticular thalamic nucleus (Rt) is stained for perineuronal nets (PNN) with Wisteria floribunda agglutinin (WFA). Enlarged images of the Rt corresponding to the white boxes in a-e are given in a'-e'. (a''-e'') PNN-staining and staining of neurofilament (NF)-positive fibers. Images correspond to the outlined areas in a'-e'. (a'''-e'') Boxed areas in a''-e'' are further enlarged to highlight the organization of NF-positive fibers. Scale bars represent 1000 µm in a-e and 100 µm in a'-e'''.
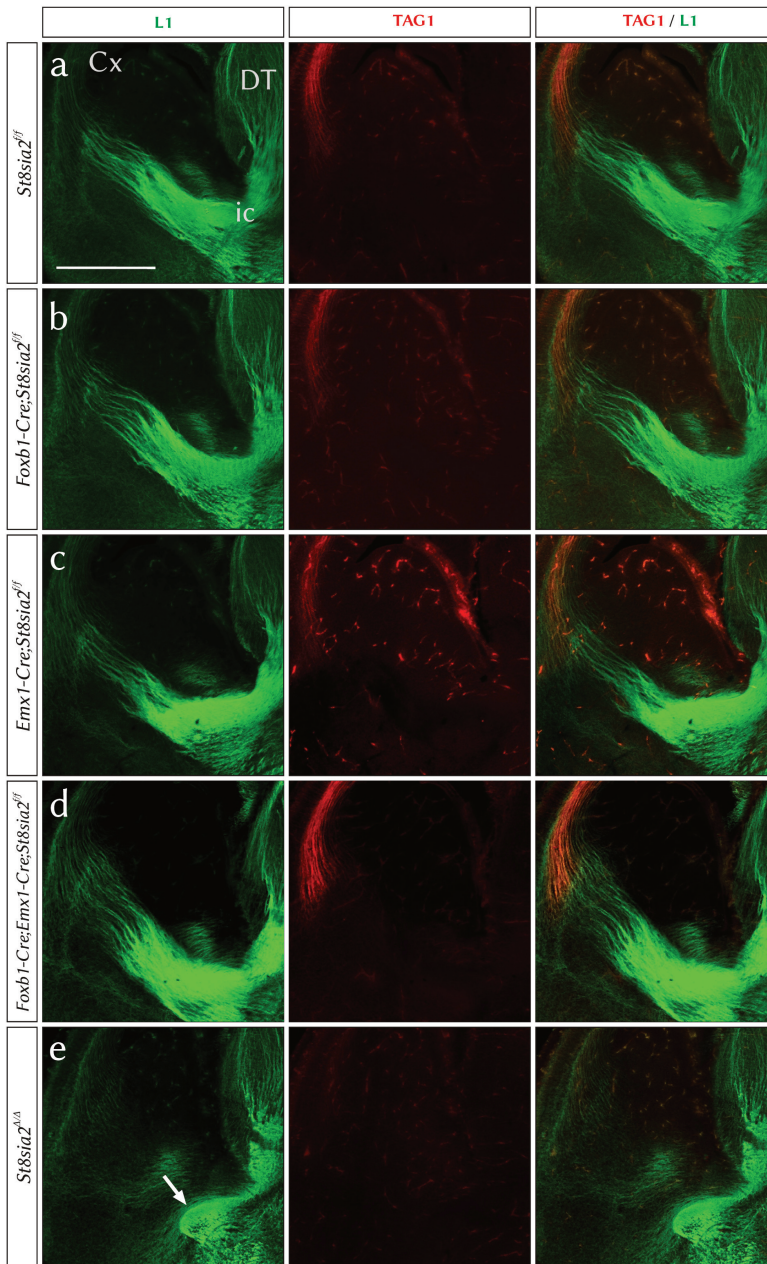
Figure 4.4: Defective pathfinding of thalamocortical fibers in *St8sia2*-negative mice at E14.5. Representative images of coronal brain sections of E14.5 old *St8sia2$^{f/f}$* controls, *Emx1-Cre;St8sia2$^{f/f}$*, *Foxb1-Cre;St8sia2$^{f/f}$*, *Foxb1-Cre;Emx1-Cre;St8sia2$^{f/f}$* and *St8sia2$^{\Delta/\Delta}$* animals. Thalamocortical fibers were stained with an antibody targeting L1 (green) and corticofugal fibers with an antibody targeting TAG1 (red). Merged pictures visualize the handshake of L1- and TAG1-positive fibers at the subpallial-pallial boundary. Scale bar represents 500 μm. Cx = cortex, DT = dorsal thalamus, ic = internal capsule.
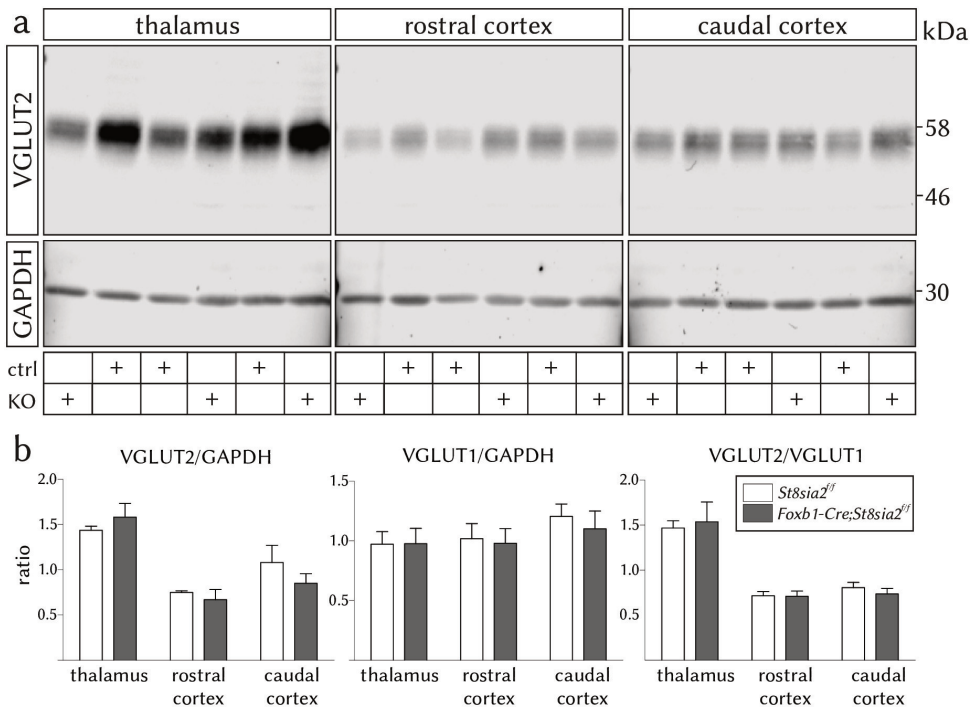
Figure 4.5: Normal glutamatergic input into the cerebral cortex of *Foxb1-Cre;St8sia2$^{f/f}$* mice. Western blot analysis of VGLUT2 and VGLUT1 in samples obtained from thalamus, rostral and caudal cortex of *St8sia2$^{f/f}$* and *Foxb1-Cre;St8sia2$^{f/f}$* at P90. GAPDH was stained as a loading control on the same blot membranes. After stripping, the same membrane was stained for VGLUT1 and GAPDH. (a) Representative blot for VGLUT2 and GAPDH. (b) Densitometric evaluation. Ratios of VGLUT1 and VGLUT2 to GAPDH and of VG-LUT2 relative to VGLUT1 were calculated for each lane on four independent Western blot replicates per sample. Values are depicted as mean ± s.e.m. of $n = 3$ *St8sia2$^{f/f}$* (ctrl) and *Foxb1-Cre;St8sia2$^{f/f}$* (KO) embryos. Statistical analysis by two-way ANOVA did not reveal any differences in the expression of VGLUT1 and VGLUT2.

Chapter 4
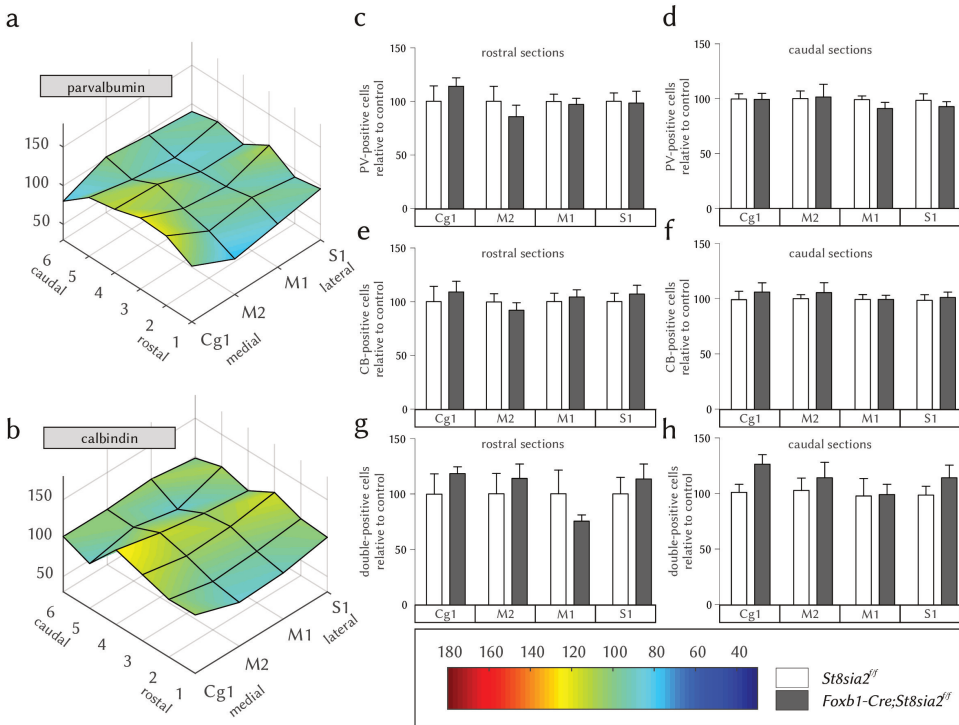
Figure 4.6: Normal interneuron distributions in the anterior cortex of *Foxb1-Cre;St8sia2^{f/f}* mice at P90. (a+b) Heatplots, representing the distribution of parvalbumin (PV)- and calbindin (CB)-expressing interneurons over six rostral to caudal bregma levels (1-6) and four adjacent regions (cingulated cortex 1 (Cg1), motorcortex regions M2 and M1 and the somatosensory cortex S1). Corresponding mean values ± s.e.m. of *n* = 5 animals per genotype. Rostral (1-3) and caudal (4-6) sections are depicted in (c+d) for parvalbumin, (e+f) for calbindin and (g+h) for double-positive interneurons. Statistical analysis by two-way ANOVA indicated no significant differences. Colored scale bar represents the shading of the heatplots indicating the number of interneurons normalized to control animals.

no alterations of parvalbumin-, calbindin- or double-positive interneurons were detected in the analyzed regions of the anterior cortex of adult *Foxb1-Cre;St8sia2^{f/f}* animals. These results are consistent with the unaltered morphology of the internal capsule, the reticular thalamic nucleus as well as with the demonstrated normal pathfinding of thalamocortical and corticofugal fibers in *Foxb1-Cre;St8sia2^{f/f}* mice. Together, these data demonstrate that ST8SIA2-depletion in the thalamus and the cortex does not result in disturbed thalamus-cortex connectivity or alterations of the cortical inhibitory system.

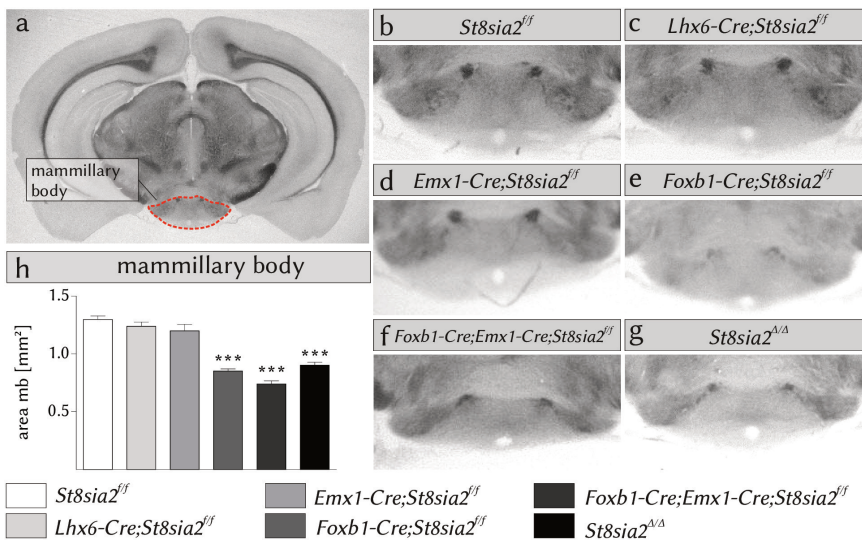**Figure 4.7:** Hypoplasia of the mammillary body is recapitulated by ST8SIA2-inactivation in *Foxb1*-expressing cells. (a) Representative image of a coronal brain section of a P90 old *St8sia2$^{f/f}$* control at the level of the closure of the third ventricle (bregma -2.8 mm according to Paxinos and Franklin 2001). The area of the mammillary body (mb) was determined as depicted by the dotted line. (b-g) Representative images of the mb obtained from animals with the indicated genotypes. (h) Areas of the mammillary body are presented as mean values ± s.e.m. of $n = 17$ controls, $n = 6$ *Lhx6-Cre;St8sia2$^{f/f}$*, $n = 5$ *Emx1-Cre;St8sia2$^{f/f}$*, $n = 6$ *Foxb1-Cre;St8sia2$^{f/f}$*, $n = 4$ *Foxb1-Cre;Emx1-Cre;St8sia2$^{f/f}$* and $n = 6$ *St8sia2$^{\Delta/\Delta}$* animals. One-way ANOVA indicated significant differences (P < 0.0001) and Bonferroni post-test for comparisons against the control was applied (***, P < 0.001).

Inactivation of ST8SIA2 by Foxb1-Cre leads to hypoplasia of the mammillary body and the mammillothalamic tract

The mammillothalamic tract is one of the axon tracts with pronounced hypoplasia in the completely polySia-negative *St8sia2$^{-/-}$ St8sia4$^{-/-}$* mice (Weinhold *et al.* 2005). To assess, if loss of ST8SIA2 affects the mammillothalamic tract and the mammillary body, morphometric analyses were performed in adult *St8sia2$^{\Delta/\Delta}$* mice and all of the available lines with conditional knockout of *St8sia2* (Fig. 7). In comparison with *St8sia2$^{f/f}$* (Fig. 7a, b), evaluation of the mammillary body in *St8sia2$^{\Delta/\Delta}$* mice revealed a pronounced size-reduction (Fig 4.7g, h). As expected, neither *Lhx6-Cre;-St8sia2$^{f/f}$* nor *Emx1-Cre;St8sia2$^{f/f}$* animals displayed any alterations (Fig. 7c, d, h), whereas the size reduction of the mammillary body was fully reproduced in *Foxb1-Cre;St8sia2$^{f/f}$* and *Foxb1-Cre;Emx1-Cre;St8sia2$^{f/f}$* animals (Fig 4.7e, f, h).
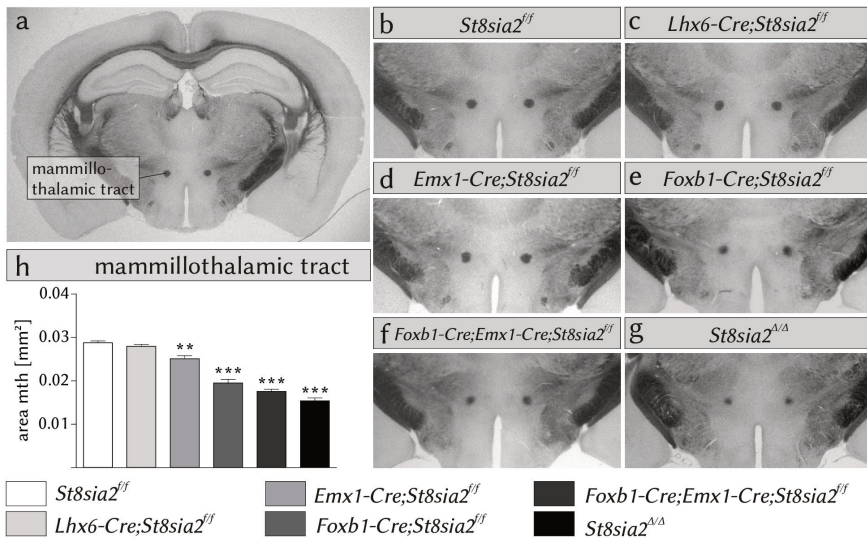
Figure 4.8: Hypoplasia of the mammillothalamic tract depends on ST8SIA2 in *Emx1-* and *Foxb1-*expressing cells. (a) Representative image of a coronal brain section obtained from a *St8sia2^{f/f}* control at P90. The location of the mammillothalamic tract (mth) is indicated. Images were chosen at a level where the mth and the dorsal part of the zona incerta are adjacent to each other (bregma -1.82, based on Paxinos and Frankling, 2001). (b-g) Representative images of the mb obtained from animals with the indicated genotypes. (h) The cross-sectional areas of the mth are depicted as mean values ± s.e.m. of $n = 19$ controls, $n = 6$ *Lhx6-Cre;St8sia2^{f/f}*, $n = 5$ *Emx1-Cre;St8sia2^{f/f}*, $n = 6$ *Foxb1-Cre;St8sia2^{f/f}*, $n = 5$ *Foxb1-Cre;Emx1-Cre;St8sia2^{f/f}* and $n = 6$ *St8sia2^{Δ/Δ}* animals. Per animal, mean values of left and right mth were determined. One-way ANOVA indicated significant differences ($P < 0.0001$) and Bonferroni post-test for comparisons against the control was applied (**, $P < 0.01$; ***, $P < 0.001$).

Corresponding analyses of the cross-sectional areas of the mammillothalamic tracts (Fig. 8) revealed a pronounced hypoplasia in *St8sia2^{Δ/Δ}* mice (Fig 4.8g+h). In contrast to the mammillary body, this hypoplasia was mimicked not only by *Foxb1-Cre;St8sia2^{f/f}* and *Foxb1-Cre;Emx1-Cre;St8sia2^{f/f}* animals but also by *Emx1-Cre;-St8sia2^{f/f}*, although to a lesser extent (Fig 4.8d, e, h). Notably, *St8sia2*-deficiency not only resulted in smaller cross-sectional areas of the mammillothalamic tract but also in a less defined appearance, which might arise from less dense fasciculation or myelination (Fig 4.8e-g). As expected, *Lhx6-Cre;St8sia2^{f/f}* animals displayed a normal size of the mammillothalamic tract (Fig 4.8c and h).

By immunohistochemical analysis of the mammillothalamic tract at E18.5 (Fig 4.9 a-c), the possibility of an early development of the mth-hypoplasia was assessed in *St8sia2*-negative and *Foxb1-Cre;St8sia2^{f/f}* mice. As illustrated by neurofilament stainings in Fig. 9a'-c', the principal mammillary tract is emerging normally from
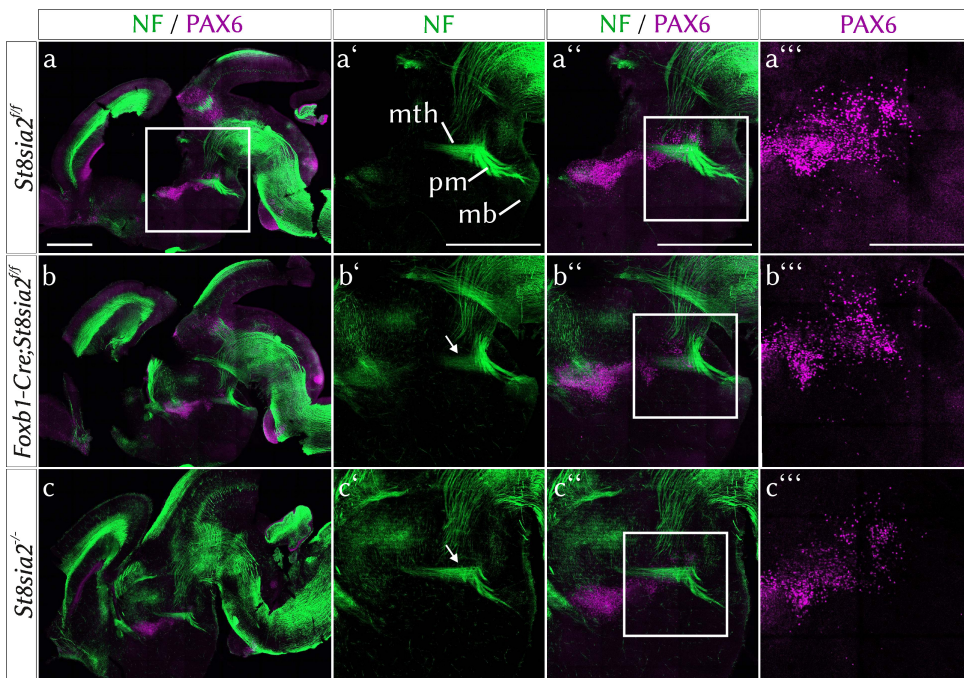
Figure 4.9: Normal pathfinding of fibers exiting the mammillary body of *Foxb1-Cre;-St8sia2^{f/f}* embryos at E18.5. Representative images of E18.5 sagittal brain sections obtained from (a) *St8sia2^{f/f}* (b) *Foxb1-Cre;St8sia2^{f/f}* (c) and *St8sia2^{−/−}* animals. Sections were stained for neurofilament (NF, green) and PAX6 (magenta). The mammillary body (mb), principal mammillary tract (pm) and mammillothalamic tract (mth) are indicated in a'. Areas marked by white boxes in a and a''-c'' are magnified in a'-c'' and a'''-c''', respectively. Scale bars represent 500 μm in a, a' and 250 μm in a'''.

Chapter 4

the mammillary body and trajectories of the mammillothalamic tract were unaltered in *Foxb1-Cre;St8sia2^{f/f}* and *St8sia2^{−/−}* mice (arrows in Fig. 9b' and c'). This is consistent with the normal distribution of PAX6-positive guidepost cells (Fig 4.9a'''-c'''), because these cells are crucial for the sprouting and pathfinding of collateral branches of the principal mammillary tract (Szabo 11). Although not systematically evaluated, the mammillothalamic tract in *Foxb1-Cre;St8sia2^{f/f}* and *St8sia2^{−/−}* mice appeared slightly smaller and less dense. In light of the marked hypoplasia of the mammillothalamic tract in adult animals, this argues for a developmental origin of the mammillothalamic tract hypoplasia, which is aggravated by subsequent degeneration of mammillothalamic tract fibers or myelination deficits.
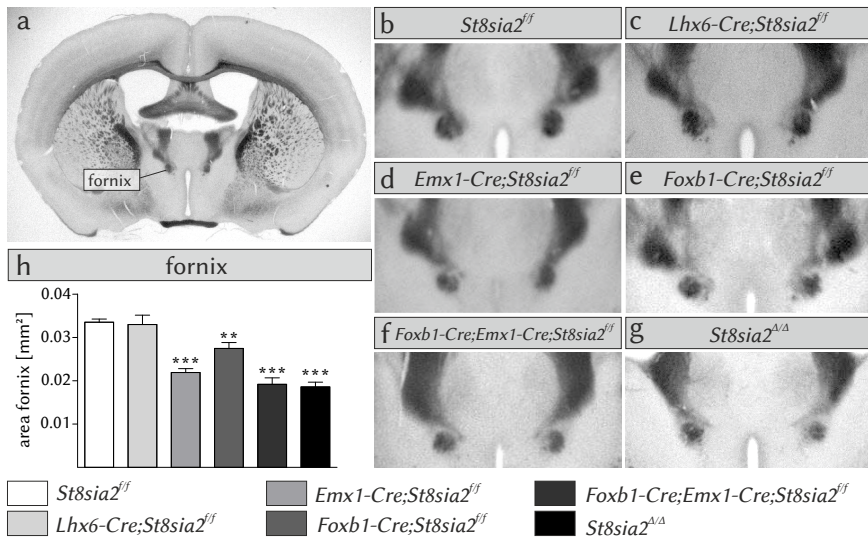
Figure 4.10: Hypoplasia of the fornix can be reproduced by inactivation of ST8SIA2 in *Emx1-* and *Foxb1*-expressing cells. (a) Representative image of a coronal brain sections of a P90 old *St8sia2$^{f/f}$* control at the level of segregation of the fornix from the stria medullaris of the thalamus (bregma -0.22 mm according to Paxinos and Franklin, 2001). (b-g) Representative images of the fornix obtained from animals with the indicated genotypes. (h) Cross-sectional areas of the fornix are presented as mean values ± s.e.m. of *n* = **19** controls, *n* = **6** *Lhx6-Cre;St8sia2$^{f/f}$*, *n* = **5** *Emx1-Cre;St8sia2$^{f/f}$*, *n* = **6** *Foxb1-Cre;St8sia2$^{f/f}$*, *n* = **5** *Foxb1-Cre;Emx1-Cre;St8sia2$^{f/f}$* and *n* = **6** *St8sia2$^{\Delta/\Delta}$* animals. Per animal, mean values of left and right fornix were determined. One-way ANOVA indicated significant differences (P < **0.0001**) and a Bonferroni post-test for comparisons against the control was applied (** P < **0.01**; *** P < **0.001**).

Inactivation of ST8SIA2 by Foxb1- and Emx1-Cre leads to hypoplasia of the fornix

Interestingly, hypoplasia of the mammillothalamic tract was also observed by loss of ST8SIA2 driven by *Emx1-Cre*, which should only target cells of the cortex. We therefore evaluated the size of the postcommissural fornix, which originates in the hippocampus and innervates the mammillary body and detected a pronounced hypoplasia in *St8sia2$^{\Delta/\Delta}$* mice that was fully mimicked by *Emx1-Cre;St8sia2$^{f/f}$* and *Foxb1-Cre;Emx1-Cre;St8sia2$^{f/f}$* but, as expected, not by *Lhx6-Cre;St8sia2$^{f/f}$* animals (Fig 4.10c, d, f-h). Unexpectedly, however, *Foxb1-Cre;St8sia2$^{f/f}$* mice partially reproduced this phenotype (Fig 4.10e, h).

4.4 Discussion

Based on the previously described reductions of cortical interneurons and markedly disturbed thalamus-cortex connectivity in *St8sia2⁻/⁻* mice, we analyzed and compared neuropathological changes in mice with conditional knockout of *St8sia2* in the diencephalon (*Foxb1-Cre;St8sia2^{f/f}*) or in the cortex (*Emx1-Cre;St8sia2^{f/f}*). *Foxb1-Cre;St8sia2^{f/f}*, *Emx1-Cre;St8sia2^{f/f}* and *Foxb1-Cre;Emx1-Cre;St8sia2^{f/f}* animals demonstrated normal thalamus-cortex connectivity, suggesting that reduced polySia-levels on developing thalamocortical and corticofugal fibers due to loss of ST8SIA2 in respective thalamic and cortical projection neurons is not sufficient to reproduce the fasciculation deficits or the hypoplasia of the internal capsule previously detected in adult *St8sia2⁻/⁻* mice (Hildebrandt *et al.* 2009; Schiff *et al.* 2011). Likewise, aberrant trajectories of thalamocortical axons and lack of corticofugal fibers described here for the first time in *St8sia2*-negative embryos were not recapitulated in any of the conditional knockout lines. Together, these data indicate that deficits of thalamus-cortex connectivity are caused by loss of *St8sia2* in cells that are not targeted by *Foxb1*- or *Emx1-Cre* driven recombination. One possible explanation is a delayed onset of polySia-reduction after inactivation of ST8SIA2, i.e. polySia on thalamocortical or corticofugal axons might only be reduced after a developmental event for which the presence of polySia is critical. Another possibility would be that polySia-reductions on cells that are derived neither from the diencephalon nor from the cortex lead to the pathfinding defects observed in *St8sia2*-negative mice. A cell population that is crucial for thalamocortical pathfinding is characterized by *Islet1*-expression (López-Bendito *et al.* 2006). These cells form a permissive corridor in the embryonic striatum adjacent to the medial ganglionic eminence. They arise from tangential migration within the ventral telencephalon and express markers characteristic for derivatives of the lateral ganglionic eminence. Although these *Islet1*-expressing corridor cells are present in polySia-negative *St8sia2⁻/⁻ St8sia4⁻/⁻* mice (Schiff *et al.* 2011), it remains a possibility that polySia on these or other cells in the ventral telencephalon is critical for thalamocortical axons to turn towards the cortex after crossing the diencephalon-telencephalon boundary. Since FOXG1 is one of the earliest transcription factors expressed throughout the developing telencephalon (Shimamura *et al.* 1995; Xuan *et al.* 1995), this area can be targeted by utilizing *Foxg1-Cre* animals (Kawaguchi *et al.* 2016). If polySia produced by ST8SIA2 in the ventral telencephalon is essential for proper pathfinding of thalamocortical fibers, *Foxg1-Cre;St8sia2^{f/f}* animals should mimic the respective phenotype of *St8sia2*-negative mice.

In contrast to polySia-negative, NCAM-positive *St8sia2⁻/⁻ St8sia4⁻/⁻* mice, *Ncam*-deficient animals display normal thalamocortical pathfinding and no hypoplasia of the internal capsule (Hildebrandt *et al.* 2009; Schiff *et al.* 2011), indicating that these defects result from the untimely presence of polySia-negative NCAM. As

Chapter 4

shown by a comparative analysis of early postnatal $St8sia2^{-/-}$ and $St8sia4^{-/-}$ mice, loss of ST8SIA4 can be fully compensated by the remaining ST8SIA2 (Galuska *et al.* 2006; Oltmann-Norden *et al.* 2008). In contrast, the loss of ST8SIA2 was only partially compensated, leading to the appearance of polySia-negative NCAM without major changes in the lengths of the remaining polySia chains. It therefore can be assumed that deletion of ST8SIA2 in the developing brain results in a subset of NCAM molecules devoid of polySia. Thus, interactions of polySia-negative NCAM should be the reason, why thalamocortical fibers in $St8sia2^{-/-}$ and polySia-negative animals fail to turn dorsally in the ventral telencephalon. Therefore, analyses of *Foxg1-Cre;St8sia2$^{f/f}$* mice would also be interesting with regard to the erroneous interactions of polySia-negative NCAM. Defective pathfinding of thalamocortical fibers in *Foxg1-Cre;St8sia2$^{f/f}$* mice would indicate that interaction of NCAM in the environment with either polySia-NCAM or a different receptor on the surface of thalamocortical fibers causes pathfinding defects. However, homophilic binding between polySia-negative NCAM on thalamocortical fibers and polySia-negative NCAM in their environment could be the basis for the aberrant development in $St8sia2^{-/-}$ embryos. This could be addressed by the generation of *Foxg1-Cre;Foxb1-Cre;St8sia2$^{f/f}$* double mutants.

Evaluation of the long-range connectivity of the mammillary body revealed hypoplasia of the mammillary body, the mammillothalamic tract and the fornix in *Foxb1-Cre;St8sia2$^{f/f}$* animals. This is consistent with studies reporting expression of *Foxb1* in the mammillary body (Alvarez-Bolado *et al.* 2000; Radyushkin *et al.* 2005; Zhao *et al.* 2007) and with the observed hypoplasia of the mammillothalamic tract in $St8sia2^{-/-}St8sia4^{-/-}$ animals (Weinhold *et al.* 2005). Similar to the more severe hypoplasia of the internal capsule in $St8sia2^{-/-}St8sia4^{-/-}$ mice, as compared to $St8sia2^{-/-}$ mice (Hildebrandt *et al.* 2009) the size reduction of the mammillothalamic tract reported for $St8sia2^{-/-}St8sia4^{-/-}$ mice by Weinhold *et al.* 2005 appears to be more pronounced than the hypoplasia in $St8sia2^{\Delta/\Delta}$ and *Foxb1-Cre;St8sia2$^{f/f}$* animals presented in the current study. Likewise, we now demonstrate a reduced rostrocaudal extent of the corpus callosum in $St8sia2^{\Delta/\Delta}$ and *Emx1-Cre;St8sia2$^{f/f}$* animals. Again, this deficit is clearly more pronounced in $St8sia2^{-/-}St8sia4^{-/-}$ mice (Hildebrandt *et al.* 2009). In line with the previous study, the current results therefore provide strong evidence that polySia produced by ST8SIA4 is also relevant for normal development of the mammillothalamic tract.

Unexpectedly, *Emx1-Cre;St8sia2$^{f/f}$* mice also displayed hypoplasia of the mammillothalamic tract, which was less severe than in $St8sia2^{\Delta/\Delta}$ and *Foxb1-Cre;St8sia2$^{f/f}$* animals and not associated with size-reduction of the mammillary body. *Emx1-Cre* expression is confined to the telencephalon (Gorski *et al.* 2002). Therefore, *Emx1-Cre*-mediated inactivation of *St8sia2* should not directly affect the mammillothalamic tract, however, its reduced size in *Emx1-Cre;St8sia2$^{f/f}$* mice could arise from defective innervation by the fornix, which originates in the hippocampus and

provides the major excitatory input to the mammillary body (Vann and Nelson 2015). Indeed, morphological assessment of the postcommissural fornix revealed hypoplasia in *Emx1-Cre;St8sia2$^{f/f}$* suggesting that the size reduction of the mammillothalamic tract in these mice is caused by reduced excitatory input to the mammillary body. The deficits of the mammillothalamic tract, therefore, could result from anterograde transneuronal degeneration due to defective innervation by the fornix. In this scenario, however, one would not only expect less axons but also less projection neurons, i.e. degeneration of the mammillary body (Schubert and Friede 1979). It is therefore puzzling why the size of the mammillary body was not reduced in *Emx1-Cre;St8sia2$^{f/f}$* mice. Although to a lesser degree, hypoplasia of the fornix was also observed in *Foxb1-Cre;St8sia2$^{f/f}$* animals, but in this case the axon tract defect is associated with a reduced size of the mammillary body. Inactivation of *St8sia2* by *Foxb1-Cre* should not directly affect hippocampal projections. Hence, the observed hypoplasia of the fornix in *Foxb1-Cre;St8sia2$^{f/f}$* mice seems to be an indirect effect, possibly caused by retrograde degeneration of fornical axons due to loss of their target neurons in the mammillary body.

Another possible cause for the observed hypoplasia of the mammillothalamic tract could be altered myelination. ST8SIA2, but not ST8SIA4 has been shown to play an essential role in developmental myelination and myelin maintenance (Koutsoudaki *et al.* 2010; Szewczyk *et al.* 2017; Werneburg *et al.* 2017). Moreover, in the diencephalon, *Foxb1* is expressed in cells of the oligodendrocyte lineage (Zhang *et al.* 2017). Therefore, the observed hypoplasia of the mammillothalamic tract and the fornix in *Foxb1-Cre;St8sia2$^{f/f}$* mice could be a direct result of ST8SIA2 loss. Additionally, defective excitatory input by the fornix could lead to degeneration of the myelin sheath of the mammillothalamic tract, since myelination is dependent on electrical activity (Wake *et al.* 2011; Gibson *et al.* 2014). Both explanations would be compatible with the unaltered size of the mammillary body in *Emx1-Cre;St8sia2$^{f/f}$* animals.

Together, these findings suggest a close relation between development and maintenance of the fornix and the mammillothalamic tract. To further study this relationship, the developmental time course of the mammillary system including the occurrence of apoptosis in the mammillary body and hippocampus should be comparatively analyzed in *Foxb1-Cre;St8sia2$^{f/f}$* and *Emx1-Cre;St8sia2$^{f/f}$* mice. Moreover, myelination should be analyzed. Assessment of g-ratios (ratio of axon diameter to the total diameter of a myelinated axon) might be a suitable approach to distinguish between thinning of the myelin sheath and possible axonal degeneration as a result of increased cell death.

The mammillary body has been reported to be relevant for memory storage (Beglinger *et al.* 2006). Ablation of the mammillary body or lesions of the mammillothalamic tract, but not lesions of the fornix, result in impaired spatial working memory (Vann and Aggleton 2003; Radyushkin *et al.* 2005; Vann *et al.* 2011; Vann

Chapter 4

2013). Therefore, the deficits in working memory observed in *St8sia2$^{-/-}$* mice (Kröcher *et al.* 2015) might be a result of impaired long-range connectivity of the mammillary body. To test for this possibility, future studies should dissect, if working memory deficits occur in *Foxb1-Cre;St8sia2$^{f/f}$* mice, which display a strong hypoplasia of the mammillothalamic tract, or possibly, also in *Emx1-Cre;St8sia2$^{f/f}$* animals, in which the mammillothalamic tract is only mildly affected. Based on the data presented in the current study, aberrant behavior in these mouse models would be independent from thalamus-cortex connectivity. Respective analyses in *Lhx6-Cre;St8sia2$^{f/f}$* mice would reveal, if working memory is affected by interneuron deficits independent from any detectable alterations of long range axonal connectivity.

4.5 Methods

Mice

All mice used in this study were bred at the central animal facility of Hannover Medical School. Protocols for animal use were in compliance with the German Animal Welfare Act and approved by the local authorities (Niedersächsisches Landesamt für Verbraucherschutz und Lebensmittelsicherheit, permissions no. 33.9-42502-04-10-0169 and -15/1902). All mouse strains were backcrossed with C57BL/6J mice for at least six generations. *St8sia2*$^{f/f}$ mice were crossbred with *Emx1-Cre* (Gorski *et al.* 2002, as described previously Schuster et al in preparation, see Chapter 3) and with *Foxb1-Cre* (Zhao *et al.* 2007) animals to obtain a diencephalon-confined ablation of ST8SIA2. Although Cre-insertion results in the loss of one *Foxb1*-allele, respective mice have been reported to show no abnormalities (Wehr *et al.* 1997; Alvarez-Bolado *et al.* 2000). *Emx1-Cre;St8sia2*$^{f/f}$ and *Foxb1-Cre;St8sia2*$^{f/f}$ mice were crossbred to obtain double mutants. Genotyping of *St8sia2*$^{-/-}$, *Lhx6-Cre;St8sia2*$^{f/f}$ and *Emx1-Cre;St8sia2*$^{f/f}$ mice was performed by PCR as described previously (Schuster et al. in preparation, see Chapter 3). Genotyping of *Foxb1-Cre;St8sia2*$^{f/f}$ mice was performed utilizing the following primers: Foxb1-iCre-1 (5'-CTCGGCATGGACGAGCTG TACAAG-3'), Foxb1-iCre-2 (5'-CACTGGGGATGGCGGGCAACGTCTG-3') and Foxb1-iCre-3 (5'-CATCGCTAG GGAGTACAAGATGCC-3'), for the *Foxb1-Cre* allele. For staging of embryos, the morning of the vaginal plug was considered as E0.5. For the morphometric analyses, P90 old *Foxb1-Cre;St8sia2*$^{f/f}$, *Emx1-Cre;St8sia2*$^{f/f}$, *Foxb1-Cre;Emx1-Cre;St8sia2*$^{f/f}$, *Lhx6-Cre;St8sia2*$^{f/f}$ mice and whenever possible, *St8sia2*$^{f/f}$ littermates were obtained. Results from *St8sia2*$^{f/f}$ animals of different genotype-groups did not display statistically significant differences and were grouped.

qPCR-analysis

Detection of control and recombined mRNA was conducted by qPCR of dissected thalamic tissue of *Foxb1-Cre;St8sia2*$^{f/f}$ mice as described previously (Schuster et al. in preparation, see Chapter 3).

Immunohistochemistry

Perfusion, generation of 50 μm vibratom sections and immunofluorescent staining on free-floating sections was performed as described previously (Schiff *et al.* 2011, Schuster et. al. in preparation, see Chapter 3). The following monoclonal (mAb) or polyclonal (pAb) antibodies were used: pAb rabbit anti-L1 (kind gift from F.Rathjen, Berlin, Germany, 1:1000), mAb mouse anti-165 kDa Neurofilament IgG$_1$ (2H3, Developmental Studies Hybridoma Bank, 1:500), pAb rabbit anti-CB

D28-k (Swant CB38a, 1:5000), mAb mouse anti-Tag-1 (4D7, Developmental Studies Hybridoma Bank, 1:100), mAb mouse anti-polySia IgG$_{2a}$ (Genovac, 1:2000), mAb mouse anti-PV (Swant, 1:5000), pAb rabbit anti-Pax-6 (Covance, # PRB-278P, 1:300) and respective Alexa Fluor 488 conjugated donkey anti-rabbit IgG H+L (Molecular Probes # A 21206), Alexa Fluor 488 conjugated goat anti-mouse IgG$_1$ (Molecular Probes # A 21121), Alexa Fluor 568 conjugated goat anti-mouse IgM (Molecular Probes # A 21043), Alexa Fluor 568 conjugated goat anti-mouse IgG$_{2a}$ (Molecular Probes # A 21131), Alexa Fluor 647 conjugated goat anti-rabbit IgG H+L (Molecular Probes # A 21245), anti-mouse IgG Cy3 (SIGMA # C2181) secondary antibodies. Perineuronal nets were labelled with biotinylated Wisteria floribunda agglutinin (Sigma-Aldrich, 1:1000) and detected with Cy3-conjugated streptavidin (Rockland Immunochemicals, 1:1000). Staining specificity was controlled by omission of primary antibodies.

Western Blot analysis

Thalamus and cortices of *Foxb1-Cre;St8sia2$^{f/f}$* and control animals were dissected and the rostral third of the cortex was analyzed separately from the second two, more caudal thirds. Tissue was lysed and 30µg protein was submitted to SDS-PAGE and Western blotting as described previously (Weinhold *et al.* 2005; Kröcher *et al.* 2015). The following antibodies were used: mouse monoclonal anti-GAPDH (Ambion Life Technologies, #AM4300, 1:40000), rabbit polyclonal anti-VGLUT1 and anti-VGLUT2 (Synaptic Systems, #135303 and #135402 1:5000) with respective secondary antibodies: anti-mouse IRDye680 and anti-rabbit IRDye800 (Li-COR Biosciences, P/N 926-68070 and P/N 926-32211, 1:20000). Detection and quantification were performed utilizing the Odyssey Infrared Imaging System and Image Studio 4.0 (Li-COR Biosystems). Mean values of four western blots were obtained.

Morphological assessment

The corpus callosum, the internal capsule, the mammillary body, the mammillothalamic tract and the fornix were analyzed on images of unstained 50 µm vibratome sections, obtained by modified dark field illumination. The rostrocaudal extent of the corpus callosum was determined by multiplication of the section thickness with the amount of sections in which callosal fibers cross the midline (bregma 1.10 to -2.54 mm). The rostrocaudal extent of the internal capsule was obtained analogously by multiplication with the number of sections with visible internal capsule corresponding to bregma level 0.02 to -1.82 mm for control animals. For analysis of the mammillary body, its cross-sectional area was measured with ImageJ at the level of the closure of the third ventricle (bregma -2.8 mm). The cross-sectional area of the mammillothalamic tract was analyzed on sections where the dorsal part

of the zona incerta is adjacent to the mammillothalamic tract (bregma -1.82 mm) and the area of the fornix was obtained on sections where the fornix is segregated from the stria medullaris of the thalamus (-0.22 mm). Identification of mentioned anatomical landmarks and bregma levels was conducted according to the Paxinos Mouse Brain Atlas (Paxinos and Franklin 2001). Mean values of both hemispheres were averaged.

Image acquisition and cell counting

Image acquisition and cell countings were conducted as described previously (Schuster et al. in preparation, see Chapter 3).

Statistical analysis

All statistical comparisons were conducted in Prism 4.0 (GraphPad) and all values are given as mean ± s.e.m. One- or two-way ANOVA were conducted with subsequent application of the Kruskal-Wallis post-test (for non-parametric evaluations) and the Bonferroni post-test as indicated.

Acknowledgements

Competing interests

The authors declare no competing financial interests.

Funding

4.6 Bibliography

Alvarez-Bolado G, Zhou X, Voss A K, Thomas T, and Gruss P (2000) Winged helix transcription factor Foxb1 is essential for access of mammillothalamic axons to the thalamus. Development 127:1029–1038.

Angata K, Huckaby V, Ranscht B, Terskikh A, Marth J, and Fukuda M (2007) Polysialic acid-directed migration and differentiation of neural precursors are essential for mouse brain development. Mol. Cell. Biol. 27:6659–68.

Beglinger L J, Haut M W, and Parsons M W (2006) The role of the mammillary bodies in memory: A case of amnesia following bilateral resection. Eur. J. Psychiatry 20:88–95.

Galuska S, Imke O, Geyer H, Weinhold B, Kuchelmeister K, Hildebrandt H, Rita G, Geyer R, and Mühlenhoff M (2006) Polysialic acid profiles of mice expressing variant allelic combinations of the polysialyltransferases ST8SiaII and ST8SiaIV. J. Biol. Chem. 281:31605–31615.

Gibson E M, Purger D, Mount C W, Goldstein A K, Lin G L, Wood L S, Inema I, Miller S E, Bieri G, Zuchero J B, *et al.* (2014) Neuronal activity promotes oligodendrogenesis and adaptive myelination in the mammalian brain. Science 344:1252304.

Gorski J, Talley T, Qiu M, Puelles L, Rubenstein J, and Jones K (2002) Cortical excitatory neurons and glia, but not GABAergic neurons, are produced in the Emx1-expressing lineage. J. Neurosci. 22:6309–14.

Graziano A, Liu X B, Murray K D, and Jones E G (2008) Vesicular glutamate transporters define two sets of glutamatergic afferents to the somatosensory thalamus and two thalamocortical projections in the mouse. J. Comp. Neurol. 507:1258–1276.

Hildebrandt H, Mühlenhoff M, and Gerardy-Schahn R (2010) Polysialylation of NCAM. Adv. Exp. Med. Biol. 663:95–109.

Hildebrandt H, Mühlenhoff M, Imke O, Röckle I, Burkhardt H, Weinhold B, and Rita G (2009) Imbalance of neural cell adhesion molecule and polysialyltransferase alleles causes defective brain connectivity. Brain 132:2831–8.

Kaneko T and Fujiyama F (2002) Complementary distribution of vesicular glutamate transporters in the central nervous system. Neurosci. Res. 42:243–250.

Kawaguchi D, Sahara S, Zembrzycki A, and O'Leary D D (2016) Generation and analysis of an improved Foxg1-IRES-Cre driver mouse line. Dev. Biol. 412:139–147.

Koutsoudaki P, Hildebrandt H, Gudi V, Skripuletz T, Škuljec J, and Stangel M (2010) Remyelination after cuprizone induced demyelination is accelerated in mice deficient in the polysialic acid synthesizing enzyme St8siaIV. Neuroscience 171:235–244.

Kröcher T, Malinovskaja K, Jürgenson M, Anu A, Zharkovskaya T, Kalda A, Röckle I, Schiff M, Weinhold B, Rita G, Hildebrandt H, and Zharkovsky A (2015) Schizophrenia-like phenotype of polysialyltransferase ST8SIA2-deficient mice. Brain Struct. Funct. 220:71–83.

Kröcher T, Röckle I, Diederichs U, Weinhold B, Burkhardt H, Yanagawa Y, Gerardy-Schahn R, and Hildebrandt H (2014) A crucial role for polysialic acid in developmental interneuron migration and the establishment of interneuron densities in the mouse prefrontal cortex. Development 141:3022–3032.

López-Bendito G, Cautinat A, Sánchez J A, Bielle F, Flames N, Garratt A N, Talmage D A, Role L W, Charnay P, Marín O, *et al.* (2006) Tangential neuronal migration controls axon guidance: a role for neuregulin-1 in thalamocortical axon navigation. Cell 125:127–142.

Oltmann-Norden I, Galuska S P, Hildebrandt H, Geyer R, Gerardy-Schahn R, Geyer H, and Mühlenhoff M (2008) Impact of the polysialyltransferases ST8SiaII and ST8SiaIV on polysialic acid synthesis during postnatal mouse brain development. J. Biol. Chem. 283:1463–1471.

Papez J W (1937) A proposed mechanism of emotion. Arch. Neurol. Psych. 38:725–743.

Paxinos G and Franklin K B J (2001) *The mouse brain in stereotaxic coordinates*. Academic press San Diego, CA.

Radyushkin K, Anokhin K, Meyer B I, Jiang Q, Alvarez-Bolado G, and Gruss P (2005) Genetic ablation of the mammillary bodies in the Foxb1 mutant mouse leads to selective deficit of spatial working memory. Eur. J. Neurosci. 21:219–229.

Rutishauser U (2008) Polysialic acid in the plasticity of the developing and adult vertebrate nervous system. Nat. Rev. Neurosci. 9:26–35.

Schiff M, Röckle I, Burkhardt H, Weinhold B, and Hildebrandt H (2011) Thalamocortical pathfinding defects precede degeneration of the reticular thalamic nucleus in polysialic acid-deficient mice. J. Neurosci. 31:1302–1312.

Schnaar R L, Gerardy-Schahn R, and Hildebrandt H (2014) Sialic acids in the brain: gangliosides and polysialic acid in nervous system development, stability, disease, and regeneration. Physiol. Rev. 94:461–518.

Schubert T and Friede R (1979) Transneuronal mammillary atrophy. J. Neurol. 221:67–72.

Sherman S M (2016) Thalamus plays a central role in ongoing cortical functioning. Nat. Neurosci. 19:533–541.

Shimamura K, Hartigan D, Martinez S, Puelles L, and Rubenstein J (1995) Longitudinal organization of the anterior neural plate and neural tube. Development 121:3923–33.

Szewczyk L M, Brozko N, Nagalski A, Röckle I, Werneburg S, Hildebrandt H, Wisniewska M B, and Kuznicki J (2017) ST8SIA2 promotes oligodendrocyte differentiation and the integrity of myelin and axons. Glia 65:34–49.

Vann S D (2013) Dismantling the Papez circuit for memory in rats. Elife 2:e00736.

Vann S D and Aggleton J P (2003) Evidence of a spatial encoding deficit in rats with lesions of the mammillary bodies or mammillothalamic tract. J. Neurosci. 23:3506–3514.

Vann S D, Erichsen J T, O'mara S M, and Aggleton J P (2011) Selective disconnection of the hippocampal formation projections to the mammillary bodies produces only mild deficits on spatial memory tasks: implications for fornix function. Hippocampus 21:945–957.

Chapter 4

Vann S D and Nelson A J (2015) The mammillary bodies and memory: more than a hippocampal relay. Prog. Brain Res. 219:163–185.

Wake H, Lee P R, and Fields R D (2011) Control of local protein synthesis and initial events in myelination by action potentials. Science 333:1647–1651.

Wehr R, Mansouri A, Maeyer T de, and Gruss P (1997) Fkh5-deficient mice show dysgenesis in the caudal midbrain and hypothalamic mammillary body. Development 124:4447–4456.

Weinhold B, Seidenfaden R, Röckle I, Mühlenhoff M, Schertzinger F, Conzelmann S, Marth J, Rita G, and Hildebrandt H (2005) Genetic ablation of polysialic acid causes severe neurodevelopmental defects rescued by deletion of the neural cell adhesion molecule. J. Biol. Chem. 280:42971–7.

Werneburg S, Fuchs H L, Albers I, Burkhardt H, Gudi V, Skripuletz T, Stangel M, Gerardy-Schahn R, and Hildebrandt H (2017) Polysialylation at early stages of oligodendrocyte differentiation promotes myelin repair. J. Neurosci. 37:8131–8141.

Xuan S, Baptista C A, Balas G, Tao W, Soares V C, and Lai E (1995) Winged helix transcription factor BF-1 is essential for the development of the cerebral hemispheres. Neuron 14:1141–1152.

Zhang Y, Hoxha E, Zhao T, Zhou X, and Alvarez-Bolado G (2017) Foxb1 regulates negatively the proliferation of oligodendrocyte progenitors. Front. Neuroanat. 11:53.

Zhao T, Zhou X, Szabó N, Leitges M, and Gonzalo A (2007) Foxb1-driven Cre expression in somites and the neuroepithelium of diencephalon, brainstem, and spinal cord. Genesis 45:781–7.

5

General Discussion

The aim of this thesis was to dissect the role of ST8SIA2 in brain development. To this end, conditional knockout models, targeting *St8sia2* in MGE-derived interneurons, the cortex and the diencephalon, were generated and validated. The distribution of interneurons in the anterior cortex and the developmental migration as well as the long-range connectivity of the thalamus and the mammillary body was analyzed. The first study of this thesis revealed the role of ST8SIA2 in the establishment of cortical interneuron densities in the medial prefrontal cortex as well as its role in the migration of precursor cells from the medial ganglionic eminence into the neocortex. In the second study, we used mice with conditional knockout in MGE-derived interneurons and the cortex to examine whether ST8SIA2 impacts cortical interneuron migration cell-autonomously or non-cell-autonomously. Analyses of interneuron populations in the anterior cortex and of interneuron migration in coculture assays demonstrated a strong cell-autonomous impact of ST8SIA2. MGE-specific inactivation of ST8SIA2 revealed an impaired BDNF-response of migrating interneurons *in situ*. In the third part of this thesis, we sought to dissect defective thalamus-cortex connectivity of *St8sia2*-knockout mice by *Foxb1-* and *Emx1-Cre* driven conditional deletion of *St8sia2*, targeting thalamocortical and corticofugal axons, respectively. Unexpectedly, normal connectivity was observed in *Foxb1-Cre;St8sia2$^{f/f}$* and *Emx1-Cre;St8sia2$^{f/f}$* animals. Analysis of long-range connectivity of the mammillary body, however, revealed hypoplasia of the mammillothalamic tract and the fornix in *Foxb1-Cre;St8sia2$^{f/f}$*, *Emx1-Cre;St8sia2$^{f/f}$* and *Foxb1-Cre;Emx1-Cre;St8sia2$^{f/f}$* mice and atrophy of the mammillary body in mice with *Foxb1-Cre* driven inactivation of ST8SIA2.

A major finding of the first two studies was that *St8sia2*-deficiency results in altered migration and distribution of cortical interneurons. Although the role of polySia on cortical interneuron populations has not yet been addressed by other studies, it has long been known that polySia is implicated in the migration of olfactory interneurons from the anterior SVZ into the olfactory bulb (Ono *et al.* 1994). More recently, it was demonstrated that ST8SIA2 plays an important role in this process (Röckle and Hildebrandt 2016). Although the migration of

olfactory and cortical interneurons is different in detail (Marín and Rubenstein 2003), it was not unexpected that inactivation of ST8SIA2 affects the migration of cortical interneurons. Importantly, analysis of *St8sia2*$^{-/-}$ mice revealed reduced GAD67-GFP-positive interneuron populations at P1 and the postnatal loss of PV was accompanied by a loss of perineuronal nets at P30 (Kröcher *et al.* 2014, see Chapter 2). These results argue for cellular loss rather than downregulation of the respective marker proteins. This is an important finding with regard to the question whether the observed loss of cortical interneurons can be explained by altered perception of BDNF during cortical interneuron migration. However, studies reported conflicting observations. While over-expression of BDNF results in inappropriate interneuron numbers (Alcántara *et al.* 2006), impaired BDNF-signaling has been associated with downregulation of cortical interneuron markers (Jones *et al.* 1994; Arenas *et al.* 1996; Fiumelli *et al.* 2000). Thus, it is unclear, whether altered BDNF-perception would affect interneuron numbers or marker expression.

A key finding in the second manuscript of this thesis (see Chapter 3) was that *Lhx6-Cre;St8sia2*$^{f/f}$ mice partially recapitulate the loss of interneurons in *St8sia2*$^{\Delta/\Delta}$ animals. This demonstrated that ST8SIA2 impacts cortical interneuron distributions mainly by a cell-autonomous mechanism. However, it remained unclear why *Lhx6-Cre;St8sia2*$^{f/f}$ mice did not fully mimic the phenotype observed in *St8sia2*$^{\Delta/\Delta}$ animals. One reason could be the late onset of polySia-reduction in *Lhx6-Cre;-St8sia2*$^{f/f}$ mice. Moreover, based on several lines of evidence, we suggested that ST8SIA2 expressed in the thalamus could contribute to the severe phenotype in *St8sia2*$^{\Delta/\Delta}$ animals. On the one hand, proper innervation of the adult cortex by thalamocortical fibers depends on polySia (Yamamoto *et al.* 2000; López-Bendito and Molnár 2003; Schiff *et al.* 2011; Kröcher *et al.* 2015). On the other hand, pathfinding of thalamocortical fibers occurs in close vicinity of MGE-derived interneuron migration (Flames *et al.* 2004; López-Bendito *et al.* 2006). Based on the idea that cortical interneurons migrate along corticofugal fibers (Denaxa *et al.* 2001; Denaxa *et al.* 2005), defective pathfinding of corticofugal, but possibly also thalamocortical fibers might account for differences between *Lhx6-Cre;St8sia2*$^{f/f}$ and *St8sia2*$^{\Delta/\Delta}$ mice. As demonstrated in Chapter 4, thalamocortical and corticofugal fibers display clear deficits in *St8sia2*$^{-/-}$ embryos and could therefore cause the observed differences in interneuron distributions between *Lhx6-Cre;St8sia2*$^{f/f}$ and *St8sia2*$^{\Delta/\Delta}$ mice.

We expected that ST8SIA2-inactivation targeting thalamocortical and/or corticofugal fibers would reproduce these pathfinding defects, allowing for subsequent investigation of their impact on cortical interneuron distributions. However, mice with specific inactivation of ST8SIA2 in thalamocortical or corticofugal fibers (*Foxb1-Cre;St8sia2*$^{f/f}$ and *Emx1-Cre;St8sia2*$^{f/f}$) did not recapitulate these pathfinding defects. Hence, these animals are not suitable to evaluate whether pathfinding defects impact cortical interneuron distributions.

One explanation for the normal pathfinding in *Foxb1-Cre;St8sia2$^{f/f}$* and *Emx1-Cre;-St8sia2$^{f/f}$* mice would be that pathfinding is independent of *St8sia2* expression in the thalamus and the cortex. Alternatively, late onset of *Cre*-mediated recombination, analogous to the temporal delay of the conditional knockout in *Lhx6-Cre;St8sia2$^{f/f}$* animals, could circumvent aberrant pathfinding. Due to the long time span between the formation of the mammillotegmental tract at E12 and collateral sprouting of mammillothalamic fibers, which occurs only at E18.5 (Valverde *et al.* 2000), a late onset of *Foxb1*-driven inactivation of ST8SIA2 could actually explain why deficits of the mammillothalamic, but not of thalamocortical axons were observed in *Foxb1-Cre;St8sia2$^{f/f}$* mice. Therefore, future studies should analyze whether thalamocortical fibers in *St8sia4*-negative *Foxb1-Cre;St8sia2$^{f/f}$* mice are negative for polySia. If fibers are polySia-negative and still display normal pathfinding, thalamocortical deficits of *St8sia2$^{-/-}$* mice cannot be caused by loss of ST8SIA2 in the thalamus. As proposed in Chapter 4, specific inactivation of ST8SIA2 in the environment of thalamocortical axons could be achieved and evaluated in *Foxg1-Cre;St8sia2$^{f/f}$* animals. Furthermore, evaluation of *Foxg1-Cre;Foxb1-Cre;St8sia2$^{f/f}$* mice would be of interest. On the one hand, analyses of these mice could help to dissect, whether pathfinding deficits are caused by heterophilic or homophilic NCAM-interactions. On the other hand, if these mice reproduce the thalamocortical phenotype of ST8SIA2-negative mice, this would exclude the possibility that aberrant pathfinding is circumvented by a late onset of polySia-reduction in *Foxb1-Cre;St8sia2$^{f/f}$* mice.

Evaluation of the long-range connectivity of the mammillary body in *Foxb1-Cre;-St8sia2$^{f/f}$* and *Emx1-Cre;St8sia2$^{f/f}$* mice revealed hypoplasia of the mammillothalamic tract and the fornix. As discussed in Chapter 4, the mechanisms causing the hypoplasia of these axon tracts remained elusive and should be evaluated in future studies. Of note, ST8SIA2, but not ST8SIA4 has been implicated in myelination (Szewczyk *et al.* 2017) and in the diencephalon, *Foxb1* is expressed in cells of the oligodendrocyte lineage (Zhang *et al.* 2017). Hence, *Foxb1-Cre* driven inactivation of ST8SIA2 may cause deficits in myelination, which could account for the observed hypoplasia. Mice with *Cre* expressed under an oligodendrocyte precursor-specific promotor (e.g. *Ng2-Cre* mice) could be used to address *St8sia2*-dependent myelination.

Analysis of *St8sia2$^{-/-}$* mice revealed neuropathological and behavioral deficits that are reminiscent to defects observed in schizophrenic patients (Kröcher *et al.* 2015). In addition, genetic variations in *NCAM1* and *ST8SIA2* have been repeatedly associated with schizophrenia and other psychiatric disorders (Arai *et al.* 2006; Sullivan *et al.* 2006; Atz *et al.* 2007; Tao *et al.* 2007; Anney *et al.* 2010; McAuley *et al.* 2012; Gilabert-Juan *et al.* 2013; Yang *et al.* 2015). The dissection of neuropathological changes in *St8sia2$^{-/-}$* mice was performed with the perspective to assign distinct phenotypical traits to behavioral deficits. The phenotypes analyzed in this thesis can be categorized into three groups: (i) impaired migration of cortical interneurons,

disturbed sensing of BDNF and aberrant distribution of PV$^+$interneurons in the adult cortex, (ii) disturbed thalamus-cortex connectivity comprising pathfinding defects of thalamocortical axons, postnatal degeneration of the reticular thalamic nucleus, hypoplasia of the internal capsule and impaired glutamatergic input into the adult cortex (Schiff *et al.* 2011; Kröcher *et al.* 2015) and (iii) hypoplasia of the mammillary body, mammillothalamic tract and the postcommissural fornix. Parallels between these phenotypical traits and observations in psychiatric disorders are discussed in the following.

A frequent finding in patients suffering from schizophrenia or autism is a reduction of PV$^+$interneurons in the prefrontal cortex (Benes and Berretta 2001; Todtenkopf *et al.* 2005; Lewis *et al.* 2012; Hashemi *et al.* 2016). Furthermore, genetic variations or altered levels of BDNF have been observed in both diseases (Nieto *et al.* 2013; Qin *et al.* 2016; Saghazadeh and Rezaei 2017) and alterations of BDNF or its receptor trkB result in a loss of PV$^+$interneurons (Hashimoto *et al.* 2005; Sakata *et al.* 2009; Zheng *et al.* 2011). Hence, the polySia-dependent sensing of BDNF as well as altered interneuron migration and loss of PV$^+$interneurons in the cortex of *St8sia2*$^{-/-}$ mice, reported in this thesis, matches observations in schizophrenic and autistic patients. Consequently, alterations of ST8SIA2 and dysregulation of BDNF may converge on the level of interneuron migration in brain development and subsequent loss of interneurons in the adult cortex.

Apart from deficits in the prefrontal cortex, schizophrenic patients also display alterations in thalamus-cortex connectivity. For instance, several studies reported alterations of the internal capsule (Wobrock *et al.* 2008; Rosenberger *et al.* 2012; Ellison-Wright *et al.* 2014). Furthermore, a correlation between hallucinations in schizophrenia and dysfunction of the reticular thalamic nucleus was demonstrated (Behrendt and Young 2004; Behrendt 2006). *St8sia2*$^{-/-}$ mice demonstrate schizophrenia-like behavior, such as deficits in working memory, impaired prepulse inhibition, increased amphetamine sensitivity and anhedonia suggested by a lack of sucrose preference (Kröcher *et al.* 2015). Working memory deficits and altered prepulse inhibition are hallmarks of schizophrenia (Green *et al.* 2000; Braff *et al.* 2001), whereas positive and negative symptoms in schizophrenia are tested in rodents via amphetamine-induced hyperlocomotion and the sucrose-preference test (Arguello and Gogos 2009; van den Buuse 2009; Anticevic and Corlett 2012). The authors ascribed these behavioral abnormalities to defects of thalamus-cortex connectivity demonstrated in *St8sia2*$^{-/-}$ mice (Kröcher *et al.* 2015), however results presented in this thesis reveal that these deficits might as well be attributed to defects of the cortical inhibitory system or to mammillary body connectivity.

Additionally, evaluation of both *St8sia2*$^{-/-}$ and *St8sia4*$^{-/-}$ animals revealed deficits in novel object recognition tasks associated with impaired short- and long-term memory (Kröcher *et al.* 2015). Indications for disturbed working- and reference memory were also found in a study evaluating the impact of a secondary hit on

the behavior of *St8sia2*$^{-/-}$ mice (Tantra *et al.* 2014). Possibly, impaired short- and long-term memory could arise from disturbed connectivity of the mammillary body. In rodents, ablation of the mammillary body, the mammillothalamic tract, but not the descending fornix causes defects in spatial working memory (Vann and Aggleton 2003; Radyushkin *et al.* 2005; Vann *et al.* 2011; Vann 2013). In contrast, fornix ablation in humans results in atrophy of the mammillary body (Loftus *et al.* 2000) and impaired long term, but not working memory (Tsivilis *et al.* 2008). In respect to schizophrenia, however, only one study reports reduced parvalbumin-positive neurons in the mammillary body, but normal mammillary body volumes (Bernstein *et al.* 2007). This is in stark contrast to the frequent association of interneuron-deficits and defective thalamus-cortex connectivity with schizophrenia. Associations between long-range connectivity of the mammillary body and schizophrenia should be investigated more frequently.

Conclusions and perspectives for behavioral studies

As reported earlier, simultaneous knockout of *St8sia2* and *St8sia4* results in pathfinding defects of thalamocortical fibers leading to subsequent degeneration of the reticular thalamic nucleus and hypoplasia of the internal capsule. Moreover, *St8sia2*$^{-/-}$ animals that display similar morphological phenotypes, exhibit behavioral defects reminiscent to those of schizophrenic patients (Hildebrandt *et al.* 2009; Schiff *et al.* 2011; Kröcher *et al.* 2015). Here, we established disturbances of the cortical inhibitory system as another phenotype of *St8sia2*$^{-/-}$ animals that matches observations in schizophrenic patients (Benes and Berretta 2001; Sakai *et al.* 2008; Lewis *et al.* 2012) and demonstrate novel defects in the long-range connectivity of the mammillary body in *St8sia2*$^{-/-}$ mice. With the aim to evaluate, whether different conditional knockout models are suitable to correlate distinct neuropathological phenotypes with altered behavior, we examined conditional knockouts targeting MGE-derived interneurons, the thalamus and the cortex.

Because *Emx1-Cre;St8sia2*$^{f/f}$ mice display a small impact on cortical interneurons as well as hypoplasia of the fornix and the mammillothalamic tract, these animals are not suited to assign a certain neuropathological defect to altered behavior.

Since *Foxb1*-driven knockout of *St8sia2* fail to mimic the thalamocortical phenotype in *St8sia2*$^{-/-}$ mice, future studies should evaluate a telencephalon-specific deletion (*Foxg1-Cre;St8sia2*$^{f/f}$). Given that these mice display disturbed thalamocortical pathfinding, subsequent behavioral analysis would be of interest. As FOXG1 is expressed early in the entire telencephalon (Shimamura *et al.* 1995; Xuan *et al.* 1995), it also affects *Lhx6*- and *Emx1*-expressing cells, likely to result in disturbances of the cortical inhibitory system. Based on our findings presented in the third study, affecting the *Emx1*-population should also result in disturbance

of the fornix and the mammillothalamic tract. Consequently, possible behavioral deficits of *Lhx6-Cre;St8sia2$^{f/f}$* and *Emx1-Cre;St8sia2$^{f/f}$* animals should be mimicked by *Foxg1-Cre;St8sia2$^{f/f}$* animals. Provided that *Foxg1-Cre;St8sia2$^{f/f}$* mice show defective thalamocortical pathfinding, any behavioral abnormalities confined to these mice could be ascribed to disturbed thalamus-cortex connectivity.

Lhx6-Cre;St8sia2$^{f/f}$ animals on the other hand are a valuable asset. Since these mice display a pronounced defect in the cortical interneuron system but no alterations in the long-range connectivity of the thalamus and the mammillary body, they appear suitable to investigate if the loss of cortical interneurons causes behavioral abnormalities.

Although *Foxb1-Cre;St8sia2$^{f/f}$* animals do not mimic the thalamocortical phenotype of *St8sia2$^{-/-}$* mice, these mice do exhibit strong alterations of the mammillary body and its long-range connectivities. Since our analyses confirmed that neither the cortical interneuron system nor long-range thalamic and cortical connectivity are affected by this knockout, *Foxb1-Cre;St8sia2$^{f/f}$* mice can be utilized to address a potential behavioral phenotype as a result of disturbances in long-range mammillary body connectivity.

In conclusion, future studies should examine the behavior of *Foxb1-Cre;St8sia2$^{f/f}$* and *Lhx6-Cre;St8sia2$^{f/f}$* animals as well as mice with disturbed thalamus-cortex connectivity in order to dissect the behavioral phenotype observed in *St8sia2$^{-/-}$* mice.

Appendix

Bibliography

Abe P, Mueller W, Schütz D, Fabienne M, Thelen M, Zhang P, and Stumm R (2014) CXCR7 prevents excessive CXCL12-mediated downregulation of CXCR4 in migrating cortical interneurons. Development 141:1857–1863.

Albach C, Damoc E, Denzinger T, Schachner M, Przybylski M, and Schmitz B (2004) Identification of N-glycosylation sites of the murine neural cell adhesion molecule NCAM by MALDI-TOF and MALDI-FTICR mass spectrometry. Anal. Bioanal. Chem. 378:1129–1135.

Alcántara S, Pozas E, Ibañez C F, and Soriano E (2006) BDNF-modulated spatial organization of Cajal–Retzius and GABAergic neurons in the marginal zone plays a role in the development of cortical organization. Cereb. Cortex 16:487–499.

Anderson S, Marín O, Horn C, Jennings K, and Rubenstein J (2001) Distinct cortical migrations from the medial and lateral ganglionic eminences. Development 128:353–363.

Ang E S, Haydar T F, Gluncic V, and Rakic P (2003) Four-dimensional migratory coordinates of GABAergic interneurons in the developing mouse cortex. J. Neurosci. 23:5805–15.

Angata K, Nakayama J, Fredette B, Chong K, Ranscht B, and Fukuda M (1997) Human STX polysialyltransferase forms the embryonic form of the neural cell adhesion molecule. Tissue-specific expression, neurite outgrowth, and chromosomal localization in comparison with another polysialyltransferase, PST. J. Biol. Chem. 272:7182–90.

Angata K, Huckaby V, Ranscht B, Terskikh A, Marth J, and Fukuda M (2007) Polysialic acid-directed migration and differentiation of neural precursors are essential for mouse brain development. Mol. Cell. Biol. 27:6659–68.

Angata K, Long J M, Bukalo O, Lee W, Dityatev A, Wynshaw-Boris A, Schachner M, Fukuda M, and Marth J D (2004) Sialyltransferase ST8Sia-II assembles a subset of polysialic acid that directs hippocampal axonal targeting and promotes fear behavior. J. Biol. Chem. 279:32603–32613.

Angevine J B (1970) Time of neuron origin in the diencephalon of the mouse. An autoradiographic study. J. Comp. Neurol. 139:129–187.

Anney R, Klei L, Pinto D, Regan R, Conroy J, Magalhaes T R, Correia C, Abrahams B S, Sykes N, Pagnamenta A T, *et al.* (2010) A genome-wide scan for common alleles affecting risk for autism. Hum. Mol. Genet. 19:4072–4082.

Bibliography

Anticevic A and Corlett P R (2012) Cognition-emotion dysinteraction in schizophrenia. Front. Psychol. 3:392.

Arai M, Yamada K, Toyota T, Obata N, Haga S, Yoshida Y, Nakamura K, Minabe Y, Ujike H, Sora I, Ikeda K, Mori N, Yoshikawa T, and Itokawa M (2006) Association between polymorphisms in the promoter region of the sialyltransferase 8B (SIAT8B) gene and schizophrenia. Biol. Psychiatry 59:652–659.

Arenas E, Åkerud P, Wong V, Boylan C, Person H, Lindsay R M, and Altar C A (1996) Effects of BDNF and NT-4/5 on striatonigral neuropeptides or nigral GABA neurons in vivo. Eur. J. Neurosci. 8:1707–1717.

Arguello P A and Gogos J A (2009) Cognition in mouse models of schizophrenia susceptibility genes. Schizophr. Bull. 36:289–300.

Atz M, Rollins B, and Vawter M (2007) NCAM1 association study of bipolar disorder and schizophrenia: polymorphisms and alternatively spliced isoforms lead to similarities and differences. Psychiatr. Genet. 17:55–67.

Barbeau D, Liang J J, Robitalille Y, Quirion R, and Srivastava L K (1995) Decreased expression of the embryonic form of the neural cell adhesion molecule in schizophrenic brains. Proc. Natl. Acad. Sci. U.S.A. 92:2785–2789.

Bartsch U, Kirchhoff F, and Schachner M (1990) Highly sialylated N-CAM is expressed in adult mouse optic nerve and retina. J. Neurocytol. 19:550–565.

Behrendt R P (2006) Dysregulation of thalamic sensory 'transmission'in schizophrenia: neurochemical vulnerability to hallucinations. J. Psychopharmacol. 20:356–372.

Behrendt R P and Young C (2004) Hallucinations in schizophrenia, sensory impairment, and brain disease: A unifying model. Behav. Brain Sci. 27:771–787.

Benes F M and Berretta S (2001) GABAergic interneurons: implications for understanding schizophrenia and bipolar disorder. Neuropsychopharmacology 25:1.

Ben-Hur T, Rogister B, Murray K, Rougon G, and Dubois-Dalcq M (1998) Growth and fate of PSA-NCAM+ precursors of the postnatal brain. J. Neurosci. 18:5777–5788.

Bernstein H G, Krause S, Krell D, Dobrowolny H, Wolter M, Stauch R, Ranft K, Danos P, Jirikowski G F, and Bogerts B (2007) Strongly reduced number of parvalbumin-immunoreactive projection neurons in the mammillary bodies in schizophrenia. Ann. N.Y. Acad. Sci. 1096:120–127.

Blakemore C and Molnar Z (1990) Factors involved in the establishment of specific interconnections between thalamus and cerebral cortex. Cold Spring Harb. Symp. Quant. Biol. 55:491–504.

Blokland G A, Mesholam-Gately R I, Toulopoulou T, Del R E C, Lam M, DeLisi L E, Donohoe G, Walters J T, Consortium G, Seidman L J, *et al.* (2016) Heritability of neuropsychological measures in schizophrenia and nonpsychiatric populations: a systematic review and meta-analysis. Schizophr. Bull. 43:788–800.

Bonfanti L and Theodosis D (1994) Expression of polysialylated neural cell adhesion molecule by proliferating cells in the subependymal layer of the adult rat, in its rostral extension and in the olfactory bulb. Neuroscience 62:291–305.

Bonfanti L (2006) PSA-NCAM in mammalian structural plasticity and neurogenesis. Prog. Neurobiol. 80:129–164.

Braff D, Geyer M, Light G, Sprock J, Perry W, Cadenhead K, and Swerdlow N (2001) Impact of prepulse characteristics on the detection of sensorimotor gating deficits in schizophrenia. Schizophr. Res. 49:171–178.

Braisted J E, Ringstedt T, and O'leary D D (2009) Slits are chemorepellents endogenous to hypothalamus and steer thalamocortical axons into ventral telencephalon. Cereb. Cortex 19:i144–i151.

Brandão J A and Romcy-Pereira R N (2015) Interplay of environmental signals and progenitor diversity on fate specification of cortical GABAergic neurons. Front. Cell. Neurosci. 9:149.

Brown A S (2011) The environment and susceptibility to schizophrenia. Prog. Neurobiol. 93:23–58.

Burgess A and Aubert I (2006) Polysialic acid limits choline acetyltransferase activity induced by brain-derived neurotrophic factor. J. Neurochem. 99.

Butt S J, Fuccillo M, Nery S, Noctor S, Kriegstein A, Corbin J G, and Fishell G (2005) The temporal and spatial origins of cortical interneurons predict their physiological subtype. Neuron 48:591–604.

Chazal G, Durbec P, Jankovski A, Rougon G, and Cremer H (2000) Consequences of neural cell adhesion molecule deficiency on cell migration in the rostral migratory stream of the mouse. J. Neurosci. 20:1446–1457.

Cremer H, Lange R, Christoph A, Plomann M, Vopper G, Roes J, Brown R, Baldwin S, Kraemer P, Scheff S, Barthels D, Rajewsky K, and Willie W (1994) Inactivation of the N-CAM gene in mice results in size reduction of the olfactory bulb and deficits in spatial learning. Nature 367:455–459.

Crick F (1984) Function of the thalamic reticular complex: the searchlight hypothesis. Proc. Natl. Acad. Sci. U.S.A. 81:4586–4590.

Cunningham B, Hemperly J, Murray B, Prediger E, Brackenbury R, and Edelman G (1987) Neural cell adhesion molecule: structure, immunoglobulin-like domains, cell surface modulation, and alternative RNA splicing. Science 236:799–806.

Curreli S, Arany Z, Rita G, Mann D, and Stamatos N (2007) Polysialylated neuropilin-2 Is expressed on the surface of human dendritic cells and modulates dendritic Cell-T lymphocyte interactions. J. Biol. Chem. 282:30346–30356.

Datta A K and Paulson J C (1995) The sialyltransferase sialylmotif participates in binding the donor substrate CMP-NeuAc. J. Biol. Chem. 270:1497–1500.

Datta A K, Sinha A, and Paulson J C (1998) Mutation of the sialyltransferase S-sialylmotif alters the kinetics of the donor and acceptor substrates. J. Biol. Chem. 273:9608–9614.

Bibliography

Denaxa M, Chan C, Schachner M, Parnavelas J, and Karagogeos D (2001) The adhesion molecule TAG-1 mediates the migration of cortical interneurons from the ganglionic eminence along the corticofugal fiber system. Development 128:4635–44.

Denaxa M, Kyriakopoulou K, Theodorakis K, Trichas G, Vidaki M, Takeda Y, Watanabe K, and Karagogeos D (2005) The adhesion molecule TAG-1 is required for proper migration of the superficial migratory stream in the medulla but not of cortical interneurons. Dev. Biol. 288:87–99.

Di Cristo G (2007) Development of cortical GABAergic circuits and its implications for neurodevelopmental disorders. Clin. Genet. 72:1–8.

Diestel S, Hinkle C L, Schmitz B, and Maness P F (2005) NCAM140 stimulates integrin-dependent cell migration by ectodomain shedding. J. Neurochem. 95:1777–1784.

Doetsch F (2003) A niche for adult neural stem cells. Curr. Opin. Genet. Dev. 13:543–550.

Du T, Xu Q, Ocbina P, and Anderson S (2008) NKX2.1 specifies cortical interneuron fate by activating Lhx6. Development 135:1559–67.

Eckhardt M, Bukalo O, Chazal G, Wang L, Goridis C, Schachner M, R G, Cremer H, and Dityatev A (2000) Mice deficient in the polysialyltransferase ST8SiaIV/PST-1 allow discrimination of the roles of neural cell adhesion molecule protein and polysialic acid in neural development and synaptic plasticity. J. Neurosci. 20:5234–44.

Eckhardt M, Mühlenhoff M, Bethe A, Koopman J, Frosch M, and Gerardy-Schahn R (1995) Molecular characterization of eukaryotic polysialyltransferase-1. Nature 373:715–718.

Edelman G M (1987) CAMs and Igs: cell adhesion and the evolutionary origins of immunity. Immunol. Rev. 100:11–45.

Eggers K, Werneburg S, Schertzinger A, Abeln M, Schiff M, Scharenberg M A, Burkhardt H, Mühlenhoff M, and Hildebrandt H (2011) Polysialic acid controls NCAM signals at cell–cell contacts to regulate focal adhesion independent from FGF receptor activity. J. Cell Sci. 124:3279–3291.

Ehrenreich H and Nave K A (2014) Phenotype-based genetic association studies (PGAS)—towards understanding the contribution of common genetic variants to schizophrenia subphenotypes. Genes 5:97–105.

Ellison-Wright I, Nathan P J, Bullmore E T, Zaman R, Dudas R B, Agius M, Fernandez-Egea E, Müller U, Dodds C M, Forde N J, *et al.* (2014) Distribution of tract deficits in schizophrenia. BMC Psychiatry 14:99.

Finne J, Finne U, H D, and Goridis C (1983) Occurrence of alpha 2-8 linked polysialosyl units in a neural cell adhesion molecule. Biochem. Biophys. Res. Commun. 112:482–7.

Fiumelli H, Kiraly M, Ambrus A, Magistretti P J, and Martin J L (2000) Opposite regulation of calbindin and calretinin expression by brain-derived neurotrophic factor in cortical neurons. J. Neurochem. 74:1870–1877.

Flames N, Long J E, Garratt A N, Fischer T M, Gassmann M, Birchmeier C, Lai C, Rubenstein J L, and Marın O (2004) Short-and long-range attraction of cortical GABAergic interneurons by neuregulin-1. Neuron 44:251–261.

Foley D A, Swartzentruber K G, and Colley K J (2009) Identification of sequences in the polysialyltransferases ST8Sia II and ST8Sia IV that are required for the protein-specific polysialylation of the neural cell adhesion molecule, NCAM. J. Biol. Chem. 284:15505–15516.

Fragkouli A, Wijk N, Lopes R, Kessaris N, and Pachnis V (2009) LIM homeodomain transcription factor-dependent specification of bipotential MGE progenitors into cholinergic and GABAergic striatal interneurons. Development 136:3841–3851.

Francavilla C, Cattaneo P, Berezin V, Bock E, Ami D, Marco A de, Christofori G, and Cavallaro U (2009) The binding of NCAM to FGFR1 induces a specific cellular response mediated by receptor trafficking. J. Cell Biol. 187:1101–1116.

Friedlander D R, Milev P, Karthikeyan L, Margolis R K, Margolis R U, and Grumet M (1994) The neuronal chondroitin sulfate proteoglycan neurocan binds to the neural cell adhesion molecules Ng-CAM/L1/NILE and N-CAM, and inhibits neuronal adhesion and neurite outgrowth. J. Cell Biol. 125:669–680.

Galuska S, Geyer R, Rita G, Mühlenhoff M, and Geyer H (2008) Enzyme-dependent Variations in the Polysialylation of the Neural Cell Adhesion Molecule (NCAM) in Vivo. J. Biol. Chem. 283:17–28.

Galuska S, Imke O, Geyer H, Weinhold B, Kuchelmeister K, Hildebrandt H, Rita G, Geyer R, and Mühlenhoff M (2006) Polysialic acid profiles of mice expressing variant allelic combinations of the polysialyltransferases ST8SiaII and ST8SiaIV. J. Biol. Chem. 281:31605–31615.

Galuska S, Rollenhagen M, Kaup M, Eggers K, Imke O, Schiff M, Hartmann M, Weinhold B, Hildebrandt H, Geyer R, Mühlenhoff M, and Geyer H (2010) Synaptic cell adhesion molecule SynCAM 1 is a target for polysialylation in postnatal mouse brain. Proc. Natl. Acad. Sci. U.S.A. 107:10250–10255.

Gelman D M and Marín O (2010) Generation of interneuron diversity in the mouse cerebral cortex. Eur. J. Neurosci. 31:2136–2141.

Gennarini G, Hirn M, Deagostini-Bazin H, and Goridis C (1984) Studies on the transmembrane disposition of the neural cell adhesion molecule N-CAM. Eur. J. Biochem. 142:65–73.

Geyer H, Bahr U, Liedtke S, Schachner M, and Geyer R (2001) Core structures of polysialylated glycans present in neural cell adhesion molecule from newborn mouse brain. Eur. J. Biochem. 268:6587–6599.

Bibliography

Gilabert-Juan J, Castillo-Gomez E, Marta P, Moltó M, and Nacher J (2011) Chronic stress induces changes in the structure of interneurons and in the expression of molecules related to neuronal structural plasticity and inhibitory neurotransmission in the amygdala of adult mice. Exp. Neurol. 232:33–40.

Gilabert-Juan J, Nacher J, Sanjuán J, and Moltó M D (2013) Sex-specific association of the ST8SIAII gene with schizophrenia in a Spanish population. Psychiatry Res. 210:1293–1295.

Gilabert-Juan J, Varea E, Guirado R, Blasco-Ibáñez J M, Crespo C, and Nácher J (2012) Alterations in the expression of PSA-NCAM and synaptic proteins in the dorsolateral prefrontal cortex of psychiatric disorder patients. Neurosci. Lett. 530:97–102.

Gong S, Chen Z, Doughty M L, Losos K, Didkovsky N, Schambra U B, Nowak N J, Joyner A, Leblanc G, Hatten M E, and Heintz N (2003) A gene expression atlas of the central nervous system based on bacterial artificial chromosomes. Nature 425:917.

Gorski J, Talley T, Qiu M, Puelles L, Rubenstein J, and Jones K (2002) Cortical excitatory neurons and glia, but not GABAergic neurons, are produced in the Emx1-expressing lineage. J. Neurosci. 22:6309–14.

Gower H J, Barton C H, Elsom V L, Thompson J, Moore S E, Dickson G, and Walsh F S (1988) Alternative splicing generates a secreted form of N-CAM in muscle and brain. Cell 55:955–964.

Green M F, Kern R S, Braff D L, and Mintz J (2000) Neurocognitive deficits and functional outcome in schizophrenia: are we measuring the" right stuff"? Schizophr. Bull. 26:119–136.

Grigoriou M, Tucker A, Sharpe P, and Pachnis V (1998) Expression and regulation of Lhx6 and Lhx7, a novel subfamily of LIM homeodomain encoding genes, suggests a role in mammalian head development. Development 125:2063–74.

Grumet M, Flaccus A, and Margolis R U (1993) Functional characterization of chondroitin sulfate proteoglycans of brain: interactions with neurons and neural cell adhesion molecules. J. Cell Biol. 120:815–824.

Gu C, Zhang Y, Wei F, Cheng Y, Cao Y, and Hou H (2016) Magnetic resonance imaging DTI-FT study on schizophrenic patients with typical negative first symptoms. Exp. Ther. Med. 12:1450–1454.

Guillery R, Feig S, and Lozsadi D (1998) Paying attention to the thalamic reticular nucleus. Trends Neurosci. 21:28–32.

Hammond M S, Sims C, Parameshwaran K, Suppiramaniam V, Schachner M, and Dityatev A (2006) NCAM associated polysialic acid inhibits NR2B-containing NMDA receptors and prevents glutamate-induced cell death. J. Biol. Chem.

Harduin-Lepers A, Mollicone R, Delannoy P, and Oriol R (2005) The animal sialyltransferases and sialyltransferase-related genes: a phylogenetic approach. Glycobiology 15:805–17.

Harduin-Lepers A, Vallejo-Ruiz V, Krzewinski-Recchi M A, Samyn-Petit B, Julien S, and Delannoy P (2001) The human sialyltransferase family. Biochimie 83:727–737.

Harris R M (1987) Axon collaterals in the thalamic reticular nucleus from thalamocortical neurons of the rat ventrobasal thalamus. J. Comp. Neurol. 258:397–406.

Hashemi E, Ariza J, Rogers H, Noctor S, and Verónica M (2016) The number of parvalbumin-expressing interneurons is decreased in the medial prefrontal cortex in autism. Cereb. Cortex 27:1931–1943.

Hashimoto T, Bergen S E, Nguyen Q L, Xu B, Monteggia L M, Pierri J N, Sun Z, Sampson A R, and Lewis D A (2005) Relationship of brain-derived neurotrophic factor and its receptor TrkB to altered inhibitory prefrontal circuitry in schizophrenia. J. Neurosci. 25:372–383.

He H T, Barbet J, Chaix J C, and Goridis C (1986) Phosphatidylinositol is involved in the membrane attachment of NCAM-120, the smallest component of the neural cell adhesion molecule. EMBO J. 5:2489.

He H T, Finne J, and Goridis C (1987) Biosynthesis, membrane association, and release of N-CAM-120, a phosphatidylinositol-linked form of the neural cell adhesion molecule. J. Cell Biol. 105:2489–2500.

Hekmat A, Bitter-Suermann D, and Schachner M (1990) Immunocytological localization of the highly polysialylated form of the neural cell adhesion molecule during development of the murine cerebellar cortex. J. Comp. Neurol. 291:457–467.

Hildebrandt H, Becker C, Mürau M, Gerardy-Schahn R, and Rahmann H (1998) Heterogeneous expression of the polysialyltransferases ST8Sia II and ST8Sia IV during postnatal rat brain development. J. Neurochem. 71:2339–2348.

Hildebrandt H, Mühlenhoff M, Imke O, Röckle I, Burkhardt H, Weinhold B, and Rita G (2009) Imbalance of neural cell adhesion molecule and polysialyltransferase alleles causes defective brain connectivity. Brain 132:2831–8.

Hinkle C, Diestel S, Lieberman J, and Maness P (2006) Metalloprotease-induced ectodomain shedding of neural cell adhesion molecule (NCAM). J. Neurobiol. 66:1378–1395.

Hirn M, Ghandour M, Hermine D, and Goridis C (1983) Molecular heterogeneity and structural evolution during cerebellar ontogeny detected by monoclonal antibody of the mouse cell surface antigen BSP-2. Brain Res. 265:87–100.

Hoffman S and Edelman G M (1983) Kinetics of homophilic binding by embryonic and adult forms of the neural cell adhesion molecule. Proc. Natl. Acad. Sci. U.S.A. 80:5762–5766.

Hu H (2000) Polysialic acid regulates chain formation by migrating olfactory interneuron precursors. J. Neurosci. Res. 61:480–492.

Bibliography

Hübschmann M V, Skladchikova G, Bock E, and Berezin V (2005) Neural cell adhesion molecule function is regulated by metalloproteinase-mediated ectodomain release. J. Neurosci. Res. 80:826–837.

Human Protein Atlas (2017). URL: http://www.proteinatlas.org/ENSG00000149294-NCAM1/tissue.

Inoue S, Lin S L, and Inoue Y (2000) Chemical analysis of the developmental pattern of polysialylation in chicken brain expression of only an extended form of polysialyl chains during embryogenesis and the presence of disialyl residues in both embryonic and adult chicken brains. J. Biol. Chem. 275:29968–29979.

Isomura R, Kitajima K, and Sato C (2011) Structural and functional impairments of polysialic acid by a mutated polysialyltransferase found in schizophrenia. J. Biol. Chem. 286:21535–21545.

Johnson C, Fragneto G, Konovalov O, Dubosclard V, Legrand J F, and Leckband D E (2005a) Structural studies of the neural-cell-adhesion molecule by X-ray and neutron reflectivity. Biochemistry 44:546–554.

Johnson C, Fujimoto I, Rutishauser U, and Leckband D (2005b) Direct evidence that neural cell adhesion molecule (NCAM) polysialylation increases intermembrane repulsion and abrogates adhesion. J. Biol. Chem. 280:137–145.

Jones K R, Fariñas I, Backus C, and Reichardt L F (1994) Targeted disruption of the BDNF gene perturbs brain and sensory neuron development but not motor neuron development. Cell 76:989–999.

Kalus I, Bormann U, Mzoughi M, Schachner M, and Kleene R (2006) Proteolytic cleavage of the neural cell adhesion molecule by ADAM17/TACE is involved in neurite outgrowth. J. Neurochem. 98:78–88.

Kammen D P van, Poltorak M, Kelley M E, Yao J K, Gurklis J A, Peters J L, Hemperly J J, Wright R D, and Freed W J (1998) Further studies of elevated cerebrospinal fluid neuronal cell adhesion molecule in schizophrenia. Biol. Psychiatry 43:680–686.

Kanatani S, Yozu M, Tabata H, and Nakajima K (2008) COUP-TFII is preferentially expressed in the caudal ganglionic eminence and is involved in the caudal migratory stream. J. Neurosci. 28:13582–13591.

Kanato Y, Kitajima K, and Sato C (2008) Direct binding of polysialic acid to a brain-derived neurotrophic factor depends on the degree of polymerization. Glycobiology 18:1044–53.

Karlstetter M, Kopatz J, Aslanidis A, Shahraz A, Caramoy A, Linnartz-Gerlach B, Lin Y, Lückoff A, Fauser S, Düker K, *et al.* (2017) Polysialic acid blocks mononuclear phagocyte reactivity, inhibits complement activation, and protects from vascular damage in the retina. EMBO Mol. Med. 9:154–166.

Kiermaier E, Moussion C, Veldkamp C, Rita G, Vries I, Williams L, Chaffee G, Phillips A, Freiberger F, Imre R, Taleski D, Payne R, Braun A, Förster R, Mechtler K, Mühlenhoff M, Volkman B, and Sixt M (2016) Polysialylation controls dendritic cell trafficking by regulating chemokine recognition. Science 351:186–190.

Kochlamazashvili G, Senkov O, Grebenyuk S, Robinson C, Xiao M, Stummeyer K, Gerardy-Schahn R, Engel A, Feig L, Semyanov A, Suppiramaniam V, Schachner M, and Dityatev A (2010) Neural cell adhesion molecule-associated polysialic acid regulates synaptic plasticity and learning by restraining the signaling through GluN2B-containing NMDA receptors. J. Neurosci. 30:4171–4183.

Kojima N, Yoshida Y, and Tsuji S (1995) A developmentally regulated member of the sialyltransferase family (ST8Sia II, STX) is a polysialic acid synthase. FEBS Lett. 373:119–22.

Kolkova K, Novitskaya V, Pedersen N, Berezin V, and Bock E (2000) Neural cell adhesion molecule-stimulated neurite outgrowth depends on activation of protein kinase C and the Ras-mitogen-activated protein kinase pathway. J. Neurosci. 20:2238–46.

Kornack D R and Rakic P (2001) The generation, migration, and differentiation of olfactory neurons in the adult primate brain. Proc. Natl. Acad. Sci. U.S.A. 98:4752–4757.

Krause M, Hoffmann W E, and Hajós M (2003) Auditory sensory gating in hippocampus and reticular thalamic neurons in anesthetized rats. Biol. Psychiatry 53:244–253.

Kröcher T, Malinovskaja K, Jürgenson M, Anu A, Zharkovskaya T, Kalda A, Röckle I, Schiff M, Weinhold B, Rita G, Hildebrandt H, and Zharkovsky A (2015) Schizophrenia-like phenotype of polysialyltransferase ST8SIA2-deficient mice. Brain Struct. Funct. 220:71–83.

Kröcher T, Röckle I, Diederichs U, Weinhold B, Burkhardt H, Yanagawa Y, Gerardy-Schahn R, and Hildebrandt H (2014) A crucial role for polysialic acid in developmental interneuron migration and the establishment of interneuron densities in the mouse prefrontal cortex. Development 141:3022–3032.

Kurosawa N, Yoshida Y, Kojima N, and Tsuji S (1997) Polysialic acid synthase (ST8Sia II/STX) mRNA expression in the developing mouse central nervous system. J. Neurochem. 69:494–503.

Kustermann S, Hildebrandt H, Bolz S, Dengler K, and Kohler K (2010) Genesis of rods in the zebrafish retina occurs in a microenvironment provided by polysialic acid-expressing Müller glia. J. Comp. Neurol. 518:636–646.

Lavdas A, Grigoriou M, Pachnis V, and Parnavelas J (1999) The medial ganglionic eminence gives rise to a population of early neurons in the developing cerebral cortex. J. Neurosci. 19:7881–8.

Bibliography

Lewandoski M, Wassarman K, and Martin G (1997) Zp3-cre, a transgenic mouse line for the activation or inactivation of loxP-flanked target genes specifically in the female germ line. Curr. Biol. 7:148–51.

Lewis D A, Curley A A, Glausier J R, and Volk D W (2012) Cortical parvalbumin interneurons and cognitive dysfunction in schizophrenia. Trends Neurosci. 35:57–67.

Lewis D A and Levitt P (2002) Schizophrenia as a disorder of neurodevelopment. Annu. Rev. Neurosci. 25:409–432.

Li H, Chou S J, Hamasaki T, Perez-Garcia C G, and O'Leary D D (2012) Neuregulin repellent signaling via ErbB4 restricts GABAergic interneurons to migratory paths from ganglionic eminence to cortical destinations. Neural Dev. 7:10.

Li H, Babiarz J, Woodbury J, Kane-Goldsmith N, and Grumet M (2004) Spatiotemporal heterogeneity of CNS radial glial cells and their transition to restricted precursors. Dev. Biol. 271:225–238.

Liedtke S, Geyer H, Wuhrer M, Geyer R, Frank G, Gerardy-Schahn R, Zähringer U, and Schachner M (2001) Characterization of N-glycans from mouse brain neural cell adhesion molecule. Glycobiology 11:373–384.

Little E B, Edelman G M, and Cunningham B A (1998) Palmitoylation of the cytoplasmic domain of the neural cell adhesion molecule N-CAM serves as an anchor to cellular membranes. Cell Adhes. Commun. 6:415–430.

Lodato S, Tomassy G S, De Leonibus E, Uzcategui Y G, Andolfi G, Armentano M, Touzot A, Gaztelu J M, Arlotta P, Prida L M de la, *et al.* (2011) Loss of COUP-TFI alters the balance between caudal ganglionic eminence-and medial ganglionic eminence-derived cortical interneurons and results in resistance to epilepsy. J. Neurosci. 31:4650–4662.

Loftus M, Knight R T, and Amaral D G (2000) An analysis of atrophy in the medial mammillary nucleus following hippocampal and fornix lesions in humans and nonhuman primates. Exp. Neurol. 163:180–190.

Lois C, Garcia-Verdugo J M, and Alvarez-Buylla A (1996) Chain migration of neuronal precursors. Science 271:978–980.

López-Bendito G and Molnár Z (2003) Thalamocortical development: how are we going to get there? Nat. Rev. Neurosci. 4:276.

López-Bendito G, Sánchez-Alcaniz J A, Pla R, Borrell V, Picó E, Valdeolmillos M, and Marín O (2008) Chemokine signaling controls intracortical migration and final distribution of GABAergic interneurons. J. Neurosci. 28:1613–1624.

López-Bendito G, Cautinat A, Sánchez J A, Bielle F, Flames N, Garratt A N, Talmage D A, Role L W, Charnay P, Marín O, *et al.* (2006) Tangential neuronal migration controls axon guidance: a role for neuregulin-1 in thalamocortical axon navigation. Cell 125:127–142.

Lysko D, Putt M, and Golden J (2011) SDF1 regulates leading process branching and speed of migrating interneurons. J. Neurosci. 31:1739–1745.

Marín O, Anderson S, and Rubenstein J (2000) Origin and molecular specification of striatal interneurons. J. Neurosci. 20:6063–76.

Marín O and Rubenstein J L (2001) A long, remarkable journey: tangential migration in the telencephalon. Nat. Rev. Neurosci. 2:780.

Marín O and Rubenstein J L (2003) Cell migration in the forebrain. Annu. Rev. Neurosci. 26:441–483.

McAuley E, Scimone A, Tiwari Y, Agahi G, Mowry B, Holliday E, Donald J, Weickert C, Mitchell P, Schofield P, and Fullerton J (2012) Identification of sialyltransferase 8B as a generalized susceptibility gene for psychotic and mood disorders on chromosome 15q25-26. PLoS One 7:e38172.

Milev P, Friedlander D R, Sakurai T, Karthikeyan L, Flad M, Margolis R K, Grumet M, and Margolis R U (1994) Interactions of the chondroitin sulfate proteoglycan phosphacan, the extracellular domain of a receptor-type protein tyrosine phosphatase, with neurons, glia, and neural cell adhesion molecules. J. Cell Biol. 127:1703–1715.

Miyamae T, Chen K, Lewis D A, and Gonzalez-Burgos G (2017) Distinct physiological maturation of parvalbumin-positive neuron subtypes in mouse prefrontal cortex. J. Neurosci. 37:4883–4902.

Miyoshi G, Butt S, Takebayashi H, and Fishell G (2007) Physiologically distinct temporal cohorts of cortical interneurons arise from telencephalic Olig2-expressing precursors. J. Neurosci. 27:7786–98.

Moberg P J, Kamath V, Marchetto D M, Calkins M E, Doty R L, Hahn C G, Borgmann-Winter K E, Kohler C G, Gur R E, and Turetsky B I (2013) Meta-analysis of olfactory function in schizophrenia, first-degree family members, and youths at-risk for psychosis. Schizophr. Bull. 40:50–59.

Molnár Z and Blakemore C (1995) How do thalamic axons find their way to the cortex? Trends Neurosci. 18:389–397.

Mühlenhoff M, Rollenhagen M, Werneburg S, Gerardy-Schahn R, and Hildebrandt H (2013) Polysialic acid: versatile modification of NCAM, SynCAM 1 and neuropilin-2. Neurochem. Res. 38:1134–1143.

Muller D, Djebbara-Hannas Z, Jourdain P, Vutskits L, Durbec P, Rougon G, and Kiss J Z (2000) Brain-derived neurotrophic factor restores long-term potentiation in polysialic acid-neural cell adhesion molecule-deficient hippocampus. Proc. Natl. Acad. Sci. U.S.A. 97:4315–4320.

Murray B A, Hemperly J J, Prediger E A, Edelman G M, and Cunningham B A (1986) Alternatively spliced mRNAs code for different polypeptide chains of the chicken neural cell adhesion molecule (N-CAM). J. Cell Biol. 102:189–193.

Nacher J, Guirado R, Varea E, G. A, Röckle I, and Hildebrandt H (2010) Divergent impact of the polysialyltransferases ST8SiaII and ST8SiaIV on polysialic acid expression in immature neurons and interneurons of the adult cerebral cortex. Neuroscience 167:825–837.

Nacher J, Alonso-Llosa G, Rosell D, and McEwen B (2002a) PSA-NCAM expression in the piriform cortex of the adult rat. Modulation by NMDA receptor antagonist administration. Brain Res. 927:111–121.

Nacher J, Blasco-Ibáñez J M, and McEwen B S (2002b) Non-granule PSA-NCAM immunoreactive neurons in the rat hippocampus. Brain Res. 930:1–11.

Nacher J, Guirado R, and Castillo-Gómez E (2013) Structural plasticity of interneurons in the adult brain: role of PSA-NCAM and implications for psychiatric disorders. Neurochem. Res. 38:1122–1133.

Nakata D, Zhang L, and Troy F A (2006) Molecular basis for polysialylation: a novel polybasic polysialyltransferase domain (PSTD) of 32 amino acids unique to the α2, 8-polysialyltransferases is essential for polysialylation. Glycoconj. J. 23:423–436.

Nelson R W, Bates P A, and Rutishauser U (1995) Protein determinants for specific polysialylation of the neural cell adhesion molecule. J. Biol. Chem. 270:17171–17179.

Niethammer P, Delling M, Sytnyk V, Dityatev A, Fukami K, and Schachner M (2002) Cosignaling of NCAM via lipid rafts and the FGF receptor is required for neuritogenesis. J. Cell Biol. 157:521–532.

Nieto R, Kukuljan M, and Silva H (2013) BDNF and schizophrenia: from neurodevelopment to neuronal plasticity, learning, and memory. Front. Psychiatry 4:45.

Oltmann-Norden I, Galuska S P, Hildebrandt H, Geyer R, Gerardy-Schahn R, Geyer H, and Mühlenhoff M (2008) Impact of the polysialyltransferases ST8SiaII and ST8SiaIV on polysialic acid synthesis during postnatal mouse brain development. J. Biol. Chem. 283:1463–1471.

Ong E, Nakayama J, Angata K, Reyes L, Katsuyama T, Arai Y, and Fukuda M (1998) Developmental regulation of polysialic acid synthesis in mouse directed by two polysialyltransferases, PST and STX. Glycobiology 8:415–24.

Ono K, Tomasiewicz H, Magnuson T, and Rutishauser U (1994) N-CAM mutation inhibits tangential neuronal migration and is phenocopied by enzymatic removal of polysialic acid. Neuron 13:595–609.

Ono S, Hane M, Kitajima K, and Sato C (2012) Novel regulation of fibroblast growth factor 2 (FGF2)-mediated cell growth by polysialic acid. J. Biol. Chem. 287:3710–3722.

Pinault D (2004) The thalamic reticular nucleus: structure, function and concept. Brain Res. Rev. 46:1–31.

Piras F, Schiff M, Chiapponi C, Bossu P, Mühlenhoff M, Caltagirone C, Gerardy-Schahn R, Hildebrandt H, and Spalletta G (2015) Brain structure, cognition and negative symptoms in schizophrenia are associated with serum levels of polysialic acid-modified NCAM. Transl. Psychiatry 5:e658.

Polleux F, Whitford K L, Dijkhuizen P A, Vitalis T, and Ghosh A (2002) Control of cortical interneuron migration by neurotrophins and PI3-kinase signaling. Development 129:3147–3160.

Poltorak M, Hemperly J J, Williams J R, El-Mallakh R, and Freed W J (1995) Disturbances in cell recognition molecules (N-CAM and L1 antigen) in the CSF of patients with schizophrenia. Exp. Neurol. 131:266–272.

Ponti G, Aimar P, and Bonfanti L (2006) Cellular composition and cytoarchitecture of the rabbit subventricular zone and its extensions in the forebrain. J. Comp. Neurol. 498:491–507.

Powell E, Mars W, and Levitt P (2001) Hepatocyte growth factor/scatter factor is a motogen for interneurons migrating from the ventral to dorsal telencephalon. Neuron 30:79–89.

Probstmeier R, Bilz A, and J. S (1994) Expression of the neural cell adhesion molecule and polysialic acid during early mouse embryogenesis. J. Neurosci. Res. 37:324–335.

Qin X Y, Feng J C, Cao C, Wu H T, Loh Y P, and Cheng Y (2016) Association of peripheral blood levels of brain-derived neurotrophic factor with autism spectrum disorder in children: a systematic review and meta-analysis. JAMA Pediatr. 170:1079–1086.

Radyushkin K, Anokhin K, Meyer B I, Jiang Q, Alvarez-Bolado G, and Gruss P (2005) Genetic ablation of the mammillary bodies in the Foxb1 mutant mouse leads to selective deficit of spatial working memory. Eur. J. Neurosci. 21:219–229.

Rapoport J, Giedd J, and Gogtay N (2012) Neurodevelopmental model of schizophrenia: update 2012. Mol. Psychiatry 17:1228.

Ren J, Aika Y, Heizmann C, and Kosaka T (1992) Quantitative analysis of neurons and glial cells in the rat somatosensory cortex, with special reference to GABAergic neurons and parvalbumin-containing neurons. Exp. Brain Res. 92:1–14.

Reyes A A, Small S J, and Akeson R (1991) At least 27 alternatively spliced forms of the neural cell adhesion molecule mRNA are expressed during rat heart development. Mol. Cell. Biol. 11:1654–1661.

Röckle I and Hildebrandt H (2016) Deficits of olfactory interneurons in polysialyl-transferase-and NCAM-deficient mice. Dev. Neurobiol. 76:421–433.

Röckle I, Seidenfaden R, Weinhold B, Mühlenhoff M, Gerardy-Schahn R, and Hildebrandt H (2008) Polysialic acid controls NCAM-induced differentiation of neuronal precursors into calretinin-positive olfactory bulb interneurons. Dev. Neurobiol. 68:1170–1184.

Rosenberger G, Nestor P G, Oh J S, Levitt J J, Kindleman G, Bouix S, Fitzsimmons J, Niznikiewicz M, Westin C F, Kikinis R, *et al.* (2012) Anterior limb of the internal capsule in schizophrenia: a diffusion tensor tractography study. Brain Imaging Behav. 6:417–425.

Bibliography

Rougon G (1993) Structure, metabolism and cell biology of polysialic acids. Eur. J. Cell Biol. 61:197–207.

Rougon G and Marshak D (1986) Structural and immunological characterization of the amino-terminal domain of mammalian neural cell adhesion molecules. J. Biol. Chem. 261:3396–401.

Rousselot P and Nottebohm F (1995) Expression of polysialylated N-CAM in the central nervous system of adult canaries and its possible relation to function. J. Comp. Neurol. 356:629–640.

Rudy B, Fishell G, Lee S, and Hjerling-Leffler J (2011) Three groups of interneurons account for nearly 100% of neocortical GABAergic neurons. Dev. Neurobiol. 71:45–61.

Rutishauser U, Acheson A, Hall A K, Mann D M, and Sunshine J (1988) The neural cell adhesion molecule-NCAM-as a regulator of cell-cell interactions. Science 240:53–58.

Rutishauser U and Landmesser L (1996) Polysialic acid in the vertebrate nervous system: a promoter of plasticity in cell-cell interactions. Trends Neurosci. 19:422–427.

Rymar V V and Sadikot A F (2007) Laminar fate of cortical GABAergic interneurons is dependent on both birthdate and phenotype. J. Comp. Neurol. 501:369–80.

Sadoul R, Hirn M, Deagostini-Bazin H, Rougon G, and Goridis C (1983) Adult and embryonic mouse neural cell adhesion molecules have different binding properties. Nature 304:347–349.

Saghazadeh A and Rezaei N (2017) Brain-derived neurotrophic factor levels in autism: a systematic review and meta-analysis. J. Autism Dev. Disord. 47:1018–1029.

Sakai T, Oshima A, Nozaki Y, Ida I, Haga C, Akiyama H, Nakazato Y, and Mikuni M (2008) Changes in density of calcium-binding-protein-immunoreactive GABAergic neurons in prefrontal cortex in schizophrenia and bipolar disorder. Neuropathology 28:143–150.

Sakata K, Woo N H, Martinowich K, Greene J S, Schloesser R J, Shen L, and Lu B (2009) Critical role of promoter IV-driven BDNF transcription in GABAergic transmission and synaptic plasticity in the prefrontal cortex. Proc. Natl. Acad. Sci. U.S.A. 106:5942–5947.

Santoni M, Barthels D, Vopper G, Boned A, Goridis C, and Wille W (1989) Differential exon usage involving an unusual splicing mechanism generates at least eight types of NCAM cDNA in mouse brain. EMBO J. 8:385–92.

Scheidegger E, Sternberg L, Roth J, and Lowe J (1995) A human STX cDNA confers polysialic acid expression in mammalian cells. J. Biol. Chem. 270:22685–22688.

Schiff M, Röckle I, Burkhardt H, Weinhold B, and Hildebrandt H (2011) Thalamocortical pathfinding defects precede degeneration of the reticular thalamic nucleus in polysialic acid-deficient mice. J. Neurosci. 31:1302–1312.

Schiff M, Weinhold B, Grothe C, and Hildebrandt H (2009) NCAM and polysialyl-transferase profiles match dopaminergic marker gene expression but polysialic acid is dispensable for development of the midbrain dopamine system. J. Neurochem. 110:1661–73.

Schnaar R L, Gerardy-Schahn R, and Hildebrandt H (2014) Sialic acids in the brain: gangliosides and polysialic acid in nervous system development, stability, disease, and regeneration. Physiol. Rev. 94:461–518.

Seki T and Rutishauser U (1998) Removal of polysialic acid-neural cell adhesion molecule induces aberrant mossy fiber innervation and ectopic synaptogenesis in the hippocampus. J. Neurosci. 18:3757–66.

Seki T and Arai Y (1991) The persistent expression of a highly polysialylated NCAM in the dentate gyrus of the adult rat. Neurosci. Res. 12:503–513.

Seki T and Arai Y (1993) Highly polysialylated neural cell adhesion molecule (NCAM-H) is expressed by newly generated granule cells in the dentate gyrus of the adult rat. J. Neurosci. 13:2351–2358.

Shahraz A, Kopatz J, Mathy R, Kappler J, Winter D, Kapoor S, Schütza V, Scheper T, Gieselmann V, and Neumann H (2015) Anti-inflammatory activity of low molecular weight polysialic acid on human macrophages. Sci. Rep. 5.

Sharp F R, Tomitaka M, Bernaudin M, and Tomitaka S (2001) Psychosis: pathological activation of limbic thalamocortical circuits by psychomimetics and schizophrenia? Trends Neurosci. 24:330–334.

Shimamura K, Hartigan D, Martinez S, Puelles L, and Rubenstein J (1995) Longitudinal organization of the anterior neural plate and neural tube. Development 121:3923–33.

Small S J and Akeson R (1990) Expression of the unique NCAM VASE exon is independently regulated in distinct tissues during development. J. Cell Biol. 111:2089–2096.

Sorkin B, Hoffman S, Edelman G, and Cunningham B (1984) Sulfation and phosphorylation of the neural cell adhesion molecule, N-CAM. Science 225:1476–1478.

Stepniak B, Papiol S, Hammer C, Ramin A, Everts S, Hennig L, Begemann M, and Ehrenreich H (2014) Accumulated environmental risk determining age at schizophrenia onset: a deep phenotyping-based study. Lancet Psychiatry 1:444–453.

Storms S D and Rutishauser U (1998) A role for polysialic acid in neural cell adhesion molecule heterophilic binding to proteoglycans. J. Biol. Chem. 273:27124–27129.

Stumm R, Zhou C, Ara T, Lazarini F, Monique D, Nagasawa T, Höllt V, and Schulz S (2003) CXCR4 regulates interneuron migration in the developing neocortex. J. Neurosci. 23:5123–30.

Sullivan P, Keefe R, Lange L, Lange E, Stroup T, Lieberman J, and Maness P (2006) NCAM1 and neurocognition in schizophrenia. Biol. Psychiatry 61:902–10.

Bibliography

Sumida M, Hane M, Yabe U, Shimoda Y, Pearce O M, Kiso M, Miyagi T, Sawada M, Varki A, Kitajima K, *et al.* (2015) Rapid trimming of cell surface polysialic acid (PolySia) by exovesicular sialidase triggers release of preexisting surface neurotrophin. J. Biol. Chem. 290:13202–13214.

Sussel L, Marín O, Kimura S, and Rubenstein J (1999) Loss of Nkx2. 1 homeobox gene function results in a ventral to dorsal molecular respecification within the basal telencephalon: evidence for a transformation of the pallidum into the striatum. Development 126:3359–3370.

Szewczyk L M, Brozko N, Nagalski A, Röckle I, Werneburg S, Hildebrandt H, Wisniewska M B, and Kuznicki J (2017) ST8SIA2 promotes oligodendrocyte differentiation and the integrity of myelin and axons. Glia 65:34–49.

Tantra M, Kröcher T, Papiol S, Winkler D, Röckle I, Jatho J, Burkhardt H, Ronnenberg A, Gerardy-Schahn R, Ehrenreich H, *et al.* (2014) St8sia2 deficiency plus juvenile cannabis exposure in mice synergistically affect higher cognition in adulthood. Behav. Brain Res. 275:166–175.

Tao R, Li C, Zheng Y, Qin W, Zhang J, Li X, Xu Y, Shi Y, Feng G, and He L (2007) Positive association between SIAT8B and schizophrenia in the Chinese Han population. Schizophr. Res. 90:108–114.

Theodosis D, Bonhomme R, Vitiello S, Rougon G, and Poulain D (1999) Cell surface expression of polysialic acid on NCAM is a prerequisite for activity-dependent morphological neuronal and glial plasticity. J. Neurosci. 19:10228–36.

Theodosis D, Rougon G, and Poulain D A (1991) Retention of embryonic features by an adult neuronal system capable of plasticity: polysialylated neural cell adhesion molecule in the hypothalamo-neurohypophysial system. Proc. Natl. Acad. Sci. U.S.A. 88:5494–5498.

Thompson J, Dickson G, Moore S E, Gower H J, Putt W, Kenimer J G, Barton C H, and Walsh F S (1989) Alternative splicing of the neural cell adhesion molecule gene generates variant extracellular domain structure in skeletal muscle and brain. Genes Dev. 3:348–357.

Tiveron M, Rossel M, Moepps B, Zhang Y, Seidenfaden R, Favor J, König N, and Cremer H (2006) Molecular interaction between projection neuron precursors and invading interneurons via stromal-derived factor 1 (CXCL12)/CXCR4 signaling in the cortical subventricular zone/intermediate zone. J. Neurosci. 26:13273–13278.

Todtenkopf M S, Vincent S L, and Benes F M (2005) A cross-study meta-analysis and three-dimensional comparison of cell counting in the anterior cingulate cortex of schizophrenic and bipolar brain. Schizophr. Res. 73:79–89.

Tsivilis D, Vann S D, Denby C, Roberts N, Mayes A R, Montaldi D, and Aggleton J P (2008) A disproportionate role for the fornix and mammillary bodies in recall versus recognition memory. Nat. Neurosci. 11:834–842.

Turetsky B I, Hahn C G, Borgmann-Winter K, and Moberg P J (2009) Scents and nonsense: olfactory dysfunction in schizophrenia. Schizophr. Bull. 35:1117–1131.

Turetsky B I, Moberg P J, Yousem D M, Doty R L, Arnold S E, and Gur R E (2000) Reduced olfactory bulb volume in patients with schizophrenia. Am. J. Psychiatry 157:828–830.

Uhlén M, Fagerberg L, Hallström B M, Lindskog C, Oksvold P, Mardinoglu A, Sivertsson Å, Kampf C, Sjöstedt E, Asplund A, *et al.* (2015) Tissue-based map of the human proteome. Science 347:1260419.

Vaithianathan T, Matthias K, Bahr B, Schachner M, Suppiramaniam V, Dityatev A, and Steinhaüser C (2004) Neural cell adhesion molecule-associated polysialic acid potentiates α-amino-3-hydroxy-5-methylisoxazole-4-propionic acid receptor currents. J. Biol. Chem. 279:47975–47984.

Valverde F, García C, López-Mascaraque L, and De Carlos J A (2000) Development of the mammillothalamic tract in normal and Pax-6 mutant mice. J. Comp. Neurol. 419:485–504.

van den Buuse M (2009) Modeling the positive symptoms of schizophrenia in genetically modified mice: pharmacology and methodology aspects. Schizophr. Bull. 36:246–270.

Vann S D (2013) Dismantling the Papez circuit for memory in rats. Elife 2:e00736.

Vann S D and Aggleton J P (2003) Evidence of a spatial encoding deficit in rats with lesions of the mammillary bodies or mammillothalamic tract. J. Neurosci. 23:3506–3514.

Vann S D, Erichsen J T, O'mara S M, and Aggleton J P (2011) Selective disconnection of the hippocampal formation projections to the mammillary bodies produces only mild deficits on spatial memory tasks: implications for fornix function. Hippocampus 21:945–957.

Varea E, Nacher J, Blasco-Ibanez J, Gomez-Climent M, Castillo-Gomez E, Crespo C, and Martinez-Guijarro F (2005) PSA-NCAM expression in the rat medial prefrontal cortex. Neuroscience 136:435–443.

Varea E, Castillo-Gómez E, Gómez-Climent M Á, Blasco-Ibáñez J M, Crespo C, Martínez-Guijarro F J, and Nàcher J (2007) PSA-NCAM expression in the human prefrontal cortex. J. Chem. Neuroanat. 33:202–209.

Varki A (2017) Biological roles of glycans. Glycobiology 27:3–49.

Vawter M P, Frye M A, Hemperly J J, VanderPutten D M, Usen N, Doherty P, Saffell J L, Issa F, Post R M, Wyatt R J, *et al.* (2000) Elevated concentration of N-CAM VASE isoforms in schizophrenia. J. Psychiatr. Res. 34:25–34.

Vawter M P, Usen N, Thatcher L, Ladenheim B, Zhang P, VanderPutten D M, Conant K, Herman M M, Kammen D P van, Sedvall G, *et al.* (2001) Characterization of human cleaved N-CAM and association with schizophrenia. Exp. Neurol. 172:29–46.

Vitry S, Avellana-Adalid V, Hardy R, Lachapelle F, and Evercooren A (1999) Mouse oligospheres: From pre-progenitors to functional oligodendrocytes. J. Neurosci. Res. 58:735–751.

Bibliography

137

von der Ohe M, Wheeler S F, Wuhrer M, Harvey D J, Liedtke S, Mühlenhoff M, Gerardy-Schahn R, Geyer H, Dwek R A, Geyer R, *et al.* (2002) Localization and characterization of polysialic acid–containing N-linked glycans from bovine NCAM. Glycobiology 12:47–63.

Vutskits L, Djebbara-Hannas Z, Zhang H, Paccaud J, Durbec P, Rougon G, Muller D, and Kiss J (2001) PSA-NCAM modulates BDNF-dependent survival and differentiation of cortical neurons. Eur. J. Neurosci. 13:1391–402.

Vutskits L, Gascon E, and Kiss J Z (2003) Removal of PSA from NCAM affects the survival of magnocellular vasopressin-and oxytocin-producing neurons in organotypic cultures of the paraventricular nucleus. Eur. J. Neurosci. 17:2119–2126.

Wang Y and Neumann H (2010) Alleviation of neurotoxicity by microglial human Siglec-11. J. Neurosci. 30:3482–3488.

Weinhold B, Seidenfaden R, Röckle I, Mühlenhoff M, Schertzinger F, Conzelmann S, Marth J, Rita G, and Hildebrandt H (2005) Genetic ablation of polysialic acid causes severe neurodevelopmental defects rescued by deletion of the neural cell adhesion molecule. J. Biol. Chem. 280:42971–7.

Werneburg S, Buettner F F, Erben L, Mathews M, Neumann H, Mühlenhoff M, and Hildebrandt H (2016) Polysialylation and lipopolysaccharide-induced shedding of E-selectin ligand-1 and neuropilin-2 by microglia and THP-1 macrophages. Glia 64:1314–1330.

Werneburg S, Buettner F F, Mühlenhoff M, and Hildebrandt H (2015) Polysialic acid modification of the synaptic cell adhesion molecule SynCAM 1 in human embryonic stem cell-derived oligodendrocyte precursor cells. Stem Cell Res. 14:339–346. URL: http://www.sciencedirect.com/science/article/pii/S1873506115000410.

Wobrock T, Kamer T, Roy A, Vogeley K, Schneider-Axmann T, Wagner M, Maier W, Rietschel M, Schulze T G, Scherk H, *et al.* (2008) Reduction of the internal capsule in families affected with schizophrenia. Biol. Psychiatry 63:65–71.

Woodruff P, McManus I, and David A (1995) Meta-analysis of corpus callosum size in schizophrenia. J. Neurol. Neurosurg. Psychiatry 58:457–461.

Xu Q, Cobos I, De La Cruz E, Rubenstein J L, and Anderson S A (2004) Origins of cortical interneuron subtypes. J. Neurosci. 24:2612–2622.

Xuan S, Baptista C A, Balas G, Tao W, Soares V C, and Lai E (1995) Winged helix transcription factor BF-1 is essential for the development of the cerebral hemispheres. Neuron 14:1141–1152.

Yamamoto N, Inui K, Matsuyama Y, Harada A, Hanamura K, Murakami F, Ruthazer E S, Rutishauser U, and Seki T (2000) Inhibitory mechanism by polysialic acid for lamina-specific branch formation of thalamocortical axons. J. Neurosci. 20:9145–9151.

Yang P, Major D, and Rutishauser U (1994) Role of charge and hydration in effects of polysialic acid on molecular interactions on and between cell membranes. J. Biol. Chem. 269:23039–23044.

Yang S, Huh I, Baek J, Cho E, Choi M, Ryu S, Kim J, Park T, Ha K, and Hong K (2015) Association between ST8SIA2 and the risk of schizophrenia and bipolar I disorder across diagnostic boundaries. PLoS One 10:e0139413.

Young A and Wimmer R D (2017) Implications for the thalamic reticular nucleus in impaired attention and sleep in schizophrenia. Schizophr. Res. 180:44–47.

Yozu M, Tabata H, and Nakajima K (2005) The caudal migratory stream: a novel migratory stream of interneurons derived from the caudal ganglionic eminence in the developing mouse forebrain. J. Neurosci. 25:7268–7277.

Zapater J and Colley K (2012) Sequences prior to conserved catalytic motifs of polysialyltransferase ST8Sia IV are required for substrate recognition. J. Biol. Chem. 287:6441–6453.

Zhang H, Vutskits L, Calaora V, Durbec P, and Kiss J Z (2004) A role for the polysialic acid–neural cell adhesion molecule in PDGF-induced chemotaxis of oligodendrocyte precursor cells. J. Cell Sci. 117:93–103.

Zhang Y, Hoxha E, Zhao T, Zhou X, and Alvarez-Bolado G (2017) Foxb1 regulates negatively the proliferation of oligodendrocyte progenitors. Front. Neuroanat. 11:53.

Zhao T, Zhou X, Szabó N, Leitges M, and Gonzalo A (2007) Foxb1-driven Cre expression in somites and the neuroepithelium of diencephalon, brainstem, and spinal cord. Genesis 45:781–7.

Zheng K, An J J, Yang F, Xu W, Xu Z Q D, Wu J, Hökfelt T G, Fisahn A, Xu B, and Lu B (2011) TrkB signaling in parvalbumin-positive interneurons is critical for gamma-band network synchronization in hippocampus. Proc. Natl. Acad. Sci. U.S.A. 108:17201–17206.

Zikopoulos B and Barbas H (2006) Prefrontal projections to the thalamic reticular nucleus form a unique circuit for attentional mechanisms. J. Neurosci. 26:7348–7361.

Zikopoulos B and Barbas H (2012) Pathways for emotions and attention converge on the thalamic reticular nucleus in primates. J. Neurosci. 32:5338–5350.

Bibliography

Acknowledgement

Acknowledgements

141

Abbildung G.1: Monument to lab mouse. By Irina Gelbukh (Own work) [CC BY-SA 3.0 (http://creativecommons.org/licenses/by-sa/3.0)], via Wikimedia Commons

Danke auch an meine alte und neue Familie für ihr Verständnis in den vergangenen Monaten aber auch unabhängig davon für ein so familiäres Miteinander, das trotz des gemeinsamen Wortstammes heutzutage leider nicht selbstverständlich ist.

Insbesondere möchte ich meinen Eltern danken. Wenn man so will für die liebevolle Aufzucht, die Förderung und die emotionale Unterstützung während des Studiums aber ganz besonders für ihre nie endende selbstverständliche Liebe, die nicht selbstverständlich ist. Danke!

Fast zuletzt möchte ich meinem Ehemann danken. Nichts ist schöner als teilen zu können. Das gilt für die schlechten Momente, in denen du mir beistehst und mir Mut machst nicht weniger als für die schönen Momente – von gemeinsamen Seele-baumeln-lassen im Urlaub bis hin zu den allabendlichen Diskussion über Gott und die Welt, ob Biochemie oder Physik. Danke für die Unterstützung beim Debuggen von Skripten, Laborproblemen und sonstigen Dingen. Danke für deine Fürsorge in den vergangenen Monaten. Ich liebe dich!

Zu guter Letzt danke ich unserem Nachwuchs. Trotz anhaltender Inkubationszeit überwiegt die Vorfreude und hilft im Schreibprozess eine positive Grundstimmung aufrecht zu erhalten.

Curriculum Vitae

Personal Details

Name	Ute Elisabeth Schuster, formerly Diederichs
Date of Birth	May 4th, 1989
Place of Birth	Dresden
Marital Status	married
Nationality	German

Education

Since 06/2013	PhD student at the Institute of Clinical Biochemistry, Medical School Hannover
10/2011 - 04/2013	Medical School Hannover graduated with M.Sc. Biochemistry (1.1 with distinction)
10/2008 - 09/2011	Leibniz University Hannover graduated with B.Sc. Biochemistry (1.9)
07/2008	Geschwister-Scholl-Gymnasium Berenbostel Graduation with university-entrance diploma (Abitur, 1.2)

Publication List

- *A crucial role for polysialic acid in developmental interneuron migration and the establishment of interneuron densities in the mouse prefrontal cortex.*
  Kröcher T, Röckle I, **Diederichs U**, Weinhold B, Burkhardt H, Yanagawa Y, Gerardy-Schahn R, Hildebrandt H.
  Development, 2014 Aug;141(15):3022-32. doi: 10.1242/dev.111773. Epub 2014 Jul 3.

- *Glatiramer acetate increases phagocytic activity of human monocytes in vitro and in multiple sclerosis patients.*
  Pul R, Morbiducci F, Škuljec J, Skripuletz T, Singh V, **Diederichs U**, Garde N, Voss EV, Trebst C, Stangel M.
  PLoS One. 2012;7(12):e51867. doi: 10.1371/journal.pone.0051867. Epub 2012 Dec 20.

Selected Poster Presentations

11/2016	"Polysialic acid synthesis by ST8SIA2 is essential for cortical interneuron development", Annual Meeting of the Society for Glycobiology (SFG), New Orleans, USA
	Schuster UE, Rossdam C, Kröcher T, Röckle I, Kessaris N, Yanagawa Y, Weinhold B, Hildebrandt H.
11/2016	"Polysialic acid synthesis by ST8SIA2 is essential for cortical interneuron development", Annual Meeting of the Society for Neuroscience (SFN), San Diego. USA
	Diederichs U, Rossdam C, Kröcher T, Röckle I, Kessaris N, Yanagawa Y, Weinhold B, Hildebrandt H.
11/2014	"Role of polysialic acid in cortical interneuron migration", Joint Meeting of the Society for Glycobiology (SFG) and the Japanese Society of Carbohydrate Research (JSCR), Honolulu, Hawaii
	Diederichs U, Kröcher T, Röckel I, Yanagawa Y, Weinhold B, Hildebrandt H.
07/2014	"Role of polysialic acid in cortical interneuron migration", Interneuron Summer School, Amsterdam, Netherlands
	Diederichs U, Kröcher T, Yanagawa Y, Weinhold B, Burkhardt H, Hildebrandt H.

Awards and Oral Presentations

- Poster-Award with Poster-Talk for "Polysialic acid synthesis by ST8SIA2 is essential for cortical interneuron development" SFG 2016

- GBM-Diplom/Masterpreis 2013 for the Master Thesis, awarded by the „Gesellschaft für Biochemie und Molekularbiologie"